WL-TR-93-5004

SPATIAL LIGHT REBROADCASTER ARCHITECTURE STUDY

J. Cederquist
D. Angell
A. Tai
S. Cartwright
N. Subotic

Environmental Research Institute of Michigan
P.O. Box 134001
Ann Arbor, Michigan 48113-4001

DECEMBER 1992

Final Report for 4/1/90 - 9/30/92

Solid State Electronics Directorate
Wright Laboratory
Air Force Materiel Command
Wright Patterson AFB, Ohio 45433-7562

ERIM 320

REPORT DOCUMENTATION PAGE

Form Approved
OMB No. 0704-0188

1. AGENCY USE ONLY (*Leave Blank*)	2. REPORT DATE	3. REPORT TYPE AND DATES COVERED
	December 1992	Final 04/01/90 -- 09/30/92

4. TITLE AND SUBTITLE
Spatial Light Rebroadcaster Architecture Study

5. FUNDING NUMBERS
C F33615-90-C-1437
PE 62204
PR 2001
TA 02
WU AH

6. AUTHOR(S)
J. Cederquist, D. Angell, A. Tai, S. Cartwright and N. Subotic

7. PERFORMING ORGANIZATION NAME(S) AND ADDRESS(ES)
Environmental Research Institute of Michgian
P.O. Box 143001
Ann Arbor, Michigan 48113-4001

8. PERFORMING ORGANIZATION REPORT NUMBER
ERIM 226800-27-F

9. SPONSORING/MONITORING AGENCY NAME(S) AND ADDRESS(ES)
Solid State Electronics Directorate
Wright Laboratory
Air Force Materiel Command
Wright Patterson AFB, Ohio 45433-7562
WL/ELOT ATTN: Weigand 513-255-7310

10. SPONSORING/MONITORING AGENCY REPORT NUMBER
WL-TR-93-5004

11. SUPPLEMENTARY NOTES

12a. DISTRIBUTION/AVAILABILITY STATEMENT
~~Export Restrictions Apply~~
Approved for Public Release: Distribution is Unlimited

12b. DISTRIBUTION CODE

13. ABSTRACT (*Maximum 200 words*)

There is a need for a processor to perform real-time automatic target classification (ATC) that is compact and consumes little electrical power. Optical processors have the potential to provide the needed computational power in a small package. Substantial efforts have been expended in the development of spatial light modulators (SLMs) to meet the ATC requirements, but performance achieved thus far is still lacking. A new class of optical devices, spatial light rebroadcasters (SLRs) have been developed recently with potential performance far exceeding current SLMs. Instead of modulating the input light field, SLR absorbs the incident radiation and re-emits when triggered to do so. The triggering can be accomplished with an optical signal which also carries spatial information. The storage capability and the relationship between the intensities of the incident (input), triggering (readout) and emitted (output) radiations can be used to perform parallel processing of two-dimensional spatial data. In this report, several optical processing architectures were developed and five of the most promising were analyzed in detail. In addition, preliminary experiments were performed to evaluate the hardware required for two of the architectures.

14. SUBJECT TERMS
Optical Processing, Automatic Target Classification, Incoherent Optical Processing, Spatial Light Rebroadcaster

15. NUMBER OF PAGES
161

16. PRICE CODE

17. SECURITY CLASSIFICATION OF REPORT	18. SECURITY CLASSIFICATION OF THIS PAGE	19. SECURITY CLASSIFICATION OF ABSTRACT	20. LIMITATION OF ABSTRACT
Unclassified	Unclassified	Unclassified	Unclassified

PREFACE

The work reported here was performed by the Optical and Infrared Science Laboratory of the Advanced Concepts Division, Environmental Research Institute of Michigan (ERIM). The work was sponsored by the Air Force Wright Laboratory, WL/ELOT, under contract F33615-90-C-1437.

This final technical report covers work performed between April 19, 1990 and September 30, 1992. The principal investigators were Daniel Angell and Jack Cederquist. Major contributors to the effort were Carl Aleksoff, Steven Cartwright, Lauren Peterson, John Seldin, Nikola Subotic and Anthony Tai.

TABLE OF CONTENTS

LIST OF FIGURES

LIST OF TABLES

1.0 EXECUTIVE SUMMARY

The Spatial Light Rebroadcaster (SLR) Architecture Study Program was funded by Wright Laboratory WL/ELOT. The performance period of the program was from April 19, 1990 to August 14, 1992. The goal of the program is to develop, analyze and demonstrate optical processing architectures based on SLR devices.

1.1 Motivation

Spatial Light Rebroadcasters may offer higher data throughput rates if they can be incorporated into avionic's systems to alleviate the bottlenecks associated with sensor fusion, target classification, voice recognition, and interprocessor communications. Target recognition is chosen here as generally representative of all these problems because they are all plagued by a lack of high speed "smart" interconnection.

Reconnaissance and targeting are increasingly performed via electronic sensors. With the development of smart weapons and Unmanned Aerial Vehicles (UAV) as reconnaissance and autonomous weapons delivery platforms, there is a need for automatic target classifiers (ATC) that are compact and consume little electrical power. The computation and memory requirements of ATC algorithms generally increase with their effectiveness. Moreover, with the emergence of critical mobile targets, the processing hardware must be capable of very high throughput in order to meet the search rate requirement. With conventional electronic processors, higher computation speed can only be achieved at the expense of higher power consumption. At this time, the Air Force does not have any fieldable real time ATC for weapon delivery and reconnaissance systems. Optical processing technology offers a potential means to meet the computation rate and the power consumption requirements of current and foreseeable ATC systems.

Most optical processing systems being proposed are based on coherent optical processing technology which requires a spatial light modulator (SLM). Substantial efforts have been expended in the development of SLMs to meet the ATC processing requirement but the performance achieved thus far is still seriously lacking. A new class of optical devices, spatial light rebroadcasters (SLR), have been developed recently with potential performance far exceeding current SLMs. Instead of spatially modulating the input light field, an SLR absorbs the incident radiation and re-emits when triggered to do so. The triggering can be accomplished with an optical or electrical signal that carries additional spatial information. The relationship between the intensities of the incident (input), triggering (readout) and emitted (output) radiations can be used to perform massively parallel mathematical operations.

In addition to the incoherent nature of the radiation and the temporal properties, the storage and transfer characteristics of SLRs are also substantially different from those of SLMs. Optical processing architectures developed for SLMs are generally inappropriate for use with SLRs. While promising, the unique features of SLRs have not been shown definitively to offer significant advantages over conventional processors or more importantly, to provide potential performance that can meet the Air Force avionics requirements. The goals of this program are to 1) select or develop optical processing architectures most suitable for use with SLRs, 2) analyze the potential performance of the selected architectures, and 3) demonstrate the basic operations of the selected SLR-based optical processors.

1.2 Program Structure

The SLR Architecture Study program is composed of four tasks, beginning with a technology survey and finishing with concept demonstration experiments at the Air Force Wright Laboratory. The four tasks are as follows.

Task 1: Identify Air Force missions requiring high speed compact processors and define the computation requirements. Survey, analyze and invent optical processing architectures and select candidates with the best potential for satisfying the computation requirements.

Task 2: Analyze selected optical processing architectures and estimate potential performance based on projected device parameters. Select the three most promising architectures for experimental investigation. Selection criteria include potential performance, SLR requirements, current and near term SLR availability, and potential for insertion into Air Force systems.

Task 3: Identify key operations and component requirements. Perform preliminary experiments to evaluate the performance and feasibility of implementing the three optical processing architectures chosen in Task 2. Select two optical processing architecture for experimental demonstration..

Task 4: Develop and perform concept demonstration experiments on the two optical processing architectures selected in Task 3 at the Air Force Wright Laboratory.

1.3 Spatial Light Rebroadcasters (SLRs)

The generic description of an SLR is shown schematically in Figure 1-1. The input light field with data coded spatially in intensity impinges on the SLR which stores the information. The SLR emits light when triggered by either electrical or optical signals encoded spatially with a second set of data. The SLR can perform basic processor functions such as memory, summation of spatial and temporal data, multiplication of two data sets represented by the incident and readout signals, and nonlinear transformations such as thresholding.

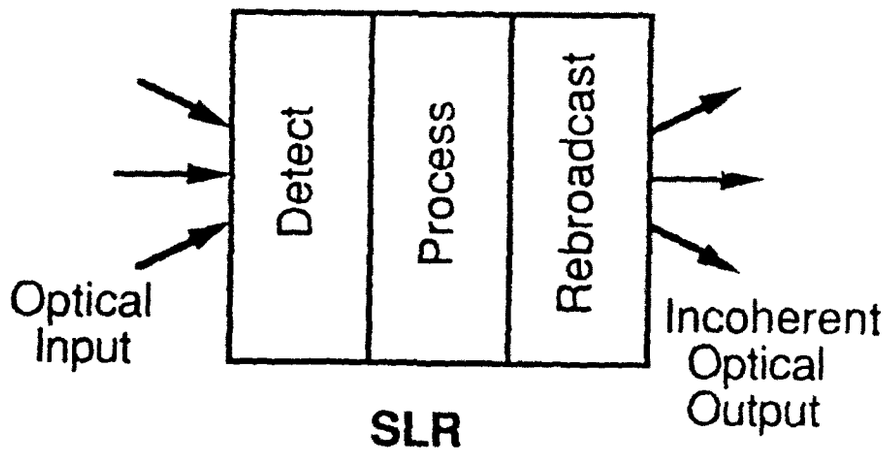

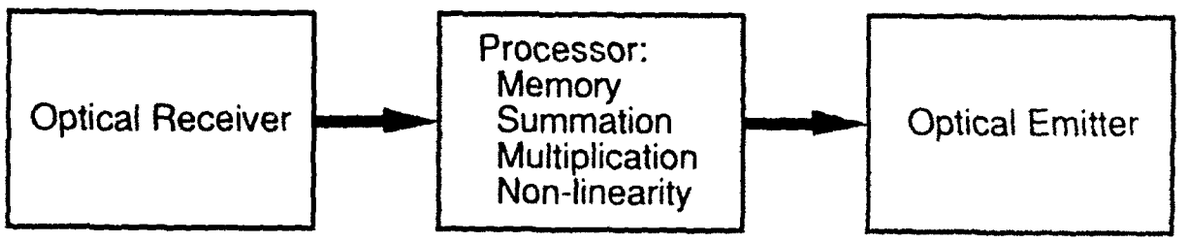

Figure 1-1. Generic Description of a Spatial Light Rebroadcaster (SLR)

SLMs and SLRs both operate with optical signals with information encoded spatially and possess read/write storage capabilities. However, there are substantial differences. The phase and coherence of the input light field are not preserved by an SLR. Therefore, information in the input and output beams can only be encoded in the intensity of the radiation. As we shall show in Section 2, this restriction impacts strongly the design of optical architectures that utilize SLRs.

There are two main types of SLRs: active and passive SLRs. While both can perform the generic functions described above, their operating characteristics are fundamentally different. Optical processing architectures that optimally utilize these two types of SLRs therefore cannot be the same.

An active SLR can be considered to be an integrated optoelectronic device with an array of elements as illustrated in Figure 1-2. Each element of the device is composed, at a minimum, of a photodetector, an electronic logic and control unit and an emitter. The input to the logic and control unit may be a signal from another photodetector. The output emission is determined by the input light intensity and the electronic control signal which may have been originated by an optical signal. An example of a series of operations that can be implemented with an SLR is to 1) multiply an input value by a weight represented by the control signal, 2) threshold the product and 3) output the binary result. This can be achieved by encoding the input value in the intensity of the input beam and the weight in the control signal. The control unit is composed of an amplifier and a comparator for thresholding. The control signal, which can be generated optically via a photodetector, controls the gain of the amplifier. The output voltage is thus proportional to the product of the input and the control signals. If the product of the two values exceeds a preset threshold, the emitter is turned on. It is interesting to note that this series of simple operations is the heart of an artificial neural network which will be described in Sections 2.4.3 and 3.2. With a two-dimensional array of these elements, the processing function

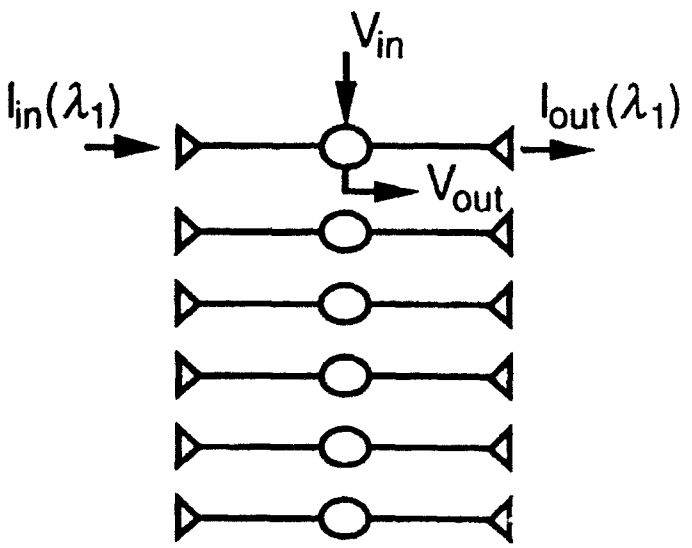

Figure 1-2. Functional Model of an Active SLR

described can be performed in parallel by all the elements in the array, achieving a very high processing throughput.

Passive SLRs operate by a very different principle even though they perform the same generic functions as active SLRs. Instead of an array of individual elements, a passive SLR typically consists of a uniform layer of an electo-optics material. An example is the electron trapping phosphor material manufactured by Quantex [Lindmayer]. Incident energy at a short wavelength (e.g., λ_i= green) is absorbed by the material, exciting electrons up to the communication band. The electrons then fall into traps where they are stored. When the material is radiated by light at a longer wavelength (e.g., λ_r=near infrared), the trapped electrons are excited out of the trapping level and fall back to the valance band, emitting light at wavelength λ_o where $\lambda_i < \lambda_o < \lambda_r$. The number of trapped electrons is determined by the product of the intensity of the input radiation and the number of trap sites. The intensity of the output emission is proportional to the number of occupied traps times the intensity of the readout beam. The products of two arrays of values can be obtained by, for example, inputting a light pattern representing the values of one of the arrays and reading the SLR out with a light pattern corresponding to the second array. The output intensity pattern of the emitted radiation is proportional to the product of the two arrays. The dynamic behavior of a passive SLR and its use in incoherent optical processing architectures are discussed in Section 3.5.

The performance of an optical processor is strongly dependent on the performance of the components used in its fabrication. To develop and evaluate optical processing architecture utilizing SLRs, the performance parameters achievable with SLRs must first be defined. In Table 1-1, the projected performances of active and passive SLRs are compared with that of an SLM. The projected performance for the active and passive SLRs are based on data from AT&T Bell Laboratory [Taylor] and Quantex Corporation [Lindmayar], respectively. The performance measure used

for comparison is space-bandwidth product rate (SBWP/T) in units of pixels/sec. If a single operation is performed each time the device goes through a read/write cycle, the SBWP/T is also the system throughput in terms of operations/sec. The potential performance of optical processors based on SLRs are orders of magnitude higher than those implemented with SLMs.

Table 1-1: **Projected Performance of an SLR**

Device	SBWP (pixels)	Frame Time (sec)	SBWP/T (pixels/sec)	Dynamic Range (dB)
Active SLR (Opto-Electronics)	$10^2 x 10^2$	10^{-9}	10^{13}	30
Passive SLR (Phosphor)	$10^{14} x 10^{14}$	10^{-3}	10^{11}	50
SLM	$10^3 x 10^3$	10^{-2}	10^8	30

There are other considerations in evaluating devices besides raw performance such as SBWP/T. The features and limitations of the two types of SLRs are summarized in Table 1-2.

Table 1-2: **Features of SLRs**

Device	Features	Limitations
Active SLR (Opto-electronics)	High speed, programmability, nonlinearity, memory, provides gain, ideal for pipelined architectures	Relatively small SBWP (100x100), high cost
Passive SLR (Phosphor)	Large SBWP, memory, low cost, write and erase simultaneously for bias subtraction	Weak nonlinearity, read out destructive, low efficiency, relatively slow, read-write at different wavelengths

1.4 Architecture Study Results

The choice of optical processing architectures is constrained by the operating characteristics of SLRs. The optical fields used to write on or read out an SLR can be coherent or incoherent, as long as they are at the proper wavelengths but the output emission is always incoherent. The output data are, therefore, represented by the beam intensity which takes on only positive real values. Moreover, an SLR does not simply modulates the intensity of the input light field, it also destroys all the phase information in the input light field. Therefore, SLRs cannot be used as direct replacement for SLMs in optical processors. Even with incoherent optical processing architectures, the destruction of the phase information limits the functions an SLR can perform. For example, an SLR cannot be used as an aperture mask in an imaging system. The SLR randomizes the phase at the aperture plane and no image can form at the output.

The active and passive SLRs also have distinct characteristics that affect the selection of optical processing architectures. Being passive devices, passive SLRs offer no gain. Moreover, the input and output wavelengths are substantially different. Together, they make it almost impossible to cascade SLRs to perform sequential or

iterative operations. On the other hand, active SLRs can provide optical gain and the devices can be easily cascaded. Active SLRs can, therefore, be used in optical processing architectures that perform sequential or iterative operation. This is important because the SBWP of the device is relative small ($< 100 \times 100$). Image processing functions cannot be performed on large images in a single pass. Partitioning the image and the processing algorithm is often necessary. Compensating for its small SBWP is the very fast (nsec) cycle time achievable with active SLRs. The time constants for the fluorescence and the stimulated photoluminescence are relative long which limits the cycle time of a processor utilizing passive SLR. However, the space-bandwidth product (SBWP) provided by a passive SLR can be very large. The spatial resolution of a phosphor based SLR can be as high as 40 lp/mm. With a 25mm x 25mm sample, the number of resolvable elements or SBWP is 1000 x 1000. Optical processing architectures utilizing passive SLRs must not demand fast cycle time and should take full advantage of their large SBWP.

A pre-selection was performed that resulted in seven candidates for evaluation. The unique operating characteristics of active and passive SLRs were taken into account in the preliminary selection of optical processing architectures. The selection was based primarily on the functionality, versatility and practicality of the architecture. The architectures chosen for study were 1) Scanning Correlator, 2) Interferometric processor, 3) OTF synthesis Optical Preprocessor, 4) Artificial Neural Network, 5) Quadratic Processor, 6) Morphological Processor and 7) Multispectral Optical Processor.

The scanning correlator [Lee] utilizes the capability of a passive SLR to store image information and produce an output that is proportional to the product of the stored image data and the image data encoded in the read beam. The interferometric processor [Tai, Aleksoff] performs Fourier transformation on the intensity distribution of an incoherent input field. The large dynamic range provided by a passive SLR is used with its simultaneous write-erase capability to enhance the output of an interferometric

processor which is characterized by a high bias. The same features are employed in the OTF synthesis optical processor [Rhodes] to perform pre-detection spatial filtering of image data. The artificial neural network [Lippman] , the quadratic processor [Rugh] and the morphological processor [Sternberg] perform nonlinear imaging processing operations. They all require sequential sum of products operations which are particularly suited for active SLRs. The multispectral optical processor takes advantages of the fact that different wavelengths are used to write on and erase data from a passive SLR to perform real time pre-detection enhancement of the image signal-to-clutter ratio.

Of the seven, five were down selected for further analyses. The down selection was based primarily on functionality, versatility and practicality. They are the artificial neural network, the quadratic processor, the morphological processor, the interferometric processor and the OTF synthesis optical preprocessor. Reasons for their selection are described below.

Unlike, for example, a Fourier transform based processor, an artificial neural network (ANN) operates from a low level which makes it the most versatile of the architectures studied. It can be used to implement nearly all the functional elements in ATC. The basic operation required is sum of products and thresholding which can be performed very efficiently with an optical processor. In addition, the massive fan-outs in an ANN architecture can be accomplished more easily with optical interconnects than with electrical wires.

A quadratic processor performs pixel-by-pixel statistical target detection on the target scene. It utilizes local spatial variations (reflectance or emittance) as a discriminant between targets and clutter. The processing architecture can utilize the incoherent sensor image directly as the input. It allows the quadratic processor to bypass the limitations of optical to electrical and electrical to optical converters, making it particularly useful as a preprocessor. In addition, the nonlinear operations performed by

a quadratic processor provide processing capabilities not available with conventional linear optical systems.

The morphological processor is also a neighborhood processor capable of nonlinear processing functions. Instead of matching to the overall shape of a target, a morphological processor performs ATC by extracting features that define a target. Such a process tends to be more robust than matched filtering or template matching whose performance can be adversely affected by changes in aspect, lighting and operating condition. Morphological processing is typically implemented electronically using a recirculating pipeline architecture to minimize the size of the processor. With the inherent parallelism of an optical processor, the neighborhood operation can be performed simultaneously for all pixels in the image.

The last two are diffraction based incoherent optical processors whose architectures are well known. Diffraction based systems provide the largest space-bandwidth product, making them attractive for wide area search applications. The difficulty has been with the bias which could easily overwhelm the signal at the output. With both architectures, the role of the SLR is bias reduction. Since the principles of these two types of incoherent optical processors are well established, the discussion in Section 3 will concentrate on the use of a passive SLR for bias reduction.

The scanning correlator was not chosen because of its limited capability (the reference function must be real and positive) and relatively slow speed due the serial nature of the scanning operation. The multispectral optical preprocessor did not survive the down selection because the laser power required for flood illumination may be too high to be practical in view of the sensitivity of available passive SLRs . Moreover, discrimination between different sets of target and clutter may involve different combinations of wavelengths. To reprogram the preprocessor will require a change in the SLR material to one with different input and readout wavelengths.

1.5 Performance Evaluations

In this section, the predicted performances of the selected optical processing architectures are presented. The purpose of the performance evaluation is to compare the performance of the optical processors with those of their electronics counterparts in performing similar ATR/C algorithms. It is not the goal of this project to evaluate the effectiveness of various ATR/C approaches and algorithms. Therefore, the performance was evaluated in terms of processing throughput instead of the probabilities of detection and false alarms.

1.5.1 Optical Artificial Neural Network

Optical processing generally has less accuracy than electronic digital processing but greater speed. In other ERIM work, a study was done to determine the accuracy required for artificial neural network computations. The problem chosen was that of determining terrain type (forest, grass, soil) from airborne sensor imagery of the ground in five wavelength bands in the visible, near infrared, and short wave infrared. A Kohonen self-organizing network was successfully developed for this purpose. The network has five inputs, three nodes, and three outputs corresponding to the terrain classification. The network was trained with floating point computation. The network was then used to classify the input data with varying accuracy in the input data and weights. The result is that floating point performance is maintained down to 5-bit accuracy in the data and weights. Although this is only a single test, it was assumed that 6-bit accuracy is sufficient for artificial neural network computations during use, but not during training.

In Section 2.4.4, five optical neural network architectures are described. To perform the performance evaluation, a cylindrical optics architecture and a planar architecture with fixed weights were chosen. Two versions of the cylindrical optics

architecture were designed and analyzed using a lens design program. The following parameters were used in the point design for a neural network processor with cylindrical optics.

Input: 100 laser diodes at 1 mm spacing and 1 MHz operation rate, Mask: 100 by 200 1mm by 250 micron pixels

Output: 200 photodiodes at 250 micron spacing and 1 MHz operation rate.

This leads to the following performance characteristics:

Volume: L by W by H = 20 cm by 10 cm by 5 cm = 1000 cm^3 ,

Input data rate: 100 x 1 MHz = 10^8 data values/sec

Computation rate: 100 x 200 x 1 MHz = 2 x 10^{10} operations/sec.

Computations/Volume: 2 x 10^7 operations/sec/cm^3.

Power (for 1% accuracy): 100 x 40 mW = 4 W

For the planar architecture, the following parameters were used:

Input: 100 laser diodes at 100 micron spacing and 1 MHz operation rate

Mask: 100 by 200 100 micron by 50 micron pixels

Output: 200 linear photodiodes at 50 micron spacing and 1 MHz operation rate

This leads to the following characteristics:

Volume: L by W by H = 6 cm by 1 cm by 1 cm = 6 cm^3-

Input data rate: 100 x 1 MHz = 10^8 data values/sec

Computation rate: 100 x 200 x 1 MHz = 2 x 10 operations/sec

Computations/cm^3: 3 x 10^9

Power (for 1% accuracy): 100 x 40 mW = 4 W

This second architecture is superior to the first in computation/cm^3 as desired.

1.5.2 Optical Quadratic Processor

The optical implementation of a quadratic processor geared toward automatic target recognition (ATR) was considered. This processor implements the likelihood ratio detector which is used extensively in ATR activities. Our analysis has shown that the optical implementation of the quadratic processor has a number of distinct advantages over their electronic (and other optical architectures) counterparts, most notably in throughput rate and density. The number or operations performed on each input pixel is summarized as:

Multiplication by mask:	81 multiplications
Lens summation (8 adds x 9 real.)	72 additions
Multiplication by neighborhood	09 multiplications
Final summation	08 additions
Total	170 ops/input pixel

For input image sizes of 500 x 500 pixels, the system throughput rate is:

1.4 Gops/sec	(SLR response time = 30 msec)
42.5 Gops/sec	(SLR response time = 1 msec)
42,500 Gops/sec	(SLR response time = 1 μsec)

In addition, our analysis showed that the system size is approximately 41,000 cm^3 and a prime power requirement of 750 Watts. The throughput rate per unit volume is then 1 Gop/sec cm^3 and the throughput rate per unit power is 57 Gop/sec W (SLR response time = 1 μsec). The signal-to-noise ratio of the system was shown to be at approximately 17dB. These specifications make the optical implementation an extremely

viable architecture. In addition, it should be noted that this architecture requires no optical/electronic/optical transduction, it operates directly on the imaging sensor pre-detected output.

1.5.3 Optical Morphological Processor

The ideal processor architecture for morphological processing in terms of performance is the parallel full array. All image pixels are transformed simultaneously, providing a tremendously high throughput. Its implementation, unfortunately, is not feasible with current microelectronics fabrication technology. The inherent massive parallelism of an optical processor, however, may make it possible to implement a parallel full array in a reasonably compact package, resulting in orders of magnitude improvement in system throughput.

The heart of an optical morphologic image processor is the computation unit which is composed simply of an input SLR, an imaging lens, a programmable pupil mask and an output SLR as described in Section 3.4. This basic module can be cascaded and arranged in a feedback architecture. The data circle back after passing through and processed by the N stages. The processing throughput of such a processor is maximized when the time required to alter the transmittance of the SLMs is matched to the processing time through the N stages. If for example, the switching time of the SLR is 1 nsec and N = 50, the SLM and the SLR logic must be programmable within 50 nsec to keep up. Otherwise, the processing speed must be slowed down or the number of processing stage has to be increased.

Let us assume that the structure element is composed of 3 x 3 neighborhood pixels, a single transformation will require a minimum of nine multiplies and one summation for a total of ten arithmetic operations. If the space-bandwidth product (SBWP) of the SLRs is 256 x 256 pixels, then with the speed assumed in Table 1 for the

active SLR devices, the processing speed of the optical morphological processor will be 256^2 x 10 ops/1 nsec = 6 x 10^{14} ops/sec.

A rough estimate of the processor size is about 5cm x 5cm x 10cm for each optical stage. The optics of a 10 stage system will occupy about 2500 cm^3. Adding another 10,000 cm^3 for the control and driving electronics, the total processor volume is about 12,500 cm^3. The processor throughput per unit volume is then equal to 5 x 10^{10} operations/sec/cm^3.

If we use a more modest and realistic processor size and the throughput becomes SLM switching time limited, then with a SLM switching speed of 1 μsec, the processing speed is lowered to 256^2 x 10 x 10 ops/ 1 μsec = 6.5 x 10^{12} ops/sec. The processing speed per unit volume achieved with these rather conservative parameters is then equal to 5.2 x 10^8 ops/sec/cm^3 which is still very high.

1.5.4 Interferometric Processor

The interferometric processor can be implemented with a different architecture. Since the optical input to an interferometric processor is incoherent, the natural target scene can theoretically be used directly. However, the amount of light available in a natural scene at the write wavelength of an SLR may not be enough to write on the SLR at a high rate. To perform image processing at high speed, the write beam must have sufficient amount of optical power. One optical architecture considered is based on acousto-optics scanners/modulators. Let the aperture time be τ, N be the number of pixels on a carrier in the A-O cell and M^2 be the space-bandwidth product of the processor output. The processing speed of the processing system is then equal to M^2N/τ. As an example, with a Crystal Tech 4075 A-O modulator, the carrier frequency f_c = 75MHz, the bandwidth BW = 50MHz, τ = 80μsec and M = N = 4000. The processing speed is then equal to 1.25 x 10^{13} op/sec. The optics in the interferometric

processor should occupy about 8700 cm^3 Including all the driving electronics, the overall processor size is estimated to be approximately 3×10^4 cm^3. The predicted system performance of the optical interferometric processor per unit volume is about 4.2×10^8 ops/sec/cm^3.

1.6 Conclusion

The Spatial Light Rebroadcaster, particularly of the active type, can potentially be a powerful device that can serve as the heart of a compact high speed processor. The devices, however, are still in a very early developmental stage and they require significant amount of further development before they can be competitive in optical processing architectures such as those described in this report.

Passive SLRs such as those implemented with electron-trapping materials, exist today. Some of these materials were developed for wavelength down-conversion to visualize near infrared radiation and they are commercially available. The performance of these passive SLR materials and devices, however, require substantial improvement in several of areas to make them competitive.

1) The slow temporal response of the passive SLR, particularly in erasure, limits the cycling rate. The throughput achievable is too slow to be competitive at this time.

2) Compounding the problem of low cycling rate is the low optical efficiency. The output is so dim that the output must be integrated over a significant amount of time to gather enough photons to provide the needed signal dynamic range.

3) The erasure is often incomplete unless very strong light or heat is used. The need for a powerful source for rapid and complete erasure impacts negatively on power consumption.

One solution to the problem may be to develop an SLR that emits light directionally (current devices radiate isotopically, over 4π radian). Improving the optical

efficiency would allow the use of a thin layer of rebroadcasting material and improve the cycling speed of the device.

More serious are some of the inherent characteristics of passive SLRs which limit their usefulness.

1) The readout is destructive. The material requires constant refreshing to keep the data stored in the device. A trade off between output brightness and the number of number of times the stored in formation can be readout is required.

2) The input and readout wavelengths are different which precludes the cascading of devices to perform sequential operations even if adequate optical efficiency can be achieved.

3) The nonlinearities exhibited by passive SLRs are weak and they can not be easily changed. The type of operation that can be performed is therefore restricted.

With these inherent limitations, passive SLR devices are less likely to have a significant impact on the optical processor development.

Active SLR devices have the inherent flexibility and power to be a significant player in the future development of compact high speed processing systems. They may be utilized as interconnects in an electronic processor, or as the processing elements in an hybrid electronic/optical processor. The programmable gain and nonlinearity provided by the device are particularly crucial to many optical computing architecture. The development of these devices, however, is still in an early stage. Specific area that requires further development includes the following.

1) Space-Bandwidth Product. The advantage offered by an optical processor is the massive parallelism of the computation. This advantage can be realized only if the space-bandwidth product of the input and output devices are sufficiently large. Devices being fabricated at this time are very small. The manufacturing technology to fabricate a large array with acceptable cost and yield remains to be developed.

2) Packing Density. The most attractive promise of optical processing is high speed processing in a small physical package with low power consumption. To fulfill this

promise, the large space-bandwidth product must be accomplished in a small package that draws little power. Therefore, the device size must be small and the packing density must be very high. Considering that each element in an active SLR consists of a detector, a signal conditioner and an emitter, a 3-dimensional structure is likely to be required to achieve the density desired.

3) Addressing Schemes. To maintain a high throughput, particularly with a pipelined, recirculating processing architecture, an efficient means must be available to address and program the elements in the SLR in parallel.

Optical processing and computing approaches typically fall into one of two categories. The optical processor either performs complete high level operations such as correlation for matched filtering or it is designed to perform low level logic operations that emulate electronic processors. Performing the bulk of the ATR functions optically will restrict the ATR algorithms to linear filtering operations which severely limits the power and robustness that can be accomplished. On the other hand, optics has limited success in challenging the well developed and entrenched electronics technology in performing low level logic operations. The optical processing architectures presented in this report offer an alternative approach where optics and electronics share the burden, each doing what it does best. Such a hybrid processing architecture has the potential to combine the speed and efficiency provided by optical processors with the flexibility and programmability offered by electronic processors. Five promising optical processing architectures were developed and analyzed. Based on the projected performance of the passive and active SLRs, the performance of the five processing systems were estimated and the results are summarized in Table 1-3.

Table 1-3. Summary of Predicted Performance of Five Optical Processor Architectures

Architecture	Device	Rate/Vol. (ops/sec/cm^3)	Minimum Power/Vol. (mw/cm^3)	Volume (cm^3)
Neural Network				
ANN 1	Active	$1x10^7$	2	$1x10^3$
ANN 2	Active	$3x10^9$	33	$6x10^0$
Planar ANN	Active	$2x10^{10}$	400	$0.5x10^0$
Quadratic Processor	Active	$1x10^9$	18	$41x10^3$
Morphological	Active	$6x10^{10}$	33	$3x10^3$
OTF Synthesis	Passive	$1x10^6$	33	$3x10^2$
Interferometric Processor	Passive	$4x10^8$	20	$9x10^3$

2.0 TASK 2: ARCHITECTURE STUDY

The goal of this task is to identify several promising optical processing architectures that can take advantages of the unique features of SLRs, evaluate their applicability to Air Force problems, perform preliminary analyses of their potential performance, and select five candidates for in depth evaluation in Task 2.

2.1 Architecture Study Methodology

The methodology used for the architecture study is summarized in Figure 2.1-1. The study began with an examination of Air Force applications and identified automatic target classification (ATC) as a primary application for high speed processors. ATC was first broken down into functional elements. The processing algorithms for these ATC functional elements were surveyed and the mathematical operations required were identified. Next, optical processing architectures that can be used to perform ATC functions were assessed. The assessment started with existing optical processing architectures that may be utilized to implement the ATC algorithms. Each architecture was analyzed to determine if and how processing performance can be improved by the use of SLRs. Based on the insight gained by the assessments, modifications of the existing architectures were made and new architectures were developed to better utilize the characteristics of SLRs. The architecture selection was influenced from the top by the potential of the optical processing architecture to satisfy specific needs of the Air Force and from the bottom by the availability of an SLR with the required performance characteristics.

2.2 ATC Application Requirements and Functional Elements

An automatic target classifier assigns target categories with associated confidence measures to the detected targets. The level of classification is dependent on the mission.

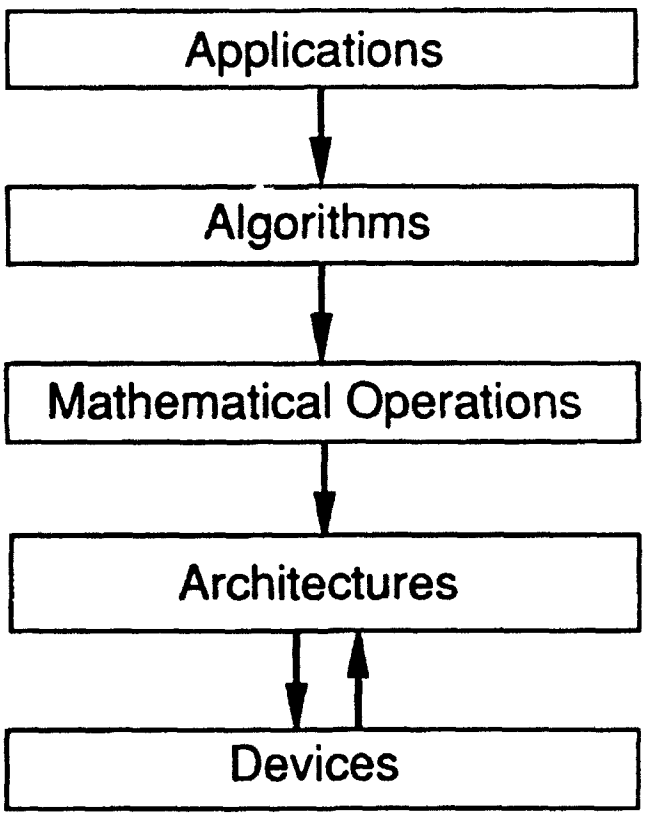

Figure 2.1-1. Architecture Study Methodology

The classification can range from coarse (e.g., tree clutter versus vehicle) to very fine (e.g., an M-1 tank with Allied markings versus an M-1 tank with markings of the adversary). ATC typically begins with interest point location which defines the probability of an area having a target. It could be based on terrain information or target attributes such as target brightness and contrast or multispectral signature. Areas identified as points of interest are then segmented further into regions such as vehicles, trees, roads, houses, hangers, etc. Segmentation may be based on the overall dimension of the region, surface roughness or spectral properties. If required, even finer features in the segmented areas can be extracted. Features of interest could include wheels, tracks, gun barrels, raised deck or recessed bay, antennae, camouflage and other markings. The final step is to classify or assign target categories with associated confidence measures to the segmented regions in the image, identifying them as clutter, friendly targets, and hostile targets of high or low value. The functional elements in a automatic target classifier [ATRWG] are summarized graphically in Figure 2.2-1.

The ultimate figures of merit for an ATC are the probabilities of detection and false alarm. The goal of this project, however, is not to develop or optimize ATC algorithms. The goal is to study the feasibility of implementing existing ATC algorithms with optical processors that employ SLRs. The figure of merit that will be used is how well the optical processor can perform the ATC algorithms.

As a first order estimate of the processing throughput requirement for ATC, consider two imaging systems: 1) a pushbroom imager with 10^4 linear pixels providing 1 ft ground resolution on a airborne platform travelling at 600mph, and 2) a focal plane imager with 512 x 512 pixel refreshing at 30 frames/sec. For both sensors, the pixel rate is 10^7 pixels/sec. Let us assume that it requires 10 operations /pixel to perform a simple detection algorithm. The required system throughput is then 10^8 ops/sec which is within the range of state-of-the art all electronic processors. However, simple detection algorithms are generally not robust enough for Air Force applications. They tend to

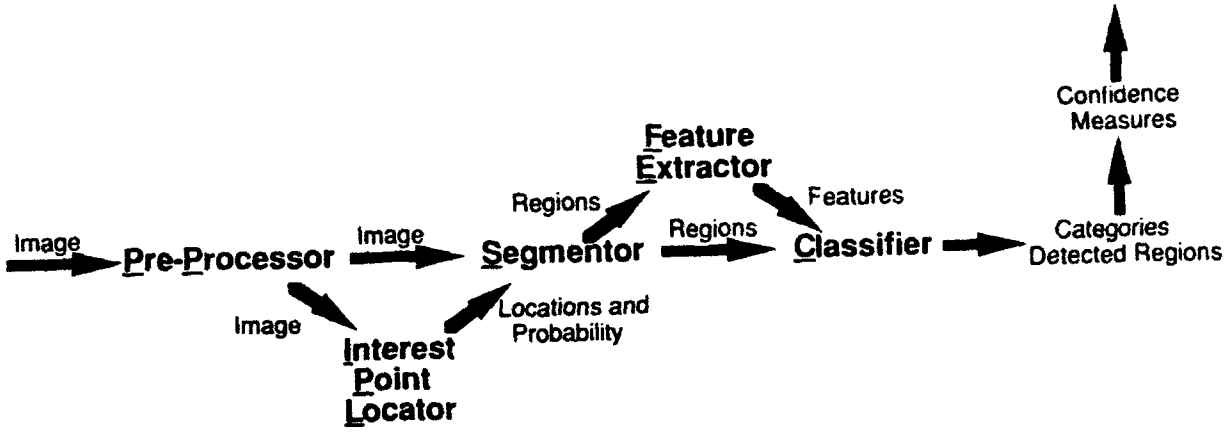

Figure 2.2-1. Functional Elements in an Automatic Target Classifier

degrade substantially with target and clutter variability. More robust adaptive ATC algorithms typically require $>>$ 10 operations/pixel to implement. The processor throughput requirement is, therefore, in the range of 10^9 ops/sec.

Optical processors are most effective as special purposed "hardwired" processing units where their strengths are optimally utilized and its weaknesses are circumvented. Therefore, it is generally more practical and efficient to implement one or more functional elements of ATC by an optical processor instead of an entire automatic target classifier. In the following section, incoherent optical processing techniques are first reviewed. Candidate processor architectures are then described in Section 2.4 and the ATC functions that can be performed by each architecture are discussed.

2.3 Incoherent Optical Processing Techniques Overview

An SLR does not modulate the input or the readout radiation, it absorbs the input radiation and re-emits. There is no correlation between the phases of the input, the readout and the output light waves. Moreover, the output radiation is spatially incoherent and, in most cases, temporally incoherent as well. Optical processing architectures utilizing SLMs must therefore employ incoherent optical processing techniques. In this section, basic operations that can be accomplished with incoherent optical processing techniques using an SLR are described, starting from low level operations such as addition and multiplication to high level operations such as Fourier transformation. The optical processing architectures described later all make use of one or more of these techniques.

2.3.1 Arithmetic Operations

Addition and multiplication are natural operations for incoherent optical processing with an SLR. Processing algorithms requiring only additions and

multiplications are most efficiently performed. Other operations such as division are also possible but requires more complexity or steps.

Addition, $I_o(x,y) = I_1(x,y)+I_2(x,y)$:

Passive SLR - The number of the excited and trapped electrons is proportional to the total absorbed energy. With two input light patterns incident on the SLR simultaneously, the number of trapped electrons is given by the sum of the intensities. With the storage capability of the SLR, the summation can also be performed by two input patterns incident on the device sequentially. The ability to sum sequential inputs is the primary benefit of SLR over a conventional detector.

Active SLR - Data can be stored as charges in capacitors and summation can be performed serially or in parallel as with a passive SLR.

Multiplication, $I_o(x,y) = I_1(x,y)I_2(x,y)$:

Passive SLR -The light pattern $I_1(x,y)$ is input to the SLR and stored. The SLR is then readout with light pattern $I_2(x,y)$. The emitted output light pattern is proportional to $I_1(x,y)I_2(x,y)$ provided that the number of trapped electrons depleted by the readout beam is small compared to the total number of trapped electrons.

Active SLR - Multiplication can be achieved by using one input value to control the gain of the amplifier. The amplified output is then proportional to the product of the input value and the stored value controlling the gain.

Contrast Reversal, $I_o(x,y) = C - I_1(x,y)$

Passive SLR - A uniform pattern is input and store, then read out with $I_1(x,y)$. What remains stored in the trap sites of the material is $C_1 - I_1(x,y)$. Reading the SLR out again with a uniform beam produces $I_o(x,y) = C_2[C_1 - I_1(x,y)]$.

Active SLR - Contrast reversal can be accomplished with an inverting amplifier.

Subtraction, $I_o(x,y) = I_1(x,y) - I_2(x,y)$

Passive SLR - Contrast reversal is first performed on the input pattern $I_1(x,y)$ as described above and obtain $[C_1 - I_1(x,y)]$. The input second light pattern $I_2(x,y)$ is then read out with a uniform beam. The emitted output is given by $I_o(x,y) = C1 + I_2(x,y) - I_1(x,y)$.

Active SLR - Charges stored in capacitors can be depleted by the desired amount to perform subtraction.

Division, $I_o(x,y) = I_2(x,y) / I_1(x,y)$

Passive SLR - Division can be performed with a device having a nonlinear input/output transfer characteristic described by $I_o = I_i^{-\gamma}$ above the toe region where $\gamma=1$. It is a natural characteristic of many materials to have a negative input-output transfer characteristic which gradually reaches saturation. The material acts as an invertor, i.e., $I_1'(x,y) = 1/I_1(x,y)$ for input values that are >0. Reading out the SLR with a light pattern $I_2(x,y)$, we have $I_o(x,y) = I_2(x,y)\, I_1'(x,y) = I_2(x,y) / I_1(x,y)$.

Active SLR - The same nonlinearity can be used to implement division.

We note that the operations are performed in parallel on all elements of the array. If we have a large number of elements in the array, the computation rate in terms of operation/sec can be very high.

2.3.2 Higher Level Operations

Higher level operations can be implemented by combining basic arithmetic operations. However, optical phenomena can also be used to implement higher order operations directly. Coherent optical processors, for example, make extensive use of the Fourier transform property of a lens. Equivalent operations can also be performed with incoherent optical processors.

2.3.2.1 Matrix Multiplication

The most well known higher order operations accomplished by combining basic arithmetic operations are vector-matrix multiplications, $\mathbf{A}_N = \mathbf{B}_M\mathbf{C}_{MN}$ and matrix-matrix multiplications, $\mathbf{A}_{MN} = \mathbf{B}_{MK}\mathbf{C}_{KN}$. The elements in the output vector in a vector-matrix multiplication are given by:

$$A_n = \sum_{m=1}^{M} B_m C_{mn} \quad . \tag{1}$$

For matrix-matrix multiplication, the output matrix is equal to:

$$A_{mn} = \sum_{k=1}^{K} B_{mk} C_{kn} \quad . \tag{2}$$

Both involve sum of products operations requiring only additions and multiplications which can be performed very efficiently by an optical processor. Sum of products is the heart of many processing algorithms including Fourier transformation and spatial frequency filtering, convolution, correlation, quadratic processing and artificial neural networks.

2.3.2.2 Fourier Transformation

Fourier transformation:

$$F(u, v) = \mathcal{F}[f(x, y)] = \int_{-\infty}^{\infty}\int_{-\infty}^{\infty} f(x, y)\, e^{-i2\pi(ux + vy)}\, dxdy \tag{3}$$

or its discrete form:

$$F(u, v) = \mathcal{F}[f(x_m, y_n)] = \sum_{m=-\infty}^{\infty} \sum_{n=-\infty}^{\infty} f(x_m, y_n)\, e^{-i2\pi(ux_m + vy_n)} \tag{4}$$

can be implemented as vector-matrix multiplications. The Fourier transform kernel is complex (i.e., with real and imaginary parts). Even if the input is composed only of positive real values, the processor must still be able to perform complex multiplications and additions. With an incoherent optical vector- matrix or matrix-matrix multiplier

which can only represent positive real values via light intensities, the computations have to be carried out with a minimum of three parallel channels.

Fourier transformation can be more efficiently accomplished by taking advantage of the properties of light propagation. With coherent light, there is a Fourier transform relationship between the complex amplitudes of the fields at two widely separated planes. The long propagation distance for Fraunhofer diffraction can be significantly shortened with the use of a lens which performs the coherent integration operation in the Fourier transformation. The Fourier transformation property of a focussing lens is the basis for coherent optical processing [Goodman. Lee]. With incoherent radiation, a Fourier transform relationship exists between the intensity distribution and the spatial coherence of the field at two widely separated planes. Once again, a lens can be used to shorten the propagation distance of the field. Interferometric optical processing architectures that make use of this coherence property of a propagating light field are described in Section 2.4.2.

2.3.2.3 Convolution and Correlation

Convolution:

$$\int\int f_1(x, y)\, f_2(\alpha-x, \beta-y)\, dxdy = \mathcal{F}^{-1}[\, F_1(u, v)\, F_2(u, v)\,] \qquad (5)$$

and correlation:

$$\int\int f_1(x, y)\, f_2^*(x-\alpha, y-\beta)\, dxdy = \mathcal{F}^{-1}[\, F_1(u, v)\, F_2^*(u, v)\,] \qquad (6)$$

can be performed by operating in the spatial or spatial frequency domain. In the above expressions, $\mathcal{F}^{-1}[\ ]$ represents inverse Fourier transformation, * denotes conjugation. Implementation in the spatial frequency domain requires sequential Fourier transformations and a multiplication. It is the usual approach taken in coherent optical processing using SLMs as the input device and the spatial filter. Incoherent optical

processing architectures using SLRs, however, are not as easily cascaded to perform sequential Fourier transformations. First of all, the wavelengths of the input, readout and output light beams may not be the same. More importantly, only positive real values can be represented by the intensity of incoherent light. Multiple separate channels and the addition of a bias are required to represent complex and bipolar values which greatly complicate the implementation of sequential operations.

For the special case where the input and reference functions, f_1 and f_2 are both positive and real, incoherent optical processing techniques can be used to perform convolution and correlation operations directly. For example, the output of an incoherent imaging system can be described by:

$$I(\alpha, \beta)=\int\int |f(x, y)|^2 \; |h(\alpha-x, \beta-y)|^2 \, dxdy \qquad (7)$$

where $I(\alpha, \beta)$ is the output image intensity, $|\ h(x,y)\ |^2$ is the incoherent point spread function and $|\ f(x,y)\ |^2$ is the intensity distribution of the input. The spatial filtering of an input image pattern can therefore be accomplished by designing the proper aperture function F(u, v) where $F(u, v) = \mathcal{F}[h(x,y)]$. It is important to note that with such an incoherent optical processor, the aperture or filter function F(u,v), which can be real or complex, must be implemented with an SLM. The aperture mask in an imaging system has to operate on the complex amplitude of the light field. A mask implemented with an SLR would destroy all the phase information of the input field. The role of the SLR in such an optical processor is therefore limited to the input and output functions such as the removal of the bias at the output of the incoherent optical processor as described in Section 3.5.

2.4 Candidate Optical Processing Architectures

The choice of optical processing architectures is constrained by the operating characteristics of SLRs. First, the optical fields used to write on or read out an SLR can

be coherent or incoherent, as long as they are at the proper wavelengths, but the output emission is always incoherent. The output data are, therefore, represented by the beam intensity which takes on only positive real values. Second, an SLR does not simply modulate the intensity of the input light field, it also destroys all the phase information in the input light field. Therefore, SLRs cannot be used as direct replacements for SLMs in optical processors. Even with incoherent optical processing architectures, the destruction of the phase information limits the functions that an SLR can perform. For example, an SLR cannot be used as an aperture mask in an imaging system. The SLR randomizes the phase at the aperture plane and no image can form at the output.

The active and passive SLRs also have distinct characteristics that affect the selection of optical processing architectures and they must be discussed separately.

Passive SLRs: Being passive devices, they offer no gain. Moreover, the input and output wavelengths are substantially different. Together, they make it almost impossible to cascade SLRs to perform sequential or iterative operations. The time constants for the fluorescence and the stimulated photoluminescence are relative long which limits the cycle time of a processor utilizing passive SLR. On the other hand, the space-bandwidth product (SBWP) provided by a passive SLR can be very large. The spatial resolution of a phosphor based SLR can be as high as 40 lp/mm. With a 25mm x 25mm sample, the number of resolvable elements or SBWP is 1000 x 1000. Optical processing architectures utilizing passive SLRs must not demand fast cycle time and should take full advantage of their large SBWP.

Active SLRs: Active SLRs can provide optical gain and the devices can be easily cascaded. Active SLRs can, therefore, be used in an optical processing architectures that perform sequential or iterative operation. This is important because the SBWP of the device is relatively small ($< 100 \times 100$). Image processing functions cannot be performed on large images in a single pass. Partitioning the image and the processing algorithm is often necessary. Compensating for its small SBWP is the very fast (nsec) cycle time achievable with active SLRs.

Passive SLRs do not possess strong nonlinearity. To implement algorithms such as neural net require strong nonlinearity, an external means must be used to produce the

nonlinearity. With an active SLR, on the other hand, the desired nonlinearity can be built into the SLR.

These unique operating characteristics of active and passive SLRs were taken into account in the preliminary selection of optical processing architectures for SLRs. The architectures chosen for study were 1) Scanning Correlator, 2) Interferometric processor, 3) OTF synthesis Optical Preprocessor, 4) Artificial Neural Network, 5) Quadratic Processor, 6) Morphological Processor and 7) Multispectral Optical Processor. The implementation of these optical processing architectures with passive or active SLRs are described below.

2.4.1 Scanning Correlator

A scanning correlator performs correlation in the spatial domain in the form of:

$$f_1(\alpha, \beta) \star f_2(\alpha, \beta) = \int\int f_1(x, y)\, f_2^*(x-\alpha, y-\beta)\, dxdy \ . \qquad (8)$$

The lateral shifting of the reference function $f_2(x, y)$ encoded on an SLM is provided by two orthogonal acousto-optic (AO) scanners as shown in Figure 2.4.1-1. The input image from the sensor is written onto an SLR and, at the same time, the scanning image of the reference is used to readout the SLR. The emitted output of the SLR corresponds to the product of the input and the reference images, $f_1(x,y)f_2(x-\alpha_o, y-\beta_o)$. The output of the SLR is then imaged onto a large area detector which detects the total incident optical power, effectively performing the spatial integration. By scanning the input image in a raster fashion, the amount of lateral shift (α, β) of the reference image is encoded into time by the relationship $\alpha = Vt/h - int(Vt/h)$ and $\beta = int(Vt/h)$ where V is the velocity of the horizontal scan, h is the length of the horizontal scan which is determined by the combined size of f_1 and f_2 , t is time and int denotes the integer function. The temporal output of the detector, therefore, represents the time encoded spatial correlation of the input and reference images.

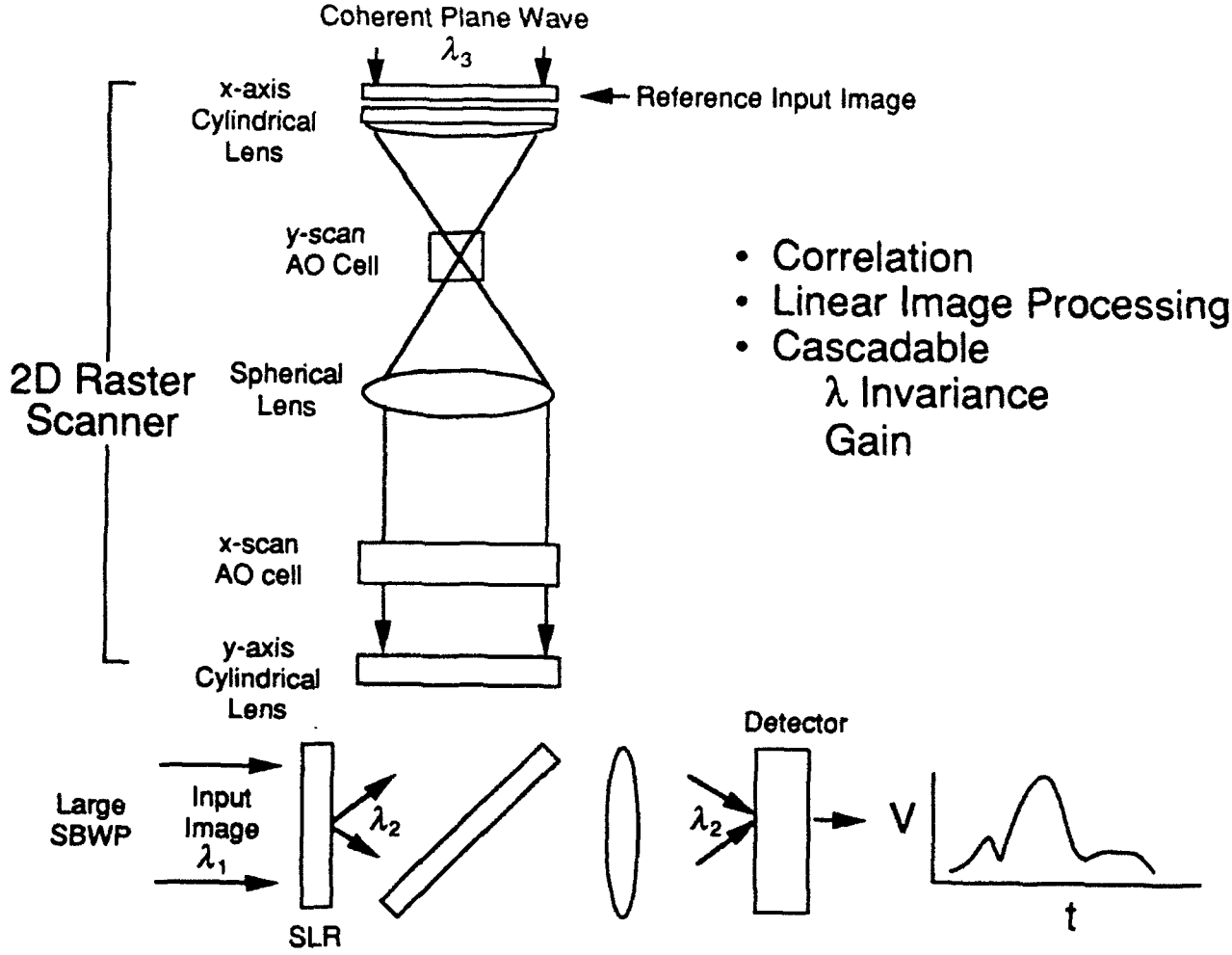

Figure 2.4.1-1. A Scanning Correlator

The scanning correlator allows the image from an optical sensor to be used as the input but it requires an SLM for the reference template. For many applications, it is not necessary to change the reference template rapidly. The use of an SLM as the reference does not represent a significant disadvantage.

There are, however, drawbacks in the use of a scanning correlator. First of all, the correlation operation is performed via sequential steps, indexing along α and β. The operating speed is, therefore, much slower than a Fourier transform based correlator that operates in the spatial frequency domain. In addition, the input and the reference functions of a scanning correlator must both be real and positive. There is a large body of work in optimizing and expanding the capabilities of correlation filters to make them invariant to the size, orientation and aspect of the target, and more tolerant of variation in lighting conditions and partial obscuration. These filters, unfortunately, require the reference function to be complex. A scanning correlator cannot take advantage of these recent advances in correlation filter design.

2.4.2 Interferometric Processor

From coherence theory, it is well known that a Fourier transform relationship exist between the intensity distribution and the coherence of the radiation in the far field [Born]. That is:

$$\mu(u,\ v) = \int\int_{\Sigma} \mathrm{I}(\alpha,\ \beta)\ e^{-i2\pi(u\alpha+v\beta)/\lambda}\ d\alpha d\beta \qquad (9)$$

where $\mu(u, v)$ s the complex degree of spatial coherence (CDSC), $\mathrm{I}(\alpha, \beta)$ is the intensity distribution of the input function and Σ is the field of view of the sensor. Using a shearing interferometer [Aleksoff, Tai] to measure the CDSC at a range of spatial frequencies simultaneously, the Fourier transform of the intensity of the target scene can be obtained at the speed of light without requiring an intervening spatial light modulator.

The output intensity of a shearing interferometer, I_o , is given by:

$$\begin{aligned} I_o(u, v) &= \int\int_{\Sigma} I_i(x, y)\{1 + \cos[2\pi(ux+vy)]\}\, dxdy \\ &= \int\int_{\Sigma} I_i(x, y)\, dxdy + \int\int_{\Sigma} I_i(x, y)\cos[2\pi(ux + vy)]\, dxdy \\ &= Bias + Re\{\mathcal{F}[I_i(x, y)]\} \quad . \end{aligned} \tag{10}$$

To obtain the imaginary part of the Fourier transform, a $\pi/2$ phase shift is inserted in one of the sheared beams to produce:

$$\begin{aligned} I_o(u, v) &= \int\int_{\Sigma} I_i(x, y)\, dxdy + \int\int_{\Sigma} I_i(x, y)\sin[2\pi(ux + vy)]\, dxdy \\ &= Bias + Im\{\mathcal{F}[I_i(x, y)]\} \end{aligned} \tag{11}$$

A rotation shearing interferometer such as a modified Köster interferometer [Aleksoff] as illustrated in Figure 2.4.2-1 can provide the two-dimensional transform of an incoherent input pattern. However, the interferometer can only operate with narrow band radiation and the image of the target scene cannot be used directly as the input. A grating interferometer is achromatic [Tai] and can operate directly on the incoherent radiation from the target scene. The grating interferometer, however, is a one-dimensional device. For a two-dimensional input, the interferometer output corresponds to a radial line in the Fourier spectrum. A two-dimensional transform of the input can be obtained by rotating the interferometer about its optical axis.

Since the bipolar output is on a bias, the signal is often overwhelmed, particularly if the size of the image support, Σ, is large. For the processor to be viable, a means to reduce the bias is necessary. The fact that the real and imaginary parts of the Fourier transform reside at the outputs of two separate channels also makes cascading the processor more difficult.

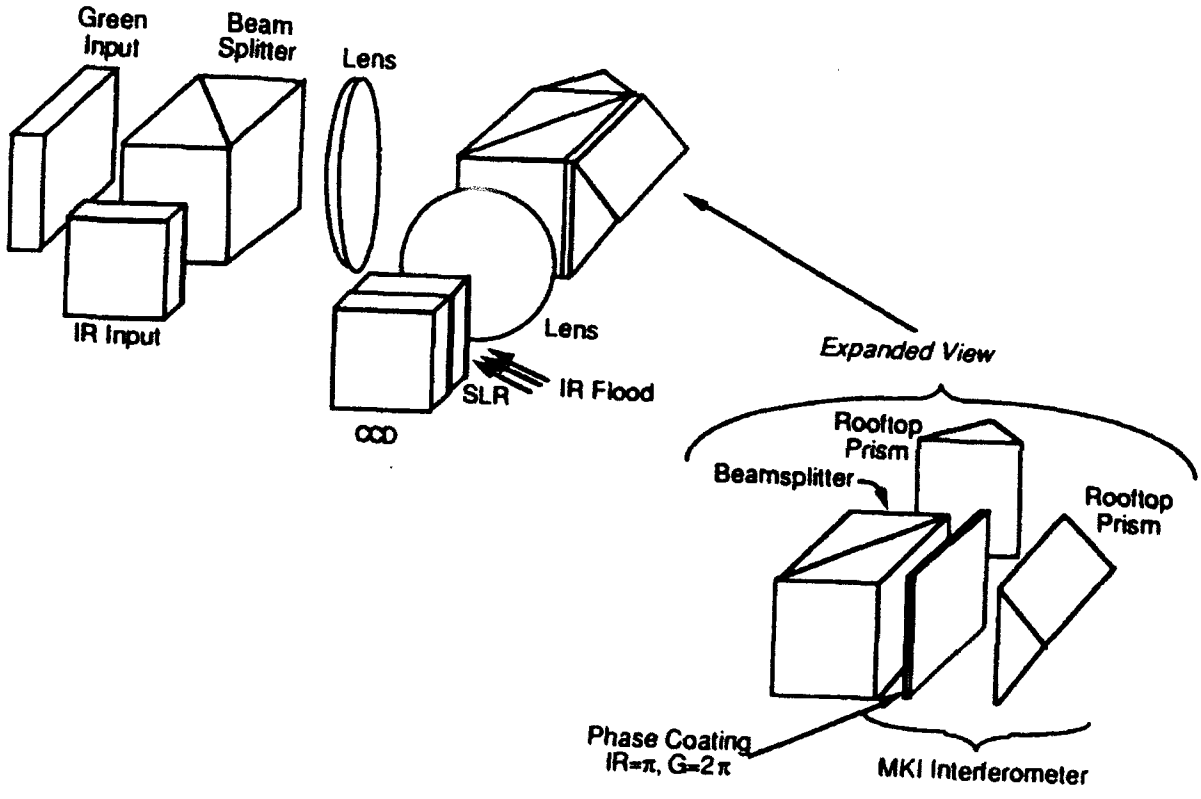

Figure 2.4.2-1. A Rotation-Shearing Interferometer

2.4.3 OTF Synthesis Optical Preprocessor

As described in Section 1.4.2.3, incoherent optical processing techniques can be used to perform convolution and correlation operations for the special case where the input and reference functions are both positive and real. Specifically, the output of an incoherent imaging system can be described by:

$$I(\alpha, \beta) = \int\int |f(x, y)|^2 \; |h(\alpha - x, \beta - y)|^2 \, dxdy \tag{12}$$

where $I(\alpha, \beta)$ is the output image intensity, $| h(x,y) |^2$ is the incoherent point spread function and $| f(x,y) |^2$ is the intensity distribution of the input. The Optical Transfer Function (OTF) of the imaging system is defined as the normalized Fourier transform of $| h(x,y) |^2$. That is, [Rhodes]:

$$OTF(u, v) = \frac{\mathcal{F}[|h(x, y)|^2]}{\int\int |h(x, y)|^2 \, dxdy} . \tag{13}$$

Spatial filtering of an incoherent input image can be accomplished by designing the proper aperture function F(u, v) where $F(u, v) = \mathcal{F}[h(x,y)]$. We note that F(u,v) can be complex. Complex operations such as matching filtering can therefore be performed.

F(u,v) must be implemented with an SLM. The filter function may be complex as we have just indicated. More importantly, the coherence and the phase of the input field must be preserved by the spatial filter which is not the case with SLRs where the input and output photons are different.

2.4.4 Artificial Neural Networks

Artificial neural networks consist of nodes (or artificial neurons) which are connected together [Lippman]. Figure 2.4.4-1 shows a node with inputs x and output y.

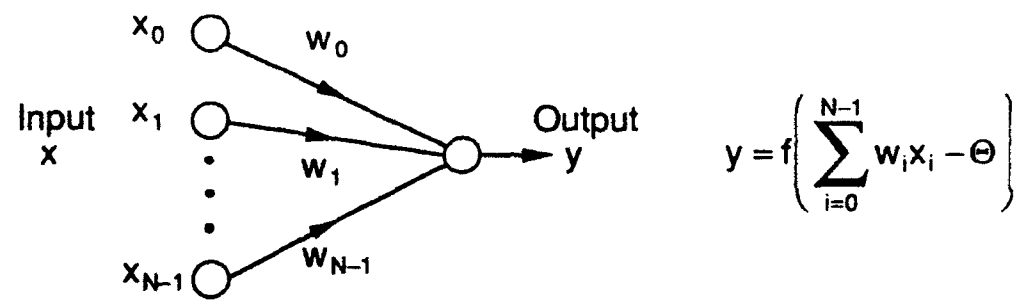

Neural network node input-output relationship

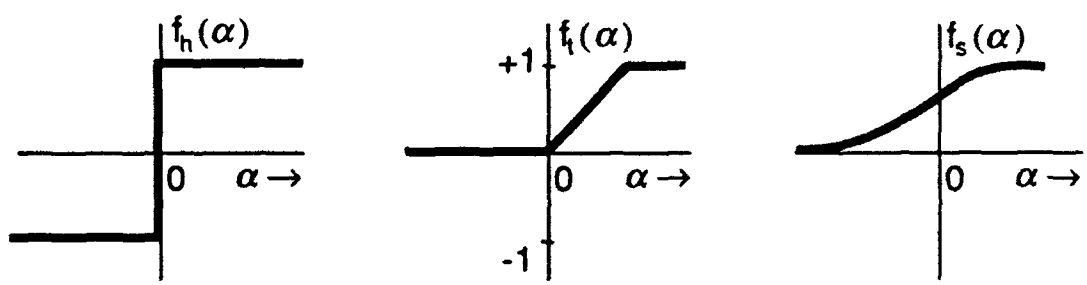

Typical nonlinearities

Figure 2.4.4-1. Basic Processing Element of an Artificial Neural Network

The node performs the function of weighting each input with a corresponding weight w, summing these weighted inputs, subtracting a threshold O, and passing the result through a nonlinearity f( ) to produce the output y. Sample nonlinear functions f are also shown in Fig. 2.4.4-1. Typically, nodes are grouped to form layers and the layers are massively interconnected. Figure 2.4.4-2 shows a three-layer perceptron artificial neural network. The N inputs x are applied to the first layer of N nodes. The N outputs x' of the first layer serve as inputs to second layer and so on to the final N outputs y. Layers which neither receive the initial input nor produce the final output are called hidden layers. Many other connections are possible including feedback connections, but a single network seldom has more than three layers. Entire networks may sometimes be cascaded, however.

The computations found in artificial neural networks are multiplication, addition, and nonlinearity. Artificial neural networks also require massive data broadcasting and reception. Linear, passive optical processing techniques can provide the multiplication and addition. Optical methods may also be used to provide the massive interconnections. Nonlinear optics or opto-electronic spatial light rebroadcasters can provide the nonlinear operations. A schematic of a possible opto-electronic node is shown in Fig. 2.4.4-3. The weighted inputs are summed as they strike detectors. Incoherent optical processing is assumed and two channels are shown to handle positive and negative weight values. The op-amp performs subtraction of the positive and negative channels and applies the nonlinearity. The output is rebroadcast to the next layer by a laser diode. Implementations with light emitting diodes are equally possible.

Five optical architectures for artificial neural networks were studied. The first three assume fixed weight values and use holographic, cylindrical, and lenslet array optics respectively to perform the interconnections. The fourth architecture assumes fixed weights and uses cylindrical optics, but uses a phosphor type spatial light rebroadcaster. The fifth architecture includes optical training or computation of the

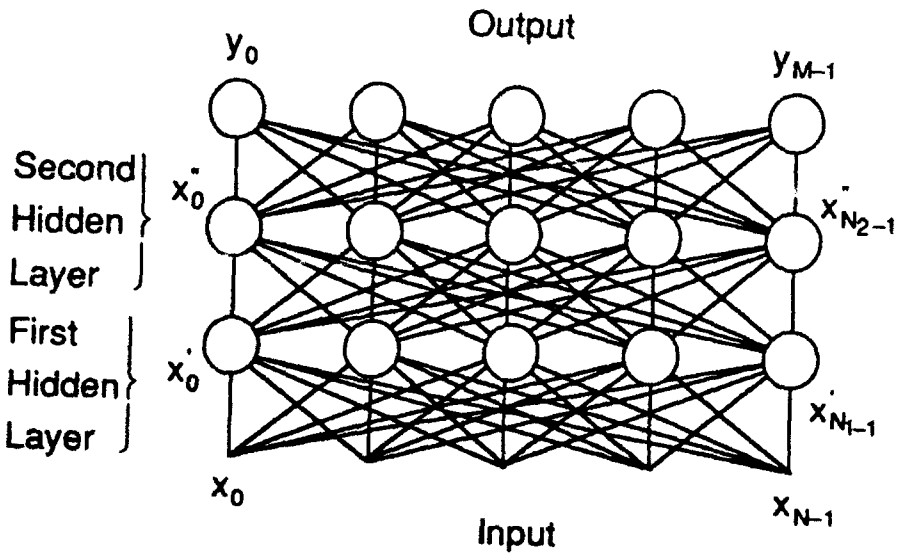

$$y_l = f\left(\sum_{k=0}^{N_2-1} w''_{kl} x''_k - \Theta''_l\right)$$

$$x''_k = f\left(\sum_{j=0}^{N_1-1} w'_{jk} x'_j - \Theta'_k\right)$$

$$x'_j = f\left(\sum_{i=0}^{N-1} w_{ij} x_i - \Theta_j\right)$$

Figure 2.4.4-2. A Three-Layer Perceptron Neural Network

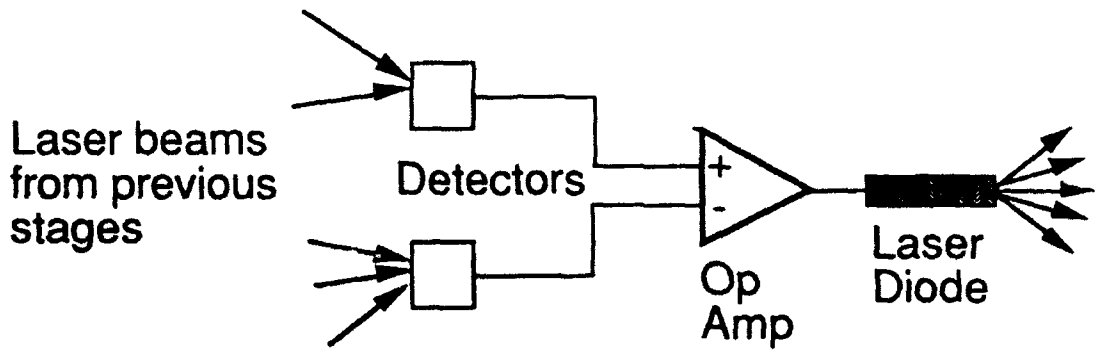

- Op Amp sums inputs and applies threshold
- Dual detectors allow bipolar inputs

Figure 2.4.4-3. An Opto-electronic Node in a Neural Network

weight values. All of the architectures are shown for a single layer artificial neural network. They would be cascaded for multiple layer networks.

2.4.4.1 Holographic Architecture

Figure 2.4.4-4 shows the holographic artificial neural network. At each node, holographic light redistribution elements are located which consist of superimposed or spatially multiplexed gratings. These elements take the output of a node, break it into multiple parts, weight each part, and send each part toward a specific node in the next layer. To do this, each grating has a diffraction angle appropriate to diffract the light to a specific node and a diffraction efficiency corresponding to the weight required for that input to the node. The nodes would be opto-electronic spatial light rebroadcasters, for example of the type shown in Fig. 2.4.4-3. Although shown as one-dimensional in the figure, the processor could operate in two dimensions.

In addition to the spatial light rebroadcasters, the critical element of this architecture is the fabrication of the holographic elements. Figure 2.4.4-5 shows one method for fabrication in which an SLM would be used to program the recording beams to write individual gratings on a holographic recording media. Binary optics fabrication techniques could also be used. It will be difficult to maintain sufficient accuracy in the weights (diffraction efficiencies). Other studies performed by ERIM have shown that 3% accuracy (5 bits) is needed at a minimum for successful neural net operation [Cederquist]. This would be difficult for the spatially multiplexed gratings, let alone for the superimposed grating approach.

2.4.4.2 Cylindrical Optics Architecture

Figure 2.4.4-6 shows a cylindrical optics based artificial neural network. The input is a linear array of laser diodes or light emitting diodes each of which is collimated

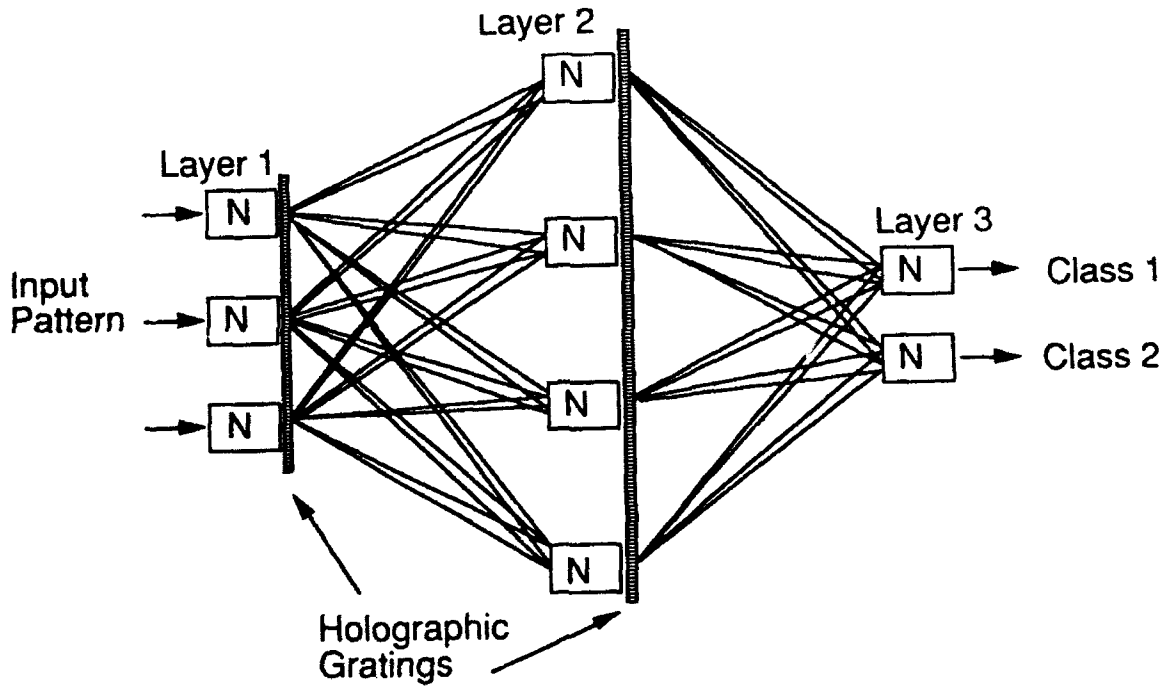

Figure 2.4.4-4. A Holographic Neural Network

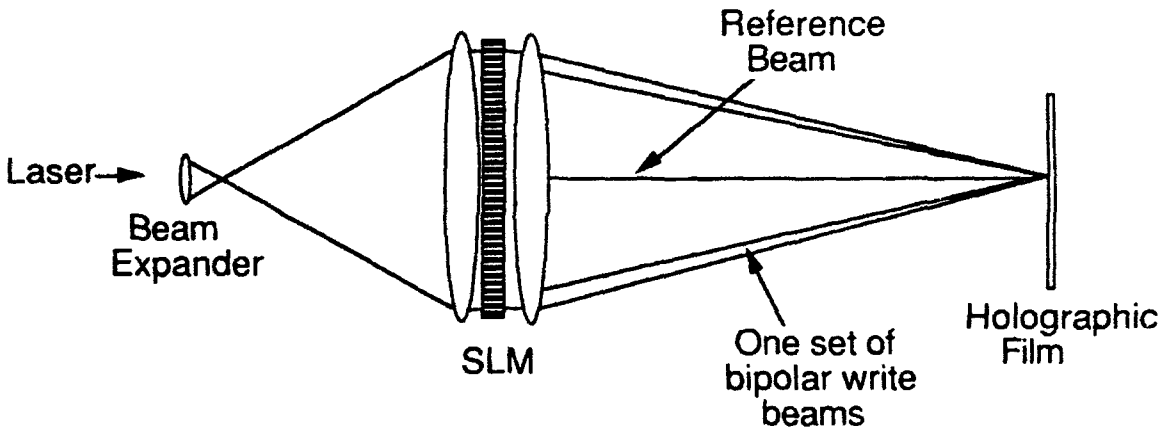

Figure 2.4.4-5. Fabrication of Holographic Grating for Neural Network

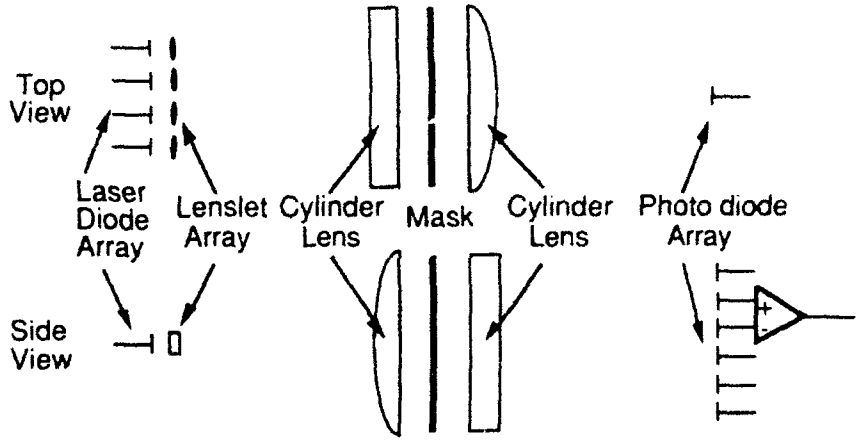

Figure 2.4.4-6. Cylindrical Optics-Based Artificial Neural Network

by the first cylindrical optic. The resulting light passes through an intensity (or gray scale) mask where it is multiplied by the weights. A second cylindrical optic oriented at 90 degrees to the first focuses this light onto a linear array of opto-electronic spatial light rebroadcasting devices. At their detectors summation is performed, nonlinearity is performed electronically, and the output is optically rebroadcast to the next layer.

The critical elements of this architecture are the performance of the cylindrical optics and the fabrication of the two-dimensional weight mask. Fabrication of a spatially multiplexed weight mask to 1% accuracy can be achieved with table look-up linearization [Cederquist and Lee]. This architecture is known in the literature and some experimental results for a matrix-vector multiplier have also already been published, so the risk of the cylindrical optics was judged to be low. Therefore, this architecture was chosen over the other approaches for in-depth analysis.

2.4.4.3 Lenslet Array Architecture

The third architecture studied is shown in Fig. 2.4.4-7. It is similar to the second architecture in that it uses a spatially multiplexed weight mask, but it uses lenslets to image the input onto the mask and lenslets to collect the light onto the detectors. The critical elements of this architecture are the performances of the two lenslet arrays. Each element of the first array must demagnify the input and image it to a specific location on the mask. This means the input FOV of the lenses is large and the lenses will have different vignetting over their FOV depending on their location in the array. This variation would have to be computed and compensated in the weight mask. Light leaving the mask does not in general propagate along the optical axis, but at an angle to it which becomes greater toward the edges of the mask. This requires lenslets of the second array to be capable of capturing and focusing light arriving at large angles to their optical axes. On balance, this architecture seemed to have no advantage of size and probable

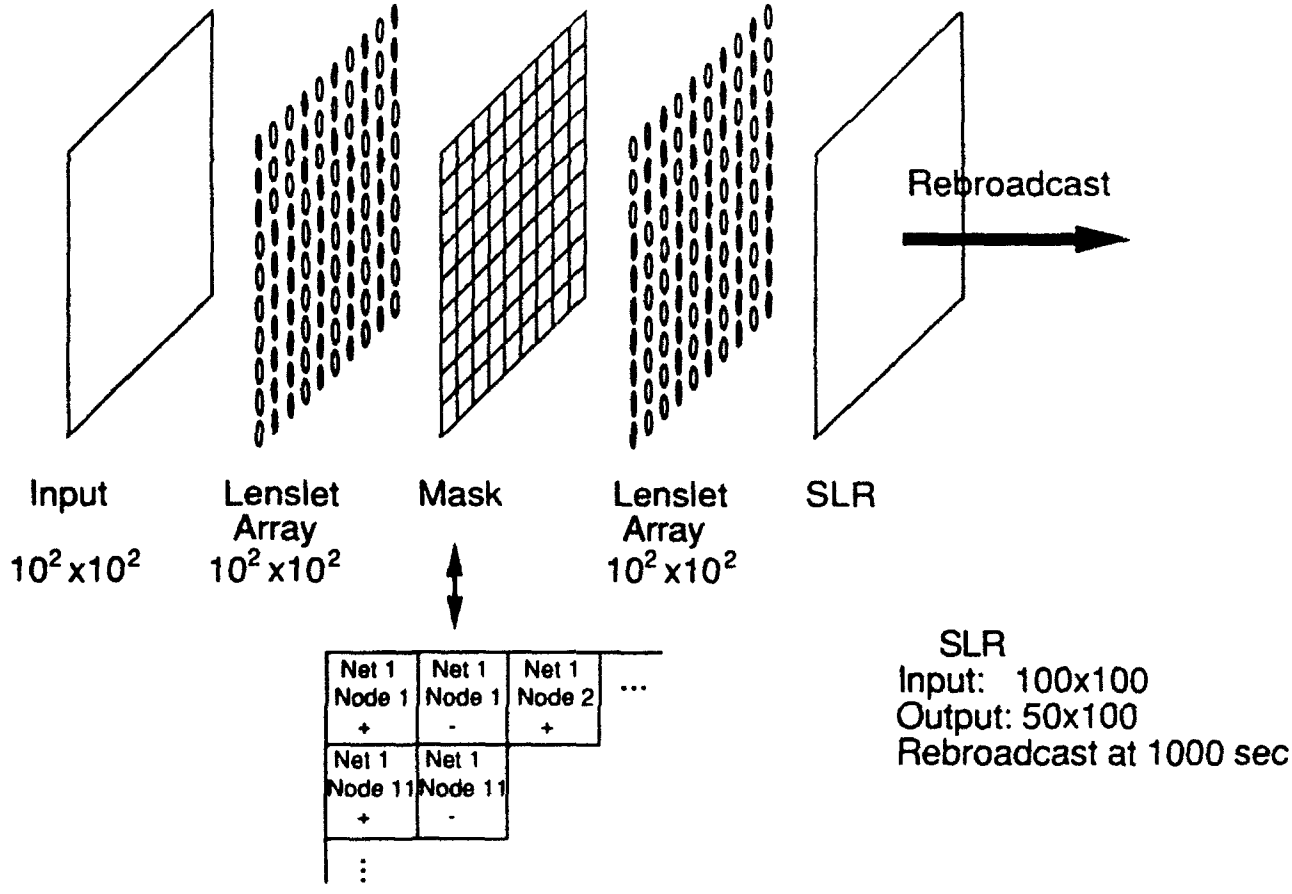

Figure 2.4.4-7. Lenslet Array Architecture for Artificial Neural Network

disadvantages in accuracy and complexity (use of lenslet arrays) over the second architecture and so was not analyzed further.

2.4.4.4 Phosphor Based Architecture

The fourth architecture studied is shown in Fig. 2.4.4-8. It uses the cylindrical optics architecture, but substitutes a phosphor type of spatial light rebroadcaster for the opto-electronic type. This is done by having two inputs, one at a write wavelength for positive weight values and one at an erase wavelength for negative weight values. Each is multiplied by the weights using a mask, but the subtraction is done optically by writing and erasing the phosphor rather than electronically in an opto-electronic spatial light rebroadcaster. The critical element of this architecture is the requirement of the spatial light rebroadcaster to perform the nonlinear operation required by artificial neural networks. As discussed in Section 3.5, accurate subtraction followed by nonlinearity is not a natural operation of phosphors. In addition, this architecture is not optically cascadable since the wavelength of the rebroadcast is not suitable for either the write or erase inputs. For these reasons, this architecture was not analyzed in depth.

2.4.4.5 Adaptive Weight Architecture

The fifth architecture studied is shown in Figure 2.4.4-9. Unlike the others, it does not use fixed weights, but electronically computes any necessary changes to the weights (such as occurs during artificial neural network training) and optically updates the weight mask. The architecture uses cylindrical optics with the weight mask written on a phosphor spatial light rebroadcaster. Since this weight mask will be partially erased each time it is read out, it is refreshed (rewritten) every 10 cycles by a weight mask in digital electronic memory and displayed on a CRT. The output of the artificial neural network processor is not only rebroadcast to the next processor, but is also input to a digital electronic processor. In the digital electronic processor, this input is used to

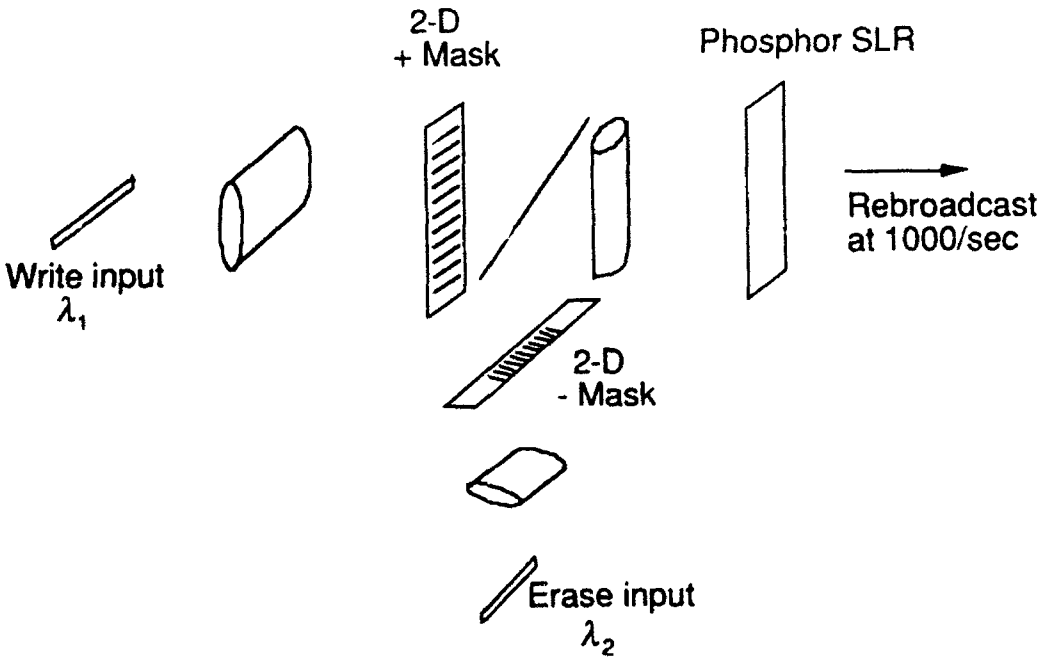

- Use write, erase wavelengths in input and subtract at SLR
- Requires phosphor SLR with nonlinearity
- Not cascadable

Figure 2.4.4-8. Phosphor Passive SLR-Based Architecture for Artificial Neural Network

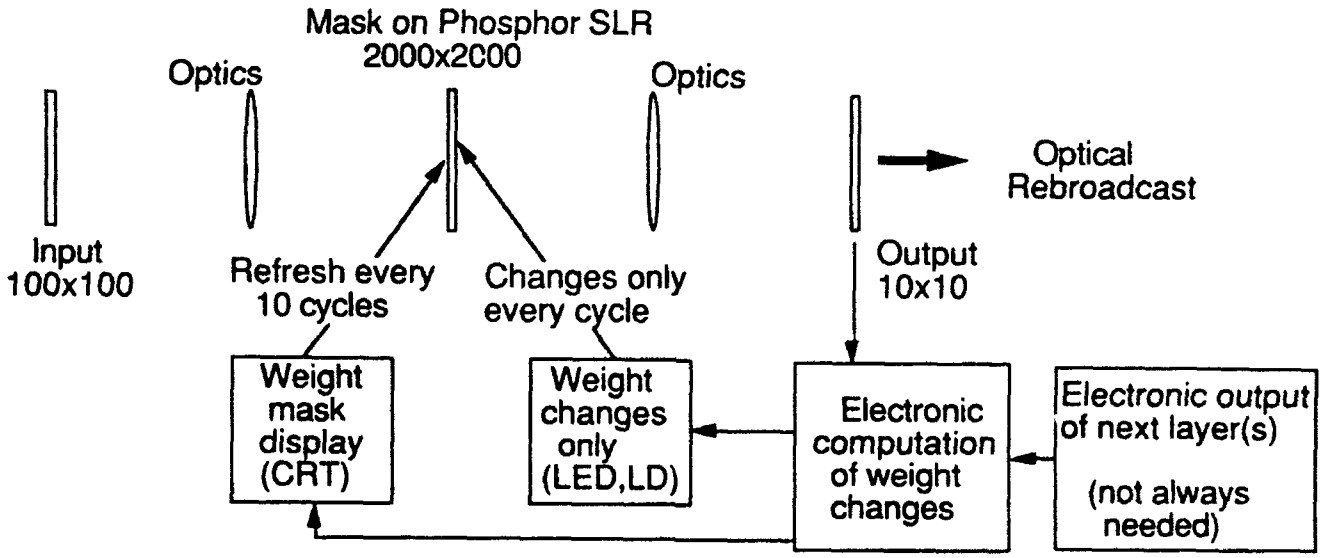

Figure 2.4.4-9. Adaptive Weight Architecture for Artificial Neural Network

compute changes to the weights (training the artificial neural network). Any changes to the weights are fed to scanned laser diodes or light emitting diodes which write or erase the weight mask stored on the phosphor spatial light rebroadcaster. For a multi-layer perceptron neural network, training would traditionally be done by the back-propagation algorithm and the computational load on the electronic processor would limit performance. Neither would an optical processor have sufficient flexibility to compute this algorithm. However, for a Kohonen self-organizing neural network, the weight modification algorithm is much simpler and only small regions of the weight mask need to be modified at each cycle. For this case, the load on the electronic processor would not be the limiting factor. Instead the overall computation rate would be determined by the space-bandwidth product of the CRT and the rate at which weight changes could be optically made. Therefore, if real-time artificial neural network training is required, then, for networks like the Kohonen, this architecture is a candidate.

2.4.5 Quadratic Processor

The optical architecture that we will discuss in this section will affect the operation of quadratic systems. Quadratic systems are extremely important in a number of applications [Rugh]. We will focus on automatic target detection operations which is the primary goal of these processors. The general input/output relationship is given as:

$$g(r) = \int f(r_1)\, f^*(r_2)\, q(r-r_1,\, r-r_2)\, dr_1\, dr_2$$

where $f(r)$ is the input and $q(r_1, r_2)$ is the kernel function. For sampled data, the quadratic processor can be rewritten in vector/matrix notation as:

$$g = f^T Q f$$

where f is the input signal vector, g is the output vector, and Q is the kernel matrix and T denotes vector transpose.

The quadratic operation is one of the most important operations in target detection. The target detection problem can be seen as a binary hypothesis test where the two hypotheses are:

H_1: clutter with distribution $p_1(f)=N(\mu_1 , \Sigma_1)$

H_2: target plus clutter with distribution $p_2(f)=N(\mu_2 , \Sigma_2)$

where N denotes multivariate Gaussian distribution, with μ_1 , and μ_2 are the mean vectors and Σ_1 , and Σ_2 as the covariance matrices of the two distributions.

The optimal test to differentiate between these two hypotheses is the likelihood ratio test (LRT) [VanTrees]. In this test, the ratios of the two probability distribution functions, $\Lambda(f) = p_1(f)/p_o(f)$ are calculated. This will produce an operation on the incoming data which is then compared to a threshold. We will assume the input signal vector f to be provided by an electro-optical sensor. In this instance, f can be composed of multispectral and/or spatial data. When f is spatial data from the local neighborhood of the pixel under test, the LRT effectively compares the local spatial texture for target detection. This has been shown to provide significant detection advantage of pure energy detection [STAR report]. For an input data vector f the LRT becomes:

$$f^T(\Sigma_o^{-1}-\Sigma_1^{-1})f - f^T(\Sigma_o^{-1}\mu_o-\Sigma_1^{-1}\mu_1) \gtrless \Gamma$$

The first term is the quadratic operation where the kernel is represented by $Q=(\Sigma_1^{-1} - \Sigma_2^{-1})$. These two covariance matrices can be computed off-line via training data of both the clutter and target. The second term is a simple linear processor with impulse response $h=\Sigma_o^{-1}\mu_o - \Sigma_1^{-1}\mu_2$. This term can be eliminated entirely when "demeaned" data are used. We will consider this case in our subsequent discussions.

An optical implementation of the quadratic operation is shown in Figure 2.4.5-1. This architecture has some significant advantages when compared to its electronic

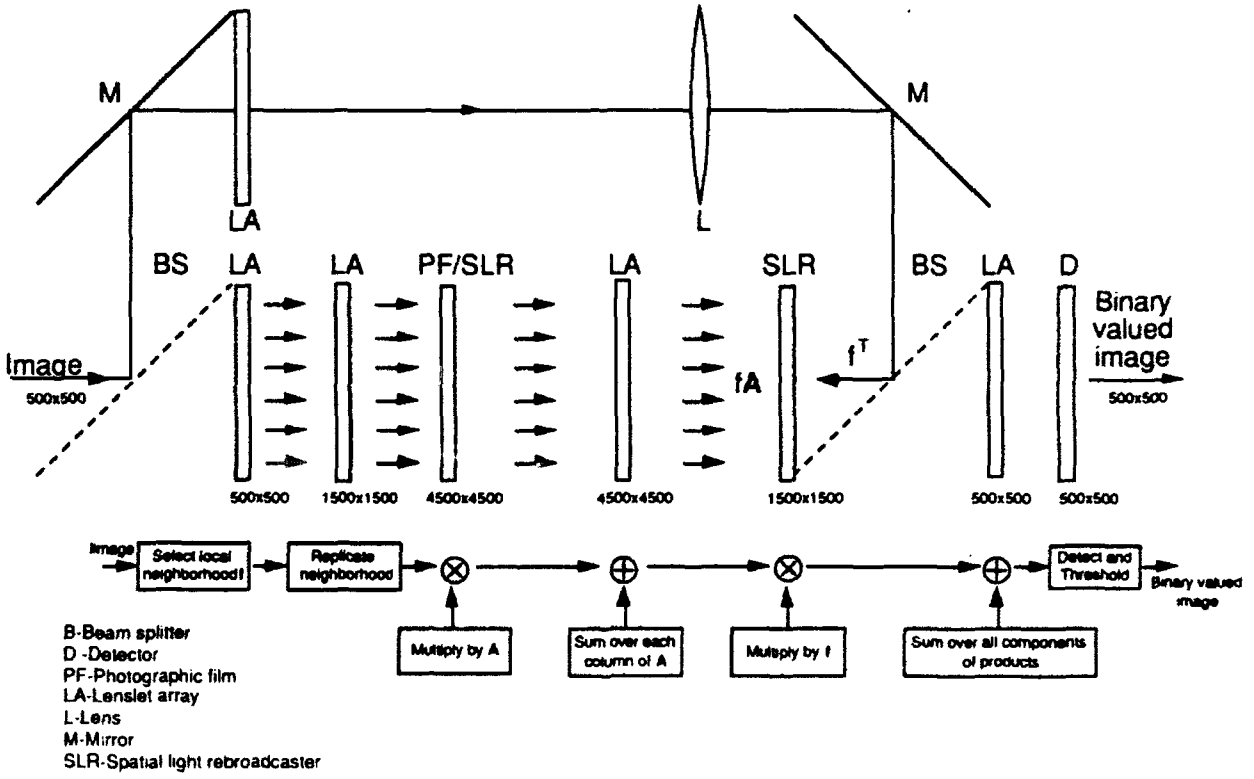

Figure 2.4.5-1. Optical Quadratic Processor

counterparts. The first and foremost is that this processor computes the LRT for each pixel in the scene simultaneously. In electronic implementations, a window is translated around the image and the LRT is computed serially. The SLR implementation allows the system to operate directly on the optical intensity at the focal plane of the sensor. No arbitrary optical/electronic-electronic/optical transduction (i.e., a detector array followed by a spatial light modulator) is required.

There are two specific technologies used in the quadratic processor architecture, the spatial light rebroacaster, and lenslet arrays. The spatial light rebroadcaster allows real time data insertion, filtering and thresholding whereas the lenslet arrays provide the means for local neighborhood isolation, pixel replication and local spatial integration. The first SLR in the architecture detects and rebroadcasts the sensor data into the optical processor. The first lenslet array selects (through reimaging) a local 3 x 3 neighborhood around each pixel in the image. This requires the same number of lenslets as the number of pixels in the input image. The second lenslet array replicates each neighborhood 3 x 3 times (also through reimaging). The replicated neighborhood are incident on the filtering SLR where the matrix Q is stored. The third lenslet array integrates each 3 x 3 segment and images the result onto the third SLR. This SLR also has the selected local neighborhood data as a readout beam incident on it via a network of two beam splitters, a lenslet array for neighborhood selection and a one-to-one imaging system. The SLR then produces the multiplication of the two data sets. A final lenslet array integrates the local 3 x 3 output of the SLR and images the result to a final active SLR which provides the thresholding operation. The output "image" of this system is a binary mapping whose pixels are either detection of target (on) or clutter (off). Refer to section 3.3 for specific operational details.

The initial assessment of benefit for the optical processor can be calculated via its throughput. We will make this calculation based on the number of operations that are applied to any specific input pixel. The key to this calculation is the realization that each

input pixel is replicated 81 times (local neighborhood selection and neighborhood replication). Note that each pixel is contained in the neighborhoods of all 9 of its neighbors. This is shown in Figure 2.4.5-2. The filtering SLR then performs 81 multiplies on a particular input pixel. The lenslet array following the filtering SLR produces 8 additions (replicated/filtered pixel being added to each element in its neighborhood) for each replicated neighborhood (9 times). This produces 72 additions on each input pixel. Multiplication by the neighborhood data at the third SLR provides another 9 multiplications per pixel. Finally, the last lenslet array sums over each local neighborhood (8 additions). The thresholding operation will be ignored in this calculation. This produces a total of 170 operations on each input pixel. This is summarized as:

Multiplication by mask:	81 multiplications
Lens summation (8 adds x 9 real.)	72 additions
Multiplication by neighborhood	09 multiplications
Final summation	08 additions
---	---
Total	170 ops/input pixel

We will assume an input image size of 500 x 500 pixels (2.5×10^5 pixels). For an SLR response time of 30 msec (30 frames/sec) the processor architecture effectively operates at a throughput rate of 1.4 Gops/sec. Conversely, for an SLR response time of 1 msec, the processor throughput rate is 42.5 Gops/sec. Clearly, this is significantly higher than any low power electronic system can achieve. Therefore, we advise that the quadratic architecture introduced in this section be further studied.

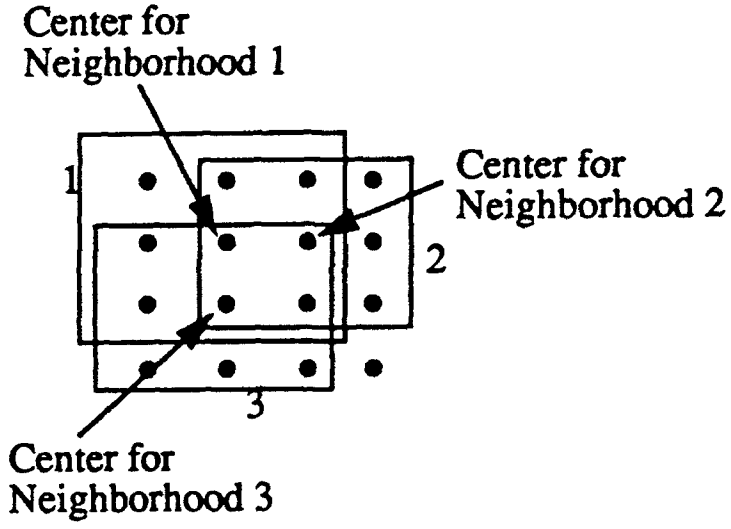

Figure 2.4.5-2. 3x3 Neighborhood Operation

2.4.6 Morphological Processor

Morphological image processing has been applied successfully in a variety of applications including automatic target recognition and classification [Sternberg, Maragos, Crimmins]. Morphological processing is based on a series of local operations and neighborhood transformations which are performed identically on all image pixels. This translation-invariant property makes morphological processing suitable for optical implementation and allows the parallelism to take full advantage of an optical processor.

In this section, morphological image processing is first reviewed and the implementations of its basic operations with an incoherent optical processor are described. Processing algorithms for ATC applications based on a series of these elementary operations and transformations are then discussed and the system architectures for a hybrid optical morphological image processor are examined.

2.4.6.1 Image Algebra

It is well known in image algebra that there are two fundamental local operations and one neighborhood transformation with which most other operations or transforms can be implemented. The two fundamental local operations are: [Serra, Huang]:

Complement of an image:

$$\bar{A} = \{(x,y) | (x,y) \in W \text{ and } (x,y) \notin A\} \tag{14}$$

where W is the image space containing all image pixels.

Union of two images A and R:

$$A \bigcup R = \{(x,y) \mid (x,y) \in A \text{ or } (x,y) \in R\} \tag{15}$$

The fundamental neighborhood transformation is

Dilation of image A by R:

$$A \oplus R = \begin{cases} \{(x_a+x_r, y_a+y_r) \in W \mid (x_a,y_a) \in A,\ (x_r,y_r) \in R\} & (A \neq \varnothing) \text{ and } (R \neq \varnothing) \\ \varnothing & \text{otherwise} \end{cases} \tag{16}$$

where $\varnothing$ denotes the null image set. In other words, dilation is the union of the translation of A by the elements in R. That is, if we let p be a pixel in W and denote the shifting of the origin of A to p by:

$$A(p) = \{a+p \mid a \in A\}$$

then dilation can also be expressed as:

$$A \oplus R = \bigcup_{r_i \in R} A(r_i) \tag{17}$$

where $A(r_1, r_2, \ldots r_N)$ are the translated images of A by the pixels in $R = \{r_1, r2, \ldots r_N\}$.

Based on these three fundamental operations and transformations, other operations and transformations can be implemented. For example:

Erosion:

$$A \ominus R = \overline{(\bar{A} \oplus \tilde{R})} \tag{18}$$

where $\tilde{R}$ denotes the symmetric set of R, that is, the rotation of R by 180°:

Difference:

$$A - R = \overline{(\bar{A} \cup R)} \tag{19}$$

Intersection:

$$A \cap R = \overline{(\bar{A} \cup \bar{R})} \tag{20}$$

Symmetric difference:

$$A \Delta R = \overline{(\bar{A} \oplus R)} \cup \overline{(A \cup \bar{R})} \tag{21}$$

Opening:

$$A_R = \overline{(\bar{A} \oplus R)} \oplus R = (A \ominus \tilde{R}) \oplus R \tag{22}$$

Closing:

$$A^R = \overline{\overline{(A \oplus R)} \oplus \tilde{R}} = (A \oplus \tilde{R}) \ominus R \tag{23}$$

The operations and transformations are illustrated in Figure 2.4.6-1 for the case $R = \tilde{R}$. Other more complex transformations include:

Hit or Miss transform:

$$A \otimes R = (A \ominus R_1) - (A \oplus R_2) = (X \ominus R_1) \cap (\bar{X} \ominus R_2) \tag{24}$$

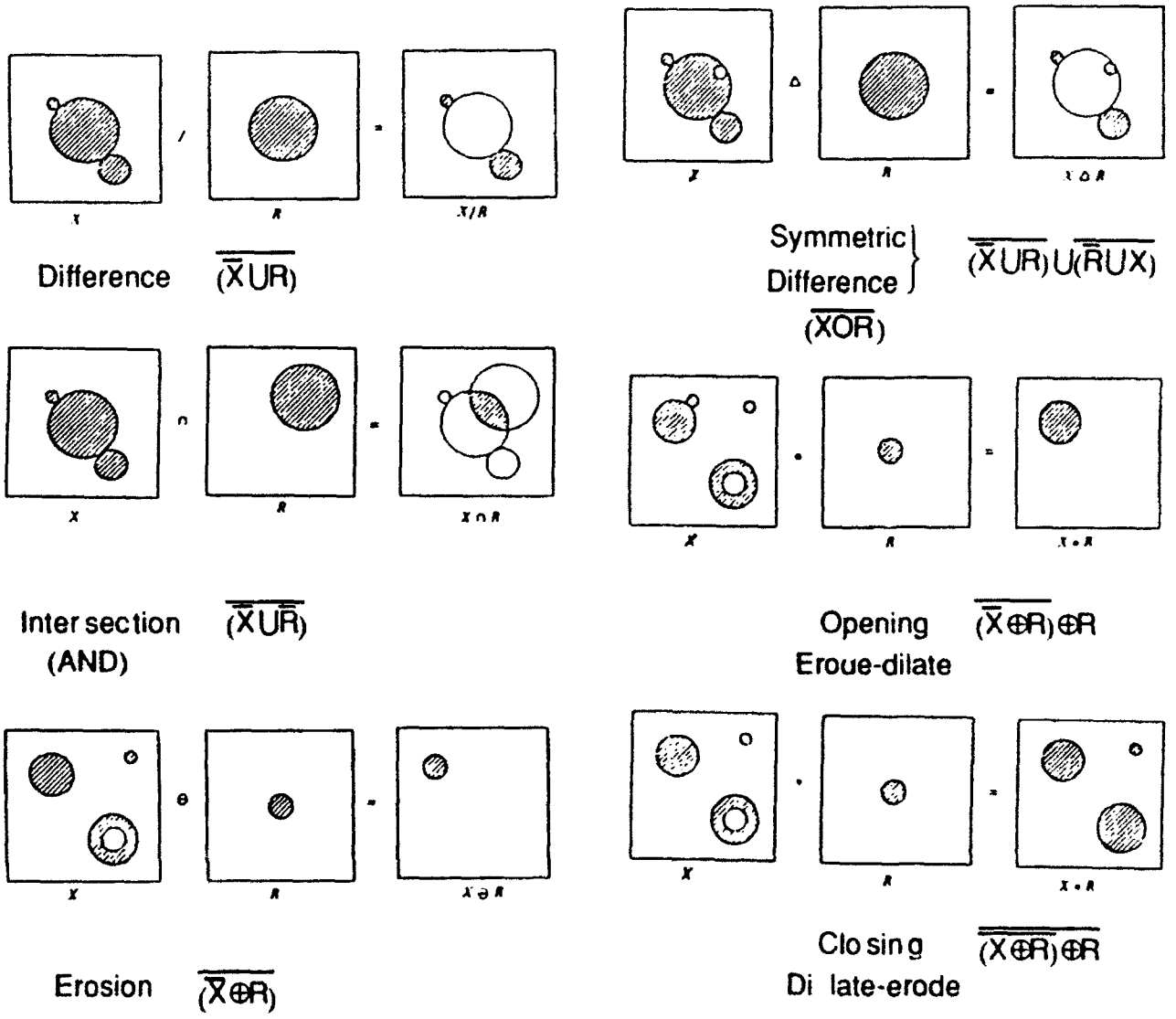

Figure 2.4.6-1. Morphological Operations and Transformations that can be Implemented with Complement, Union and Dilation.

Thinning:

$$A \circ R = A - (A \otimes R) \tag{25}$$

Thickening:

$$A \odot R = A \cup (A \otimes R) \tag{26}$$

and Skeletonization:

$$SK(A) = \bigcup_{r>0} \{(A \ominus rB)_p]\} \tag{27}$$

where rB is an open disk of radius r and p is a closed disk of the size of a single pixel, and $(\cdot)_p$ denotes the opening of $(\cdot)$ by p.

In image processing, A is generally the input image and R is referred to as the structure element which operates on A. R can be of any shape. Some commonly used shapes are circle (disk), square, line and rhombus.

2.4.6.2 Optical Implementation of Elementary Operations and Transformations

As described in Section 1.0, there are two elementary local operations and one neighborhood transformation with which other morphological operations and transformations can be implemented, namely, complement, union and dilation. In this section, the optical implementations of these elementary functions are described. The system architecture of an optical morphological processor is discussed later in Section 5.0.

Complement

Complement or negation requires a device with an input-output intensity transfer characteristic that has a negative slope. Many spatial light modulators can be made to

produce positive or negative outputs by varying the bias intensity or voltage levels. The SLR is assumed to also have the capability to be switched to produce a positive or negative output.

Union

Union is equivalent to a logical OR operation. It can be implemented with summation and thresholding operations. That is:

$$A \bigcup R = \{(x,y) | (x,y) \in [k_A(x,y) + k_R(x,y)] \geq 1\} \tag{28}$$

where A and R are binary images with values of 0 and 1, k_A and k_R are the indicator functions associated with compact sets A and R. The summation of intensity is a natural function of a square law detector such as a SLR. Two images incident on the SLR simultaneously will be summed. With the storage capability of the SLR, the summation can also be performed on images which impinge on the SLR sequentially. Thresholding can be implemented with an active SLR by the appropriate design of the electronics between the detectors and the emitters of the device.

Dilation

Dilation is the union of the translations of A by the elements in R. It can be expressed in the form of a convolution operation:

$$A \oplus R = \sigma[k_A(x,y) * k_R(x,y)] \tag{29}$$

where * denotes the convolution operation and σ indicates the support of convolution product. The convolution can be performed optically and the support can be obtained by simple thresholding.

With an incoherent imaging system, the output image intensity for an input, $k_A(x,y)$, is given by $k_A(x,y) * |h(x,y)|^2$ where $|h(x,y)|^2$ is the point spread function of the imaging system. It is related to the pupil function, $P(u,v)$, via $h(x,y) = \mathcal{F}[P(u,v)]$

where $\mathcal{F}[\ ]$ denotes Fourier transformation. Dilation can, therefore, be performed by choosing a pupil function P(u,v) whose point spread function matches the desired structure element $\boldsymbol{R}$. When the structure element is large, the pupil function becomes small, severely affecting the optical efficiency of the optical processor. A simple means to improve the optical throughput through the lens aperture is to replicate the pupil function as illustrated in Figure 2.4.6-2. The spatial separation of the pupil functions has to be large enough such that the resulting spurious fringe pattern cannot be resolved by the out detector array or SLR.

The point spread function is always real and positive. Performing the convolution with an incoherent imaging system will restrict the type of structure elements that can be realized directly. With dilation, the structure element is defined only by points which belongs to $\boldsymbol{R}$. (In hit or miss transform which will be described in the following section, the structure element is also defined by points that belong to the background or $\bar{R}$.) $k_{\boldsymbol{R}}$ is, therefore, real and positive and the convolution can be realized with an incoherent imaging system.

To summarize, $\boldsymbol{A} \oplus \boldsymbol{R}$ can be implemented by thresholding the output image obtained with an incoherent imaging system having a pupil function, P(u,v), where:

$$k_{\boldsymbol{R}}(x,y) = \left| \mathcal{F}^{-1} \left[\mathrm{P}(u,v) \right] \right|^2 . \tag{30}$$

A detailed description of the pupil function design for morphological processing will be presented later in Section 3.4.

Hit or Miss Transformation, Thinning and Thickening

In Hit or Miss transform, $\boldsymbol{A} \oplus \boldsymbol{R}$, the structure element is composed of two components $\boldsymbol{R}_1$ and $\boldsymbol{R}_2$ where $\boldsymbol{R}_1$ is defined by points that belong to **A** (shape of foreground) and $\mathbf{R}_2$ is defined by points that belong to $\bar{A}$ (shape of background). The

Pupil function that produces disk-like structure element

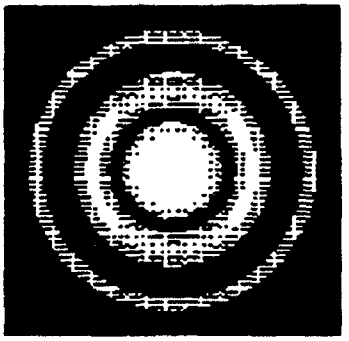

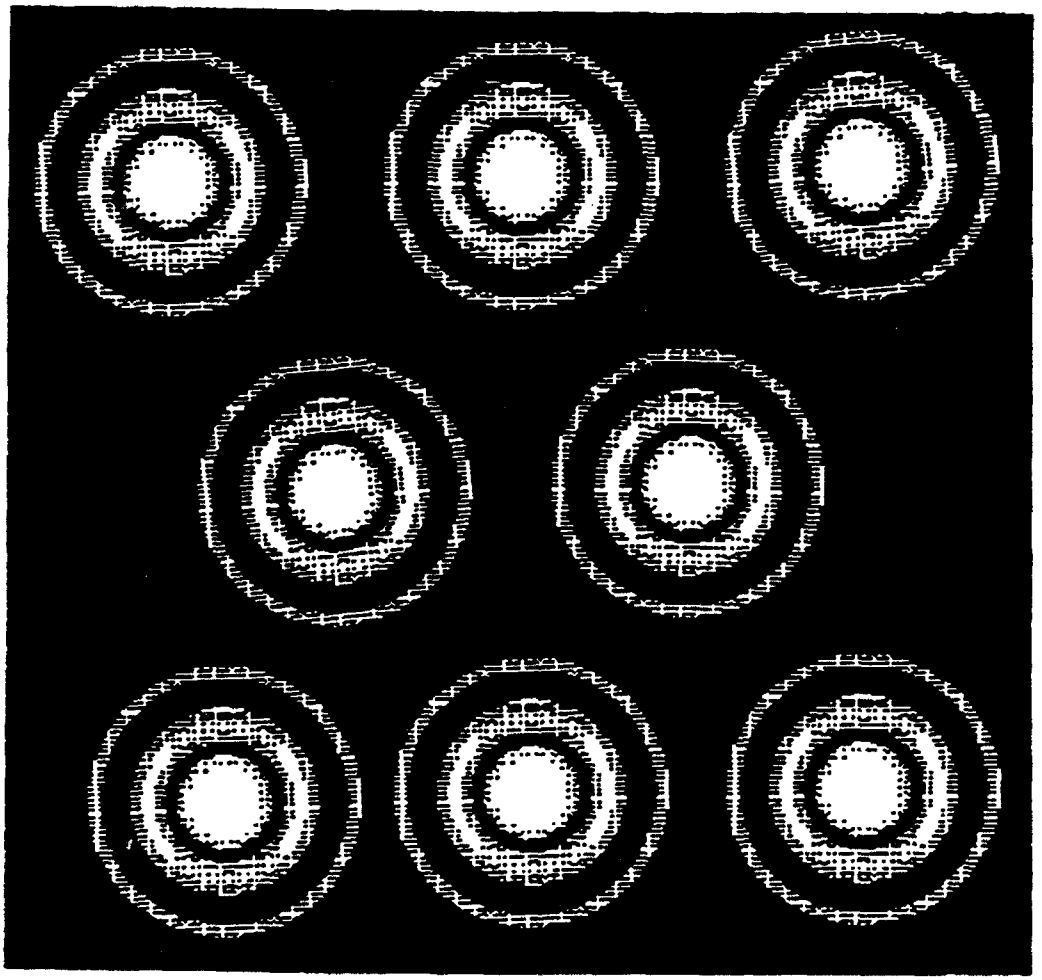

Figure 2.4.6-2. Replication of Pupil Function to Increase Optical Throughput

condition of the transform is that A matches R_1 and $\bar{A}$ matches R_2. A simple example is shown in Figure 2.4.6-3. which performs an asymmetric form of edge filtering where only the left vertical edge is enhanced.

Closely related to hit or miss transform are thinning and thickening. Thinning is obtained by subtracting $X \otimes R$ from A. Thickening is obtained by taking union of A with $A \otimes R$.

With the structure element composing of two components, the hit of miss transform (Eq. 24) can be implemented optically using two pupil masks to produce R_1 and R_2. The two parts of the hit or miss transform, $(X \ominus R_1)$ and $(\bar{X} \ominus R_2)$, can be performed with parallel imaging optics and then summed and thresholded to obtain the intersection. Alternatively, the operations can be implemented sequentially using the storage capability of the SLR.

Some commonly used structure elements are given in Figure 2.4.6-4. Notice that the centers of R_1 and R_2 are often off-set from each other. With an incoherent optical system, however, the point spread function convolving with the input image is always centered at the optical axis. A means must, therefore, be available to shift one of the two output images before they are summed and thresholded. The amount of shift required is quite small. The shift may be obtained by adding a grating structure to the pupil function if the programmable pupil mask (SLM) provides enough space-bandwidth product. Alternatively, it can be achieved with electro-mechanical means by tilting a mirror or a beamsplitter with a piezoelectric driver. The shift can also be performed electro-optically by adding a wedge of electro-optics material at the pupil plane. The application of voltage changes the amount of linear phase retardation and shifts the output image. It may also be possible to shift the image stored in an active SLR electronically by using a charge couple device structure to fabricate the SLR.

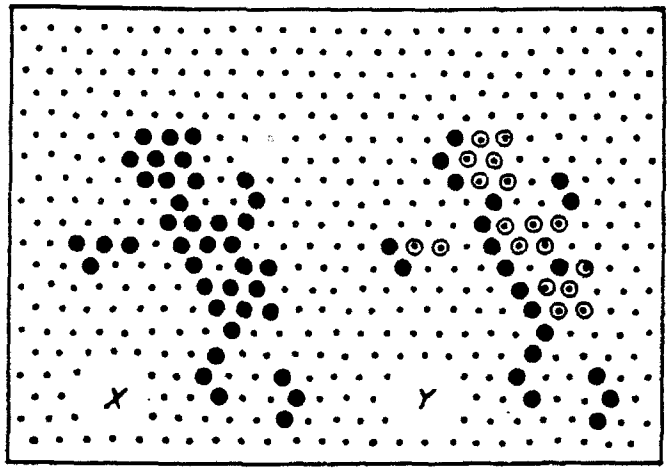

Structuring elements
For X : $B = \{\bullet\}$
For Y : $B' = b_1\ b_2 = \{\odot\ \bullet\}$ ↓

● points of the structuring element which must belong to X
⊙ points of the structuring element which must belong to $\overline{X}$

↓ location of the origin associated with the structuring element.

Figure 2.4.6-3. Example of Hit or Miss Transformation for Spatial Filtering

Symbol	*Structuring element*	*Thinning*	*Thickening*	*Hit or Miss*
L		homotopic skeleton	Conditional Segmentation	
M		homot. skeleton (rarely used)		
D		homotopic marking	Pseudo-convex hull (D^*)	
C			Hexagonal Convex hull	
E		Skeleton clipping (cond.) skiz		End points
I			Homotopic clipping	Isolated points
F				Triple points
F'				Triple points
R		Erosion (R^*)	Dilation Cond: ultimate erosion partly recons.	
H		Boundary		Erosion-dilation (H^*) Cond: part. recons. ultimate erosion
K		Sizing by circumscribed hexagons	Ferret's diameter	

● points of the structuring element which must belong to X
○ points of the structuring element which must belong to $\overline{X}$

Figure 2.4.6-4. Some Commonly Used Structure Elements

2.4.6.3 Extension to Gray Scale Images

So far, we have limited ourselves to binary input images. In this section, approaches to allow the optical morphological processor to handle gray scale images are described.

Gray scale morphological operations are very computation intensive. A gray scale opening for example, requires much more computation than a thresholding operation followed by a binary opening. For high speed processing, gray scale 2-dimensional images are typically decomposed into 2-dimensional binary images which are then processed efficiently by binary morphological operations and transformation.

Two approaches to decompose a gray scale image into binary images will be described. The most powerful approach utilizes a concept called umbra with which gray scale images can be processed in 3-space.

2.4.6.3.1 Umbra

A gray scale image can be considered to be a binary three- dimensional (i,x,y) image and morphological operations and transformations can be performed by breaking the gray scale image into a series of binary two-dimensional images. Let A^2 be a set of points in 2-space and G is a function which assigns a gray scale value $I_{x,y}$ to each point (x,y) in A^2. $G(A^2)$ is then a gray scale image having a binary representation in 3-space. p^3 is an element in A^3 if p^2 is an element in A^2 and has gray value $I_{x,y}$. A^3 essentially defines a surface in 3-space corresponding to the gray scale function. A^3 can be converted into a binary 3-dimensional image called Umbra. The umbra of A^3 is the space below the surface, it can be expressed as [Sternberg]:

$$U(A^2) = U^3 = \{(i,x,y) \mid (i,x,y) < (i,x,y) \in A^3\} \quad (31)$$

The gray scale image, its surface and umbra are illustrated in Figure 2.4.6-5 for a one-dimensional image.

For a two-dimensional gray scale image, its three-dimensional umbra can be further decomposed into slices of two-dimensional binary images:

$$A^3 = \bigcup_{n=1,N} A^2_{y_n} \quad (32)$$

Three-dimensional morphological operations can be performed by operating on two-dimensional slices and recomposing the image. For example, to perform a dilation $U^3 \oplus R^3$, the three dimensional umbra is first decomposed into slices in the y direction. Operating on the 2-D slices, an intermediate result:

$$B^3 = \bigcup_{n=1,N} A^2_{y_n} \oplus R^2_{y_n} \quad (33)$$

is obtained. Then, turning to the orthogonal direction, we have:

$$U^3 \oplus R^3 = \bigcup_{m=1,M} B^2_{x_m} \oplus R^2_x \quad (34)$$

where R^2_y and R^2_x denote the two-dimensional slicers of the three- dimensional structure: element R^3 projected onto the i-x and i-y planes respectively.

2.4.6.3.2 Threshold Decomposition

The processing approach described above is quite complex, requiring electronic buffer memory to hold the intermediate step B^3. Threshold decomposition offers a

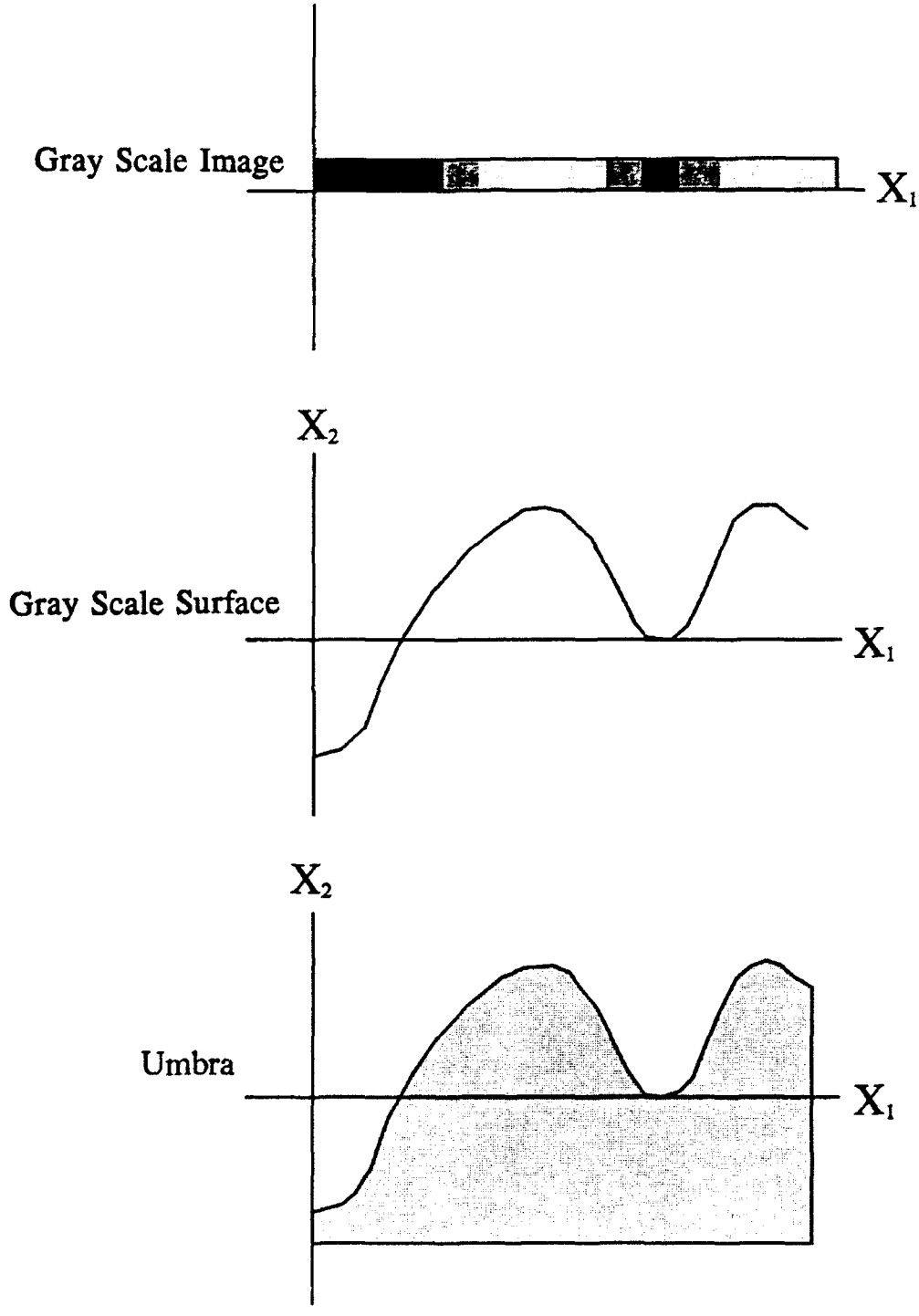

Figure 2.4.6-5. Umbra Representation of a One-dimensional Gray Scale Image

simpler approach to gray scale morphology [Shih]. It can be shown that gray scale morphological operation is the summation of a series of unioned binary operations. If the structure element is binary, the processing is reduced to the summation of a series of binary morphological operations on the gray scaled image which has been decomposed into a set of binary images according to intensity levels. The processing for the decomposed images can be performed by the optical processor in parallel. Such a plane-parallel architecture allows the processor to maintain real-time processing performance with gray scale input images. Alternatively, the decomposed images can be processed in serially, using a detector or an SLR to sum the output in order to minimize hardware complexity.

To make the results of threshold decomposition consistent, the shading or slowly varying bias of the gray scale image should first be removed. This can be achieved with the same optical processor by using the storage and gray scale properties or the SLR. Let G(x,y) be the two-dimensional gray scale input image. The slowly varying bias can be estimated by:

$$S(x,y) = G(x,y) * |h(x,y)|^2 \tag{35}$$

where $|h(x,y)|^2$ the point spread function of an incoherent imaging system which performs a low pass filtering operation. The modified gray scale image is given by $M(s,y) = G(x,y) - S(x,y)$ which can be sliced at different intensity levels into a set of two dimensional binary images.

2.4.7 Multispectral Optical Preprocessor

Many targets have spectral reflectance characteristics that are different from those of the clutter background that can be used to aid target detection. Even with camouflage paints and markings designed to make the target blends in with the background, there are measurable differences in their finer spectral structures. For example, background clutter

has chlorophyll and water absorption lines that are hard to emulate accurately with man-made materials. Similarly, synthetic material and paints may reflect particularly strongly or weakly at certain wavelengths. The target-to-clutter ratio can be enhanced by comparing the relative spectral reflectance at two different wavelengths. As an example, Figure 2.4.7-1 shows the spectral reflectance of a fictitious target and the background clutter over certain spectral region. The spectral reflectance of the target is measurably different between wavelengths λ_1 and λ_2 but for the clutter, they are about the same. If the image intensity acquired at wavelength λ_2 is subtracted from image taken at wavelength λ_1 , an enhanced image of the target is obtained. That is:

$$\begin{aligned} I_o(x,y) &= I_T(x,y;\,\lambda_1) + I_C(x,y;\,\lambda_1) - I_T(x,y;\,\lambda_2) - I_C(x,y;\,\lambda_2) \\ &\simeq I_T(x,y;\,\lambda_1) - I_T(x,y;\,\lambda_2). \end{aligned} \tag{36}$$

where $I_o(x,y)$ is the intensity distribution of the resulting image, $I_T(x,y;\,\lambda)$ is the intensity of the target at λ and $I_C(x,y)$ is the intensity of the clutter. With the specific spectral reflectance and the choice of the two wavelengths, the background clutter is largely removed.

2.4.7.1 Optical Processing Architectures for Multispectral Preprocessor

The ability of an SLR to perform subtraction can be used as multispectral preprocessor. A possible optical processing architecture is illustrated in Figure 2.4.7-2. As explained in Section 1.3, a passive SLR is written and read out at the two different wavelengths. As a multispectral preprocessor, an SLR with write-in wavelength of λ_1 and readout wavelength of λ_2 is used as the input device for the imaging sensor with a two-band spectral filter centering at λ_1 and λ_2 . For day-night operation, the object scene can also be actively illuminated with two lasers emitting at λ_1 and λ_2 . The relative brightness of the clutter image at λ_1 and λ_2 is adjusted such that the rate of build up of trapped electrons by wavelength λ_1 is about the same as the rate depletion by wavelength λ_2 . Under such a condition, the number of trapped electrons due to the

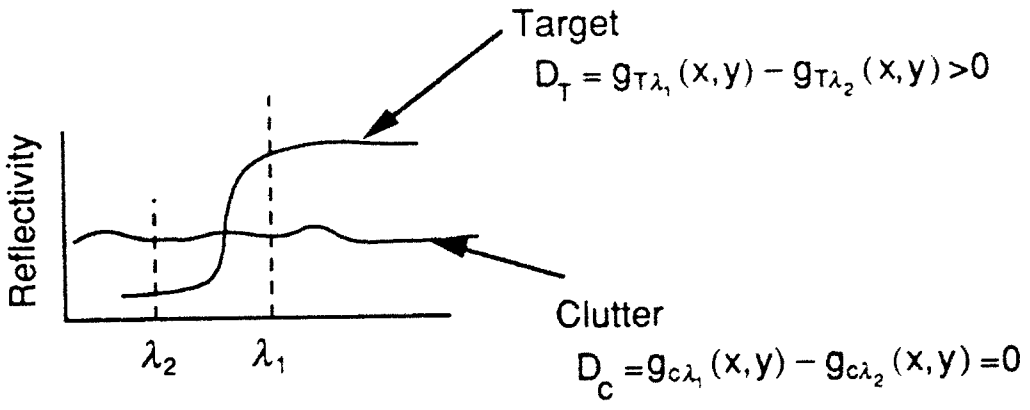

Figure 2.4.7-1. Multispectral Target-to-Clutter Ratio Enhancement

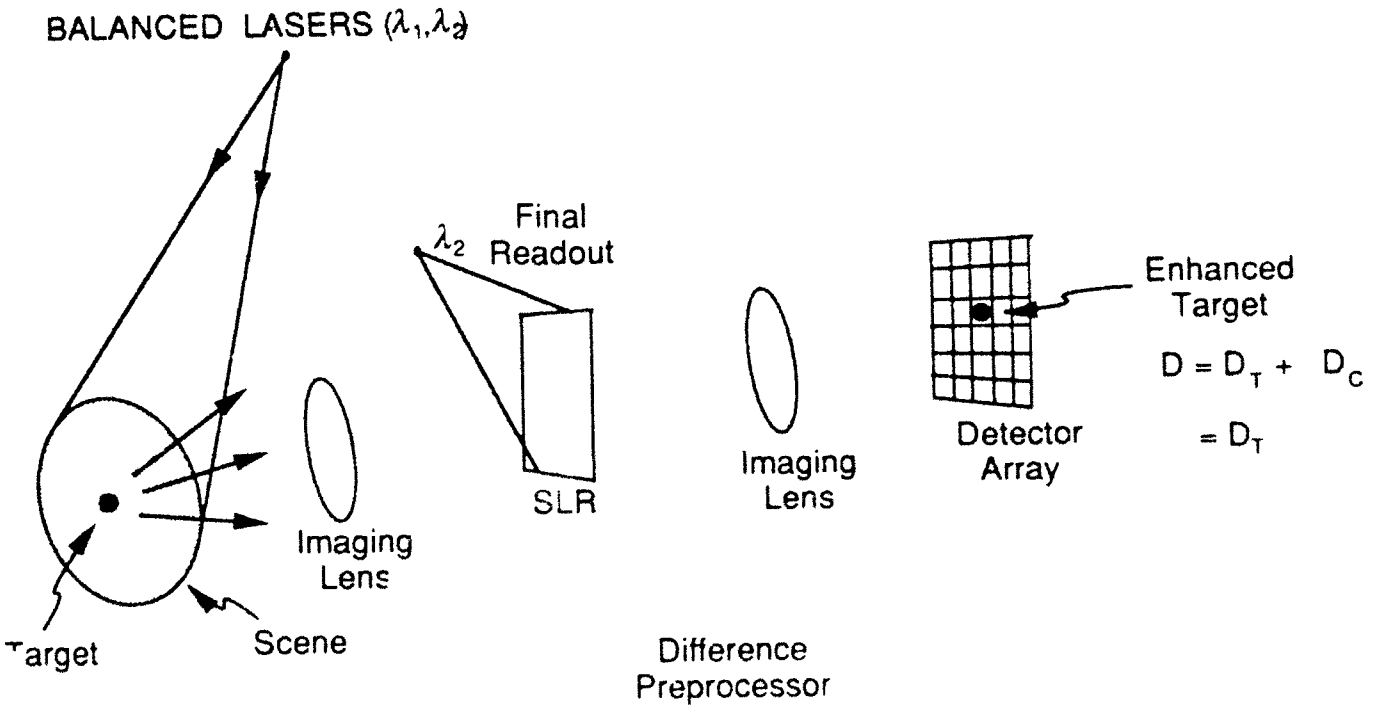

Figure 2.4.7-2 Multispectral Optical Processor

target image will increase with time since the target is brighter at λ_1 . A clutter suppressed image of the target can be obtained by simply reading the image in the SLR out with a uniform readout beam at wavelength λ_2.

If the target image is brighter at the readout wavelength, instead, the SLR can first be flooded with light at wavelength λ_1 to saturate the SLR. The number of trapped electrons due to the image will reduce with time and the result is an enhanced and contrast reversed image of the target.

2.5 Down Selection

A pre-selection was performed that resulted in seven candidates for evaluation. Of the seven, five were down selected for further analyses. They are the artificial neural network, the quadratic processor, the morphological processor, the interferometric processor and the OTF synthesis optical preprocessor. Reasons for their selection are given below.

Unlike, for example, a Fourier transform-based processor, an artificial neural network (ANN) operates from a low level which makes it the most versatile of the architectures studied. It can be used to implement nearly all the functional elements in ATC. The basic operation required is sum of products and thresholding which can be performed very efficiently with an optical processor. In addition, the massive fan-outs in an ANN architecture can be accomplished more easily with optical interconnects than with electrical wires.

A quadratic processor performs pixel-by-pixel statistical target detection on the target scene. It utilizes local spatial variations (reflectance or emittance) as a discriminant between targets and clutter. The processing architecture can utilize the incoherent sensor image directly as the input. It allows the quadratic processor to bypass

the limitations of optical to electrical and electrical to optical converters, making it particularly useful as a preprocessor. In addition, the nonlinear operations performed by a quadratic processor provide processing capabilities not available with conventional linear optical systems.

The morphological processor is also a neighborhood processor capable of nonlinear processing functions. Instead of matching to the overall shape of a target, a morphological processor performs ATC by extracting features that define a target. Such a process tends to be more robust than matched filtering or template matching whose performance can be adversely affected by changes in aspect, lighting and operating condition. Morphological processing is typically implemented electronically using a recirculating pipeline architecture to minimize the size of the processor. With the inherent parallelism of an optical processor, the neighborhood operation can be performed simultaneously for all pixels in the image.

The last two are diffraction based incoherent optical processors whose architectures are well known. Diffraction based systems provide the largest space-bandwidth product, making them attractive for wide area search applications. The difficulty has been with the bias which could easily overwhelm the signal at the output. With both architectures, the role of the SLR is bias reduction. Since the principles of these two types of incoherent optical processors are well established, the discussion in Section 3 will concentrate on the use of a passive SLR for bias reduction.

The scanning correlator was not chosen because of the its limited capability (the reference function must be real and positive) and relatively slow speed due the serial nature of the scanning operation. The multispectral optical preprocessor did not survive the down selection because the laser power required for flood illumination may be too high to be practical in view of the sensitivity of available passive SLRs. For example, to illuminate and image a 120 m x 120 m area which has an average reflectance of 0.2

from a distance of 1 km using a laser source with P watts of power and an f/2 lens with a 4 cm aperture, the image intensity on the SLR will be about 3.2×10^{-10}P watts/cm^2. The Quantex SLR requires about 10 mJ/cm^2 of exposure energy to reach saturation. With an exposure time of 0.1 second, P = 3.1×10^8 watts. The laser has to emit over 300 Mwatts of power. Moreover, discrimination between different sets of target and clutter may involve different combinations of wavelengths. To reprogram the preprocessor will require a change in the SLR material to one with different input and readout wavelengths.

3.0 TASK 2: IN-DEPTH ANALYSES

The candidate optical processing architectures were down selected in Task 2 to five: 1) Artificial Neural Network, 2) Quadratic Processor, 3) Morphological Processor, 4) OTF Synthesis Preprocessor and 5) Interferometric processor. In this section, the design of the selected architectures are analyzed in greater depth to evaluate their potential performance and viabilities.

3.1 Evaluation Criteria

The SLR-based incoherent optical processors have to compete with well entrenched electronic processors and with coherent optical processors as well as with each other. The primary performance figure for processor comparison is computation speed or system throughput in terms of the number of operations per second. However, for Air Force ATR missions, the sensors and processors have to be carried on aircraft, unmanned aerial vehicles and missiles. The processor size and weight become important issues. Electronic processors can achieve processing speed as fast or faster than any optical processor by implementing massive amount of parallelism. Such a feat is accomplished at the expense of processor size. A better performance figure for comparison is throughput per unit volume (e.g., operations per second per cm^3). Power consumption is also important issue, particularly for satellite borne processors. Rough estimates of the power requirements of the optical processors are also provided. Beside the ultimate potential performance, the near term availability of optical components for the optical processing architectures were also investigated to determine the viability of the optical processing architectures.

3.2 Artificial Neural Network

In Section 2.4.3, five architectures for artificial neural networks were discussed. The cylindrical optics architecture with a fixed weight mask was chosen for in-depth analysis. An architecture allowing real-time optical modification of the weights was also identified as a candidate for further analysis. The in-depth analysis began with a study of computing accuracy requirements and led to a decision that optical processing is neither suited for nor needed for weight computation. The cylindrical optics architecture was then analyzed in-depth. It was found that the cylindrical optics architecture requires some significant modifications. A new opto-electronic architecture based on integrated optics was then developed, analyzed, and shown to be superior in terms of size required while not sacrificing performance in any other area.

3.2.1 Accuracy and Real-Time Computation Requirements

Optical processing generally has less accuracy than electronic digital processing but greater speed. In other ERIM work, a study was done to determine the accuracy required for artificial neural network computations. That study is briefly summarized here [Cederquist et al]. The problem chosen was that of determining terrain type (forest, grass, soil) from airborne sensor imagery of the ground in five wavelength bands in the visible, near infrared, and short wave infrared. A Kohonen self-organizing network was successfully developed for this purpose. The network has five inputs, three nodes, and three outputs corresponding to the terrain classification. The network was trained with floating point computation. The network was then used to classify the input data with varying accuracy in the input data and weights. The results are shown as confusion matrices in Fig. 3.2-1. The result is that floating point performance is maintained down to 5-bit accuracy in the data and weights. Although this is only a single test, it was assumed that 6-bit accuracy is sufficient for artificial neural network computations during use, but not during training.

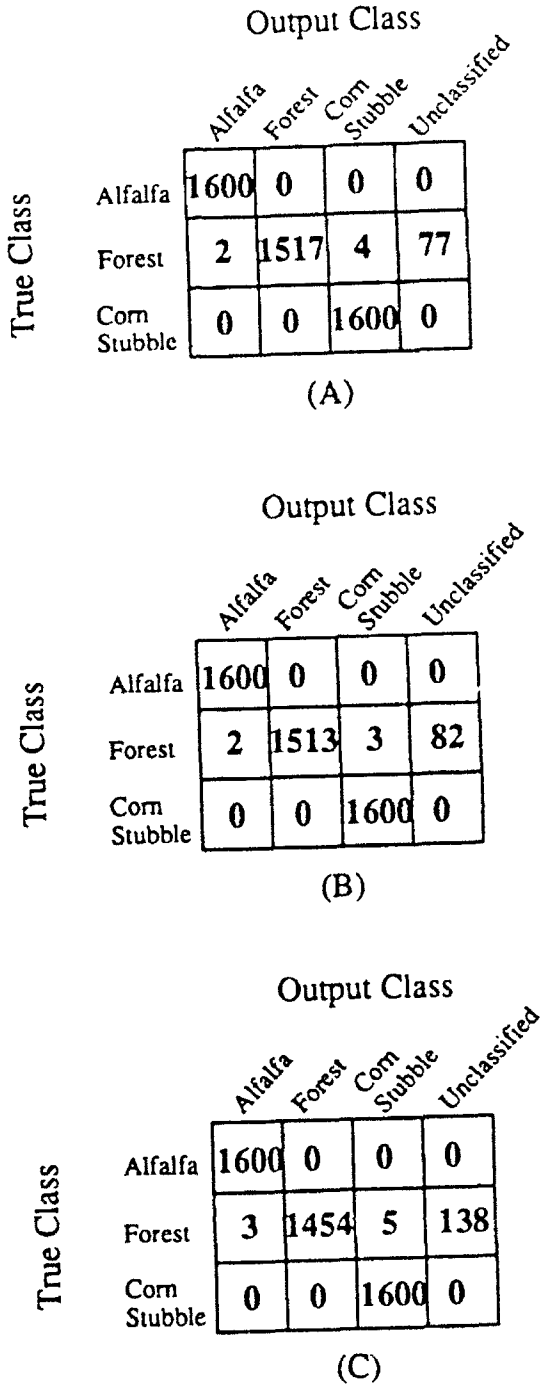

Figure 3.2-1. Confusion Matrix for Test Data with Finite Weight and Input Precision (a) Floating-point Weight and Input Precision; (b) 6-bit Weight and Input Quantization; (c) 5-bit Weight and Input Quantization

Optical computation of weight values was then considered. From ERIM experience with perceptron and Kohonen artificial neural networks for automatic target classification applications such as edge enhancement (ship wakes in SAR imagery), segmentation (terrain classification from optical multispectral imagery), and object detection (mine location in laser imagery), it is known that, during training, the changes in the weights at each cycle require much more than 6-bit accuracy. Optical processing in general and the architecture discussed in Section 2.4.5 in particular have never been shown to be capable of this greater accuracy. As an example, the few optical processors which were carefully tested for accuracy generally achieved about 5% [Cederquist and Lee].

The need for real-time computation of weights was also critically analyzed. For the automatic target classification application, which is one application of interest to the Air Force, it is very difficult to argue that weights would be computed in real-time, i.e., during an Air Force mission. Air Force doctrine requires pre-mission planning and high confidence in the success of the mission. The automatic target classification algorithms used would need to be known and tested for performance before the mission. If artificial neural networks were to be trained during the mission, there is no current knowledge that guarantees that training would be successful and no current method of measuring performance other than comparison with targets and backgrounds identified by the air crew during the mission. In short, artificial neural network training algorithms are not yet sufficiently developed to be used during a mission, so there is not a compelling reason for pursuing optical computation of artificial neural network training algorithms.

3.2.2 Cylindrical Optics Architecture Analysis

Two versions of the cylindrical optics architecture were designed using the GENII lens design software and analyzed. The first is shown in Fig. 3.2-2. A laser diode array was chosen for the linear input device. In a cascaded version, this would be the output

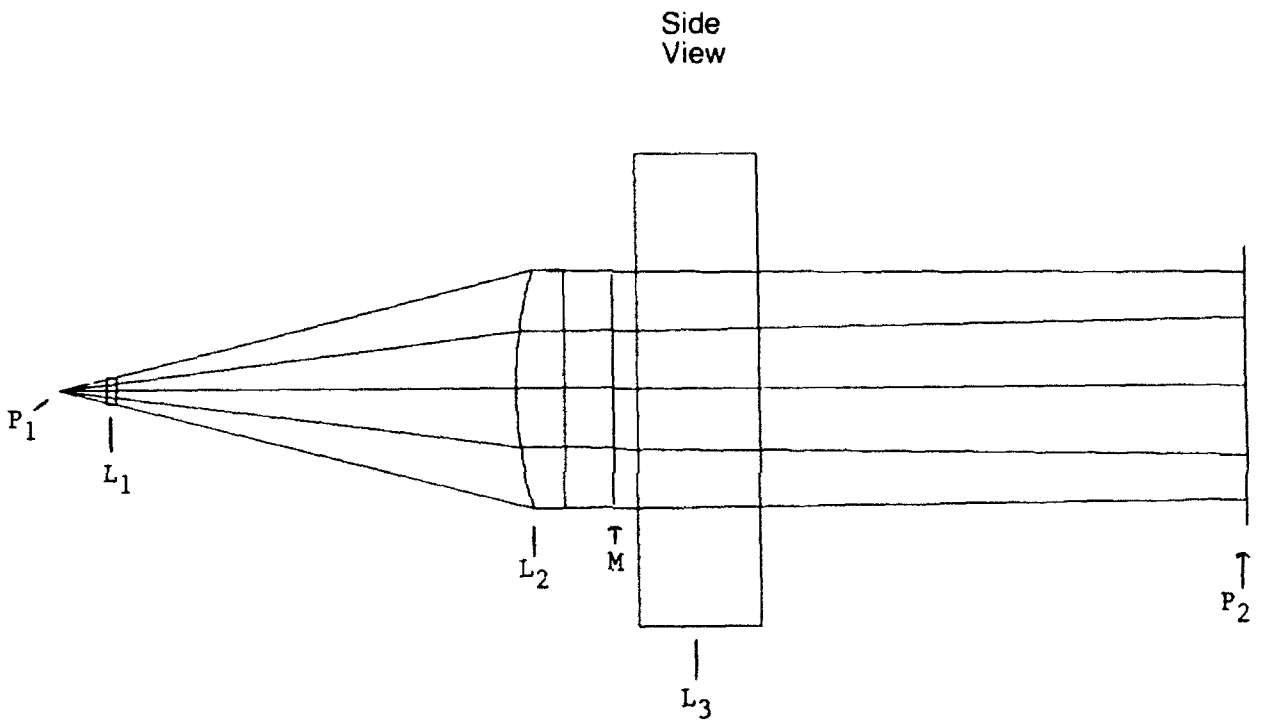

Figure 3.2-2. Ray Trace through Cylindrical Optics in Neural Network (Side View)

of the spatial light rebroadcaster. An array of cylindrical (plano-elliptical cross-section) lenses is used to collimate the asymmetrical beams from the lasers in one-dimension. The first cylinder lens is elliptical-plano in cross-section and provides collimated beams at the weight mask. The second cylinder lens is plano-hyperbolic in cross-section and focuses the beams onto a linear photo-diode array (input side of spatial light rebroadcaster). Additional raytraces are shown in Fig. 3.2-3. The mask layout is shown in Fig. 3.2-4 for cases where the number of nodes per network is small and multiple networks can, therefore, be computed simultaneously. Positive and negative weight channels are needed because of intensity detection. The point design of this architecture was completed by specifying the following:

Input: 100 laser diodes at 1 mm spacing and 1 MHz operation rate, Mask: 100 by 200 1mm by 250 micron pixels

Output: 200 photodiodes at 250 micron spacing and 1 MHz operation rate.

This leads to the following characteristics:

Volume: L by W by H = 20 cm by 10 cm by 5 cm = 1000 cm^3

Input data rate: 100 x 1 MHz = 10^8 data values/sec

Computation rate: 100 x 200 x 1 MHz = 2 x 10^{10} operations/sec

Computations/cm^3: 2 x 10^7

Power (for 1% accuracy): 100 x 40 mW = 4 W

The main disadvantage of this first architecture is the large volume resulting in a relatively low number of computations per unit volume. This large required volume is not generally recognized in the optical processing literature because other researchers have not attempted to design an actual optical system use optical raytracing design software. The literature generally shows only very simplified, schematic drawings of cylindrical optics architectures usually for matrix-vector multipliers.

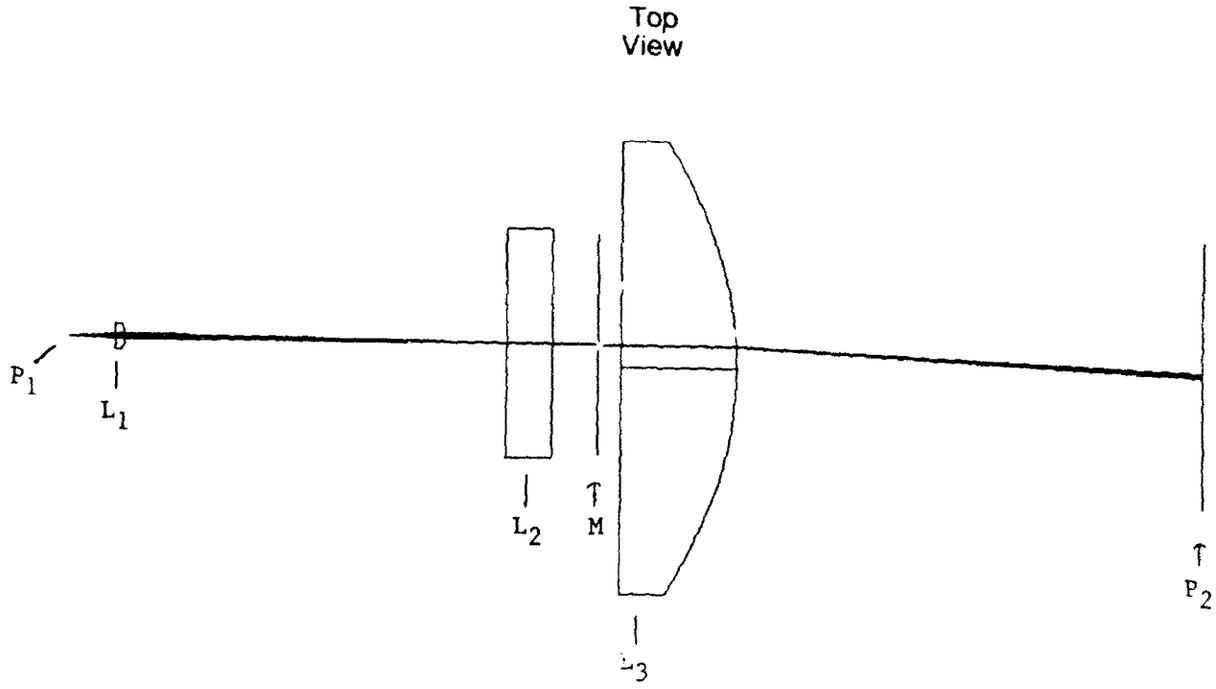

Figure 3.2-3. Ray Trace through Cylindrical Optics in Neural Network (Top View)

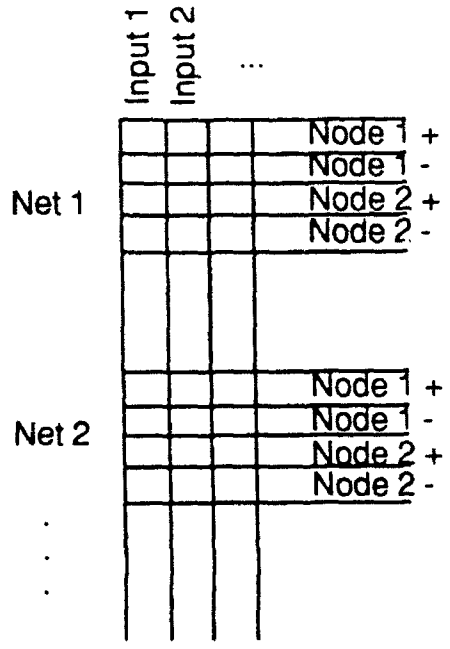

$$out_j = \sum_k in_k w_{kj}^{+} + \sum_k in_k w_{kj}^{-}$$

- 100 inputs
- 10 to 50 networks, 4 to 10 nodes each
- 100 to 200 outputs

Figure 3.2-4. Mask Layout for an Optical Artificial Neural Network

In an effort to reduce the processor volume, a second cylindrical optics architecture was developed and analyzed. The architecture is shown in Figure 3.2-5. Again, a laser diode array was chosen for the linear input device. A pair of cylinder lenses with an aperture stop is used to transfer the input to the weight mask by imaging it in one-dimension and collimating it in the other. Again, the GENII optical design software was used in our analysis. The mask layout is identical to that for the first architecture, shown in Figure 3.2-4. The main difference of this architecture from the first is that a linear array of long, narrow photodiodes is used to electrically collect the light passing through the mask rather than using optics to focus the light onto a linear array of point detectors. Using this mode of operation means that the light at the mask does not need to be collimated and thereby reduces the constraints on the cylindrical lens design. This in turn allows a more compact design. A 1 MHz readout rate is assumed for both architectures so the computation rate is not decreased. The point design of this architecture was completed by specifying the following:

Input: 100 laser diodes at 100 micron spacing and 1 MHz operation rate
Mask: 100 by 200 100 micron by 50 micron pixels
Output: 200 linear photodiodes at 50 micron spacing and 1 MHz operation rate

This leads to the following characteristics:

Volume: L by W by H = 6 cm by 1 cm by 1 cm = 6 cm^3-
Input data rate: 100 x 1 MHz = 10^8 data values/sec
Computation rate: 100 x 200 x 1 MHz = 2 x 10^{10} operations/sec
Computations/cm^3: 3 x 10^9
Power (for 1% accuracy): 100 x 40 mW = 4 W

This second architecture is superior to the first in computation/cm^3 as desired.

It was found in both these designs that the mask two-dimensional space-bandwidth product was proportional to the square root (W x H). The two designs have, of course, different proportionality constants. This result is not surprising. It is well known in the

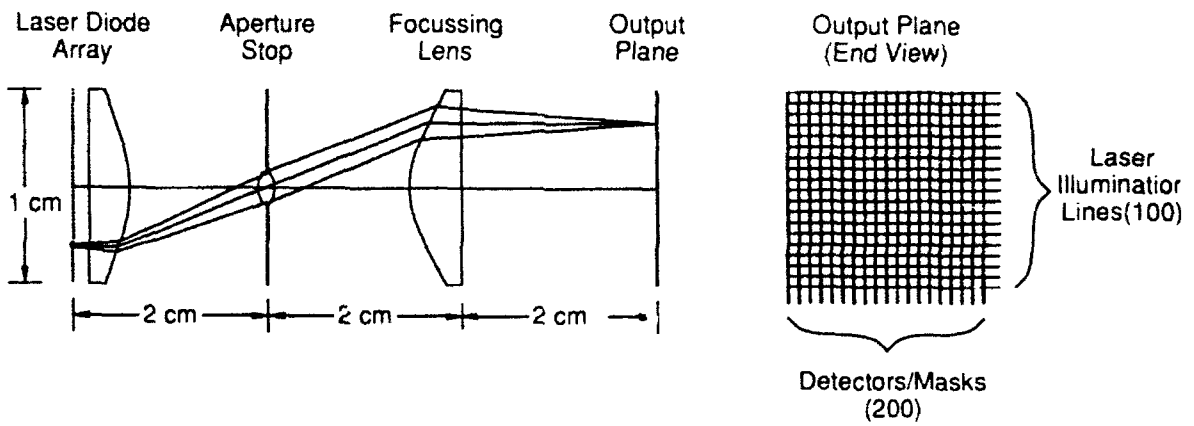

- Cylindrical optics
- Volume = 6 cm x 1 cm x 1 cm = 6 cm^3
- SBWP
- Laser diode array: 100 diodes on 100 μm centers
- Mask
  - Photographic film
  - (? μm)^2 pixel
  - >100:1 dynamic range
- Photo diode spacing

Figure 3.2-5. Alternate Cylindrical Optics Architecture for an Artificial Neural Network

optical processing literature that optical systems which can implement arbitrary optical interconnections of the input to the output (e.g., cross bar switches) have their space-bandwidth product limited by diffraction effects to the square root (W x H). To overcome this fundamental limit, a new optical architecture was developed and analyzed.

3.2.3 Integrated Optics Architecture Analysis

The integrated optics architecture is shown in Figure 3.2-6. Once again, a laser diode array was chosen for the linear input device. The lasers are coupled into a linear array of optical multimode waveguides, one laser for each waveguide. Each waveguide has, along its length, a number of devices which couple light out of the waveguide. Either by controlling the amount of light coupled out or by placing a mask next to the waveguide array, the input light is multiplied by the desired artificial neural network weights. This light is then electrically collected by a linear array of long, narrow photodiodes similar to that used in the second cylindrical optics architecture. Processing of positive and negative channels is done electronically. The results can be rebroadcast to the next layer by electrical connection to another laser diode array. Both of these functions could be done with integrated electronics to maintain a compact artificial neural network processor.

The technology required for the implementation of this processor is currently available (laser diode arrays, optical waveguides, linear photodiode arrays) or an extension of current electronic technology (integration of photodiodes with operational amplifiers and laser diodes) except for the method of coupling light out of the waveguides. Possible methods for achieving this coupling are (1) transparent windows in otherwise totally reflecting waveguide walls which would let light escape, (2) diffuse regions in the walls which would scatter light out, and (3) grating couplers which would diffract light out of the waveguide. This methods are discussed further in Section 4.3.

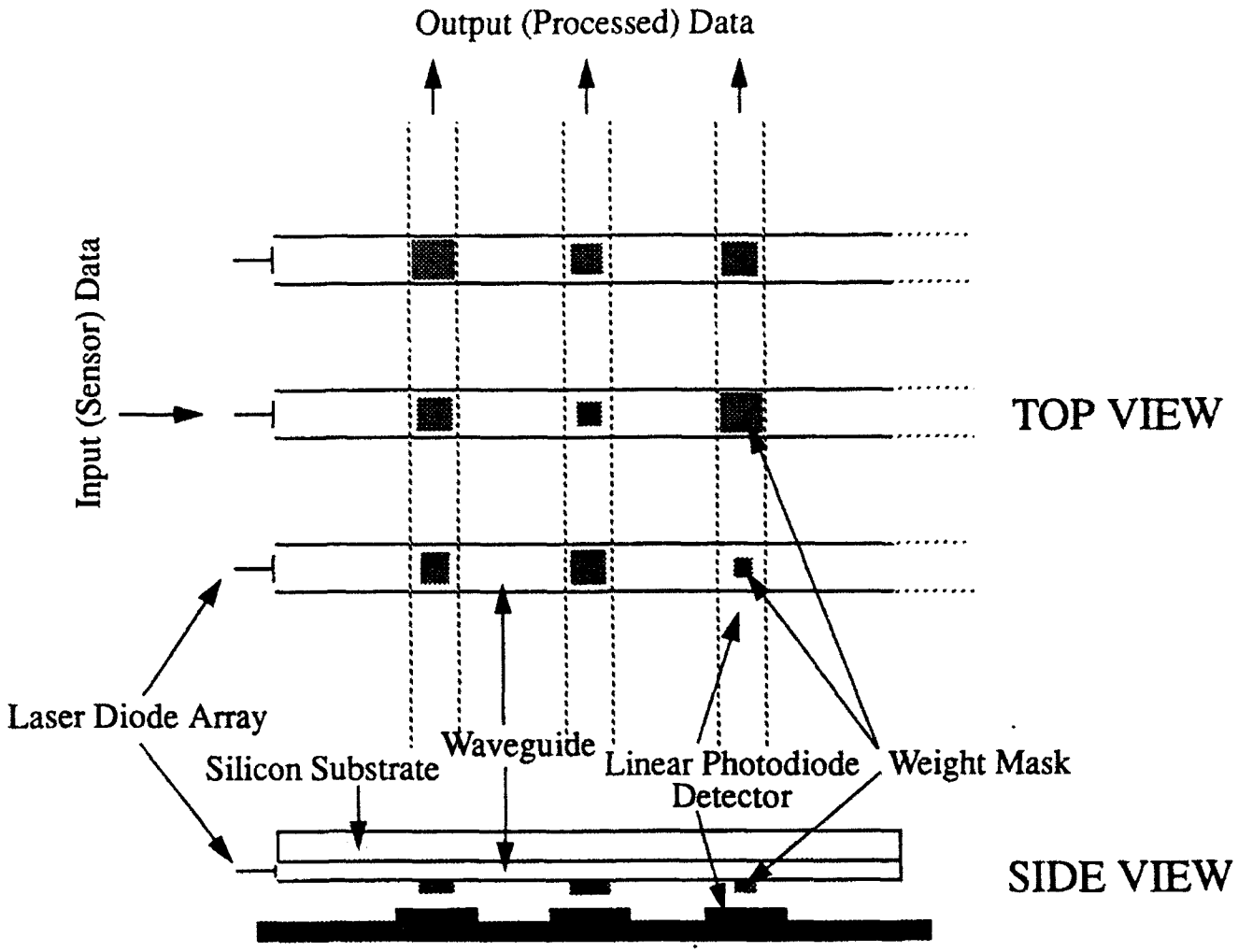

Figure 3.2-6. Integrated Optics Architecture for Artificial Neural Network

The point design of this architecture was completed by specifying the following:

Volume: L by W by H = 0.5 cm by 1 cm by 1 cm = 0.5 cm^3 (where L is measured perpendicular to the plane of the waveguides)
Input data rate: 100 by 1 MHz = 10^8 data values/sec
Computation rate: 100 x 200 x 1 MHz = 2 x 10^{10} operations/sec
Computations/cm^3: 4 x 10^{10}
Power (for 1% accuracy): 100 x 40 mW = 4 W

The length L (or more properly device thickness) is only an estimate based on integrated electronic flip chip and bump bonding practices. The integrated optics architecture has about a factor of 10 greater computations/cm^3. It should also be noted that the space-bandwidth product is proportional to W x H. This means that, if it were desired to scale the space-bandwidth product of the point designs presented in this section up by a factor of 2 in each dimension, the integrated optics architecture would grow by a factor of 4 in volume while the cylindrical architectures would grow by 16. Other advantages of the integrated optics architecture are (1) that it builds on electronic microfabrication technology and will benefit from advances in that arena and (2) that the device is a single component which should be more rugged and easier to keep in alignment than the cylindrical optics architecture with its multiple, separated optical components.

Some initial concepts were developed for further integration of the integrated optics architecture. First, multiple layers of an artificial neural net could be integrated onto a single substrate as shown in Figure 3.2-7. A two-dimensional spatial light rebroadcaster, such as the three terminal device being developed by AT&T could then be used as the optical to electrical to optical convertor and input-output device.

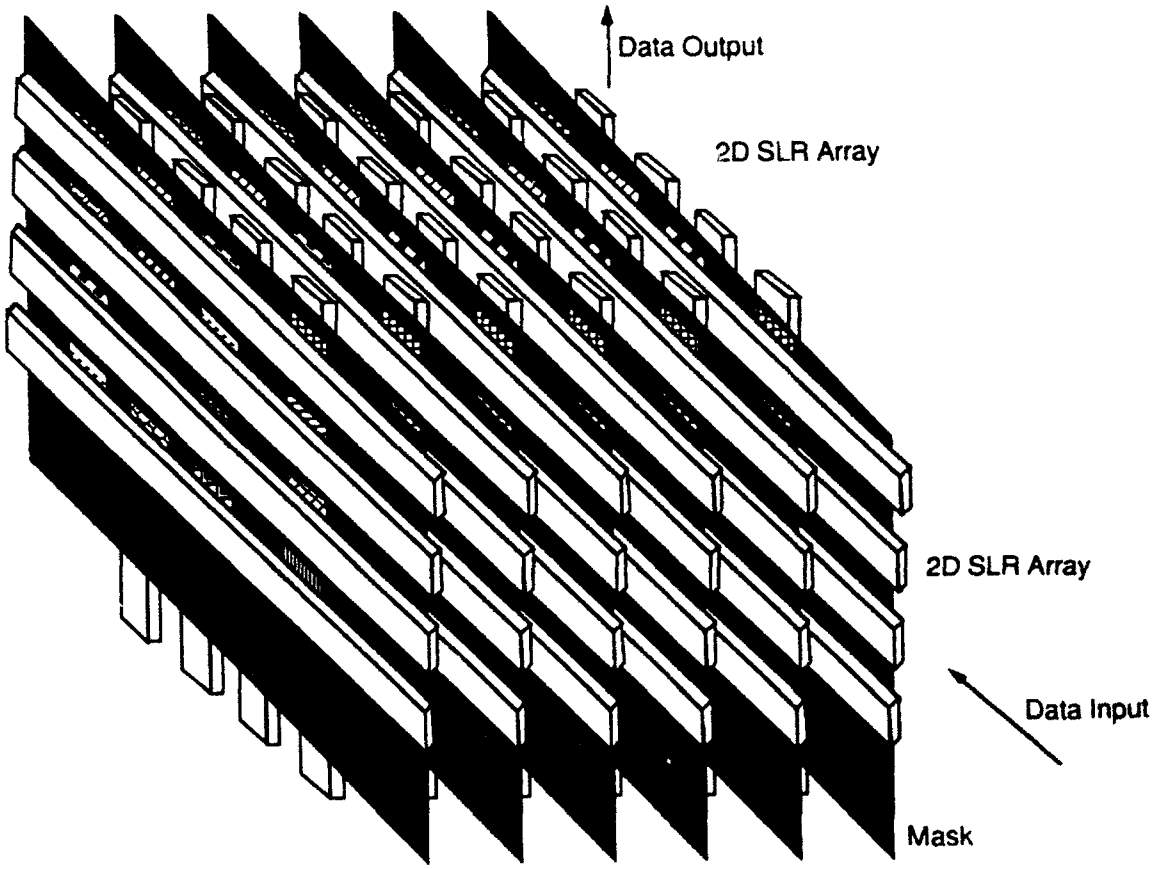

Figure 3.2-7. Multiple Layer Integrated Optics Implementation for Artificial Neural Network

3.3 Quadratic Processor

The primary function of the quadratic optical processor (shown in Figure 3.3-1) is to implement a pixel-by-pixel statistical target detection algorithm applied to 2D optical scenes. This optical processor would be a pre-detection processor whereby "detection" signifies the detection of an extended multipixel target. The main attributes of this architecture is the total parallelism in its implementations (all pixels are processed simultaneously) and the lack of optical/electronic/optical interfaces. No arbitrary detection and spatial light modulation is incorporated in the architecture.

An understanding of the salient features of the optical architecture can be facilitated through a detailed analysis of the quadratic algorithm. The quadratic operation used in the pixel-by-pixel detector is:

$$L = f^T A f > \Gamma \tag{37}$$

where f is the feature vector under consideration and A is proportional to the inverse of the covariance matrices and T denotes transpose. The feature vector f will be assumed to be the image data over a local 3 x 3 neighborhood. The covariance matrix A can be calculated off-line through training data.

The optical realization of matrix vector operations is through coefficient-by-coefficient multiplication and summation. The first part of the quadratic operation $f^T A$ can be written as:

$$g^T = f^T A = [g_1, \ldots, g_n, \ldots, g_N]. \tag{38}$$

Note that each coefficient g_n is produced by the multiplication of each member of the row vector f^T with the members of the specific column of A and then summed as:

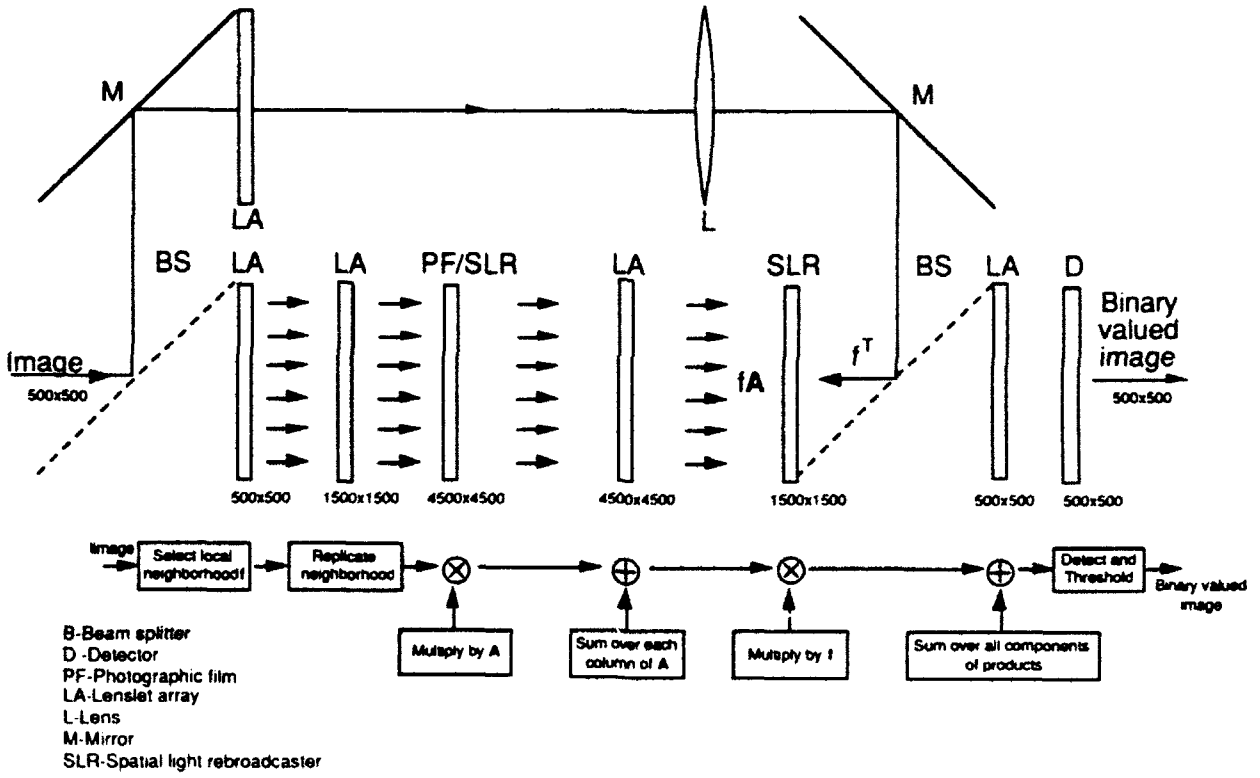

Figure 3.3-1. Optical Quadratic Processor

$$g_n = \sum_{i=1}^{N} f_i \; a_{i,n} \; . \tag{39}$$

Note that the f_i are replicated for each column n in A producing $a_{i,n}$. Lastly, the vector inner product $g^T f$ is computed as:

$$g^T f = \sum_{i=1}^{N} g_i \, f_i \; . \tag{40}$$

Recall that the input data are produced by an optical imaging sensor. The feature vector is defined as the local 3 x 3 neighborhood around a specific pixel. This physical situation requires an altered lexicographic numbering of the input vector f and filtering array A. Instead of the input vector having the form $f^T = [f_1, \ldots, f_n, \ldots, f_9]$, the input vector will be ordered as:

$$f = \begin{matrix} f_1 & f_2 & f_3 \\ f_4 & f_5 & f_6 \\ f_7 & f_8 & f_9 \end{matrix} \; .$$

which is what is physically present in the optical system. By allowing this numbering convention, no additional special optics need be applied to display the vectors in the conventional way.

The first lenslet array selects the local 3 x 3 neighborhood f. As shown in Figure 3.3-2, each pixel in the scene is contained in 9 neighborhoods. Its own and that of the 8 neighbors. Figure 3.3-2 shows how the lenslet array isolates each neighborhood. Each lens in the array has an overlapping field-of-view where two columns (or two rows for vertically oriented lenslets) of the 3 x 3 area are shared between two horizontally spaced lenslets. In order for this system to operate, three conditions must be met: 1) the number

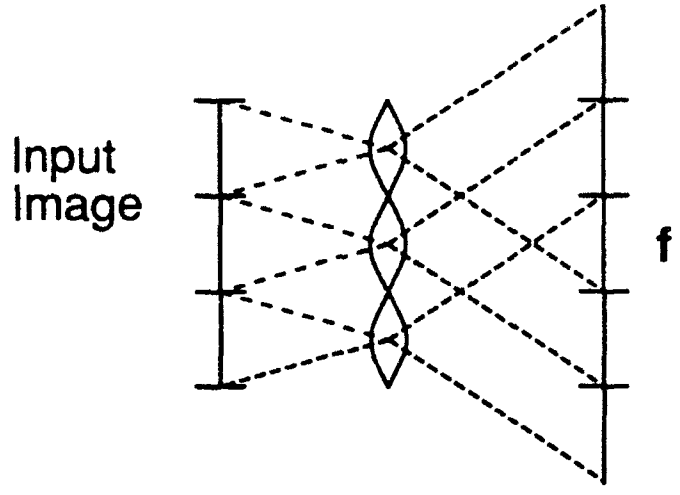

Figure 3.3-2. Selection of Neighborhood with Lenslet Array

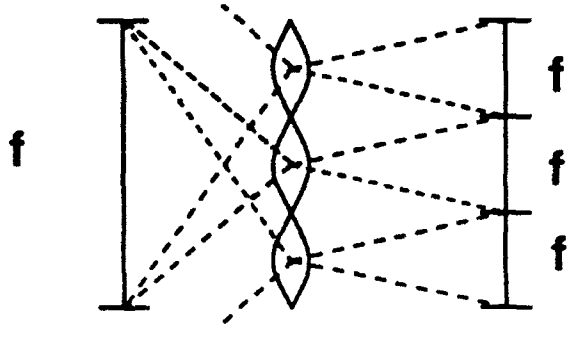

Figure 3.3-3. Replication of Local Neighborhood with Lenslet Array.

of lenslets in the array must be equivalent to the number of pixels in the input image. This is due to the fact that the number of neighborhoods is equivalent to the number of pixels. 2) the lenslet size must be less than or equal to the pixel size of the input image. When equal, the light throughput of each lenslet is maximum. The input pixel size will be assumed to be approximately 200 μm (consistent with the SLR pixel size specification). 3) When imaged, the local neighborhood will be minified by the lenslet array. This requirement attempts to control crosstalk for the next lenslet array which replicates f.

The second lenslet array replicates the local neighborhood as shown in Figure 3.3-3. This step is required to affect the vector matrix product $f^T A$ as outlined above. The input vector (the local neighborhood) is replicated and multiplied by the appropriate column in the matrix A. The basis for this step is the use of multiple lenslets with completely overlapping fields-of-view to reimage the local neighborhood numerous times. In our case 9 lenslets are required per neighborhood replicating the same neighborhood 9 times.

The multiplication of the replicated vector f by the matrix A is accomplished via point-by-point multiplication through a mask (either film or SLR). The matrix A must also be lexigraphically reordered as described previously and shown in Figure 3.3-4. Once reordered, a simple incoherent multiplication is affected by the mask. The final summation which then produces the output $g=f^T A$ is provided by the next lenslet array. In this system, each lenslet has distinct fields-of-view which are the neighborhoods in their entirety (see Figure 3.3-5). A simple integration via focusing is then accomplished. The number of lenslets in this array correspond to the number of neighborhoods.

The output $g=f^T A$ is incident on the next SLR which also has the radiation of the replicated neighborhood impinging upon it from the other side. This neighborhood data are simply the output of the sensor split from the main path of the quadratic system

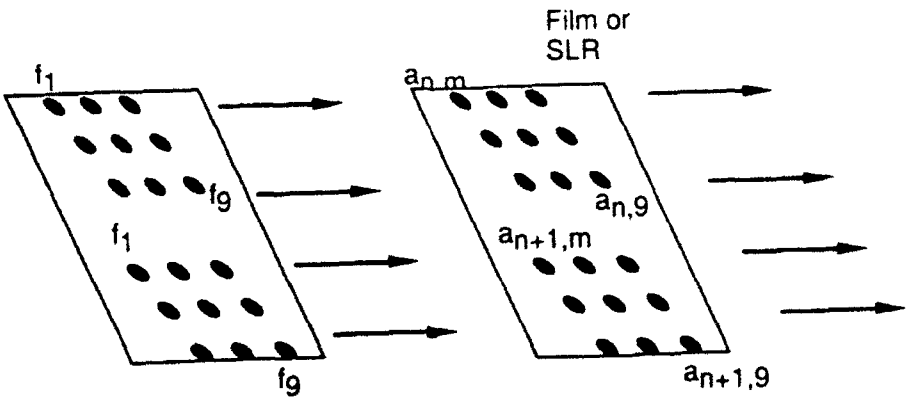

Figure 3.3-4. Lexigraphic Ordering of Matrix A and the Operation $f^T A$

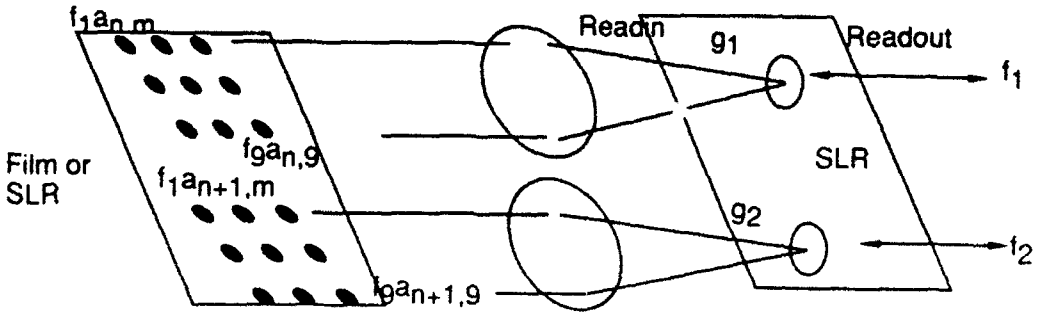

Figure 3.3-5. Summation over the Columns of the Product $f_i a_{i,n}$

via a beamsplitter as shown in Figure 3.3-1. These data have their neighborhoods selected via a lenslet array as discussed previously. The same conditions apply to the lenslet array as previous (number of lenslet are equal to the number of input points). A second lens (non-lenslet) reimages the neighborhoods onto the SLR via a second beamsplitter. A point-by-point multiplication of $g f^T$ is then produced by the SLR.

The final summation of the terms in $g f^T$ to produce the output scalar is provided by the last lenslet array of the system. Each lenslet in the array has a distinct field-of-view and provides the summation operation through focusing the energy onto a spot. The number of lenslets in this array is equal to the input number of points. The output spot must be small enough such that the finite size of the detection elements of the SLR completely cover the focused spot. Lastly, the final SLR is used as a means of setting a threshold on the incident radiation producing the final binarized output.

We will now embark on a detailed analysis of the system size and the specifications on the optical components. This analysis, in conjunction with Section 2.3.2 will allow us to completely determine the system throughput density (ops per volume per unit power) which is the performance metric useful for a comparison to digital systems. In our analysis we will rely on system geometry and simple imaging equations (lensmakers equation, F-number, magnification, and Rayleigh resolution criterion) to drive our analysis. In addition, we will also design the system to fall within well accepted specifications on the lenslet arrays described in [Borelli] and summarized here:

Lenslet diameter:	$70\mu m < D < 1000\mu m$
Lenslet spacing:	$15\mu m <$ Delta
Focal lengths:	$200\mu m < f < 50mm$
F-number:	$F\# > 1.43$

To begin our analysis, we will define the lensmakers equation as:

$$1/f=1/s_o+1/s_i \tag{41}$$

where f is the lens focal length, s_o is the object distance and s_i is the image distance. The magnification factor is given as:

$$M=-s_i/s_o=y_i/y_o \tag{42}$$

where y_i is the image size and y_o is the object size. In order to facilitate the analysis in terms of lens diameters, spacings, etc., we will define sizes in terms of the lens diameter as $y_o=k_1 D$, $y_i=k_2 D$, and $M=k_2/k_1$.. We can now calculate the object and image distances in terms of the constants k_1 and k_2 as:

$$s_o=-s_i/M=f(k_1/k_2+1). \tag{43}$$

The last required parameter for the analysis is the minimum resolvable spot size. This parameter defines the lenslet diameter. We will use the Rayleigh criterion which states $\delta = 1.22 \lambda s_i /D$ where λ is the wavelength of the radiation.

The parameters of each lenslet array are influenced by subsequent arrays in the optical system. These arrays help define required magnifications (or minifications). The requirements are also usually defined in terms of their lenslet sizes D_n and spacings Δ_n. We will now derive the numerical parameters of the neighborhood selection lenslet array in detail. The subsequent arrays are analyzed in an equivalent manner. Therefore, only their results will be given.

Figure 3.3-6 shows the lenslet geometry that will be used in this analysis. It will be assumed that the input pixel spacing is equal to the lenslet spacing. Since the field of view of the lenslet must encompass 3 input pixels, the object size to be imaged is:

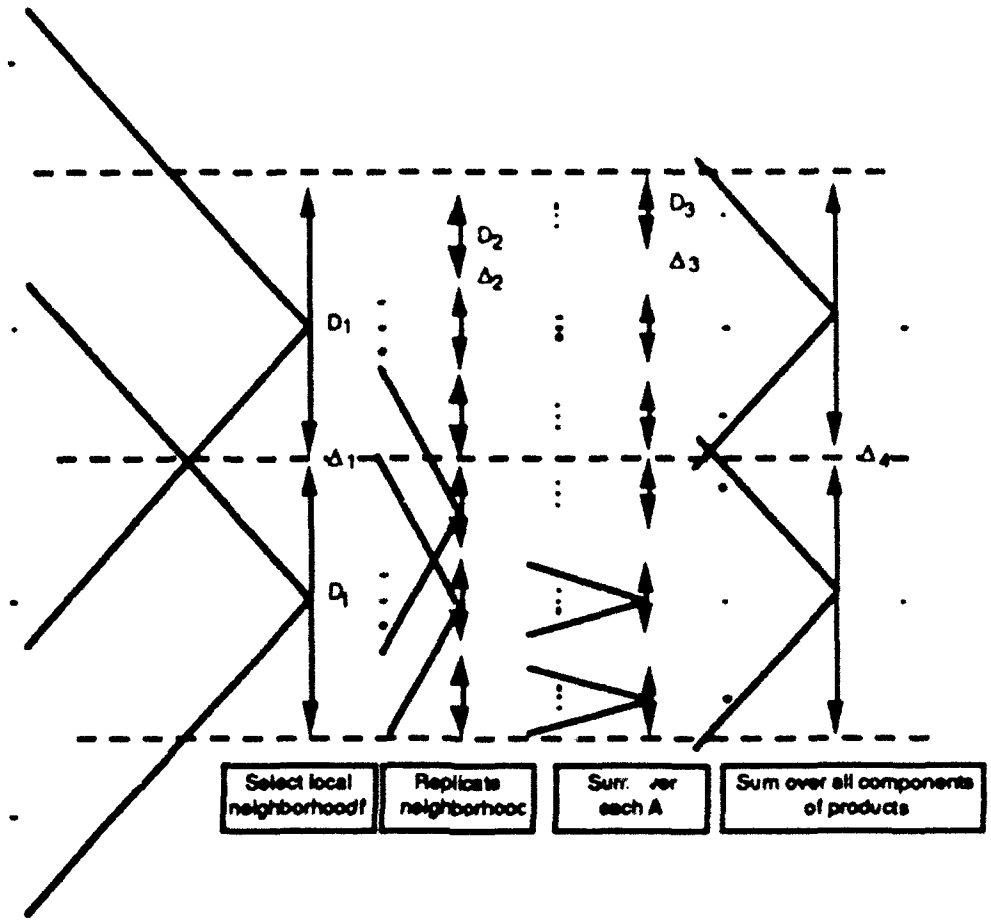

D_1=300 μm	D_2=100 μm	D_3=100 μm	D_4=300	Lenslet diameter (μm)
Δ_1=45 μm	Δ_2=15 μm	Δ_3=15 μm	Δ_4=45 μm	Lenslet spacing (μm)
$y_O=2D_1+2\Delta_1$	$y'_O=2D_2+2\Delta_2$	$y''_O=D_3$	$y'''_O=2D_3+2\Delta_3+\frac{y''_i}{2}+\frac{y''_i}{2}$	Object size
$y_i=\frac{D_1}{3}$	$y'_i=\frac{D_2}{3}$	$y''_i=\frac{D_3}{10}$	$y'''_i=\frac{D_4}{10}$	Image size
⇒ 8.9	1	0.9	8.8	Focal length f (mm)
30	9.9	9.3	29.4	F-number ($F^{\#}$)

Figure 3.3-6. Lenslet Geometry in Optical Quadratic Processor

$$y_o = 2D_1 + 2\Delta_1 = k_1 D_1 \tag{44}$$

where D_1 and Δ_1 are the lenslet diameter and spacing, respectively. Since the object consists of only 3 points, the minimum resolvable spot separation at the output is:

$$\delta = y_i / 3 = k_2 D_1 / 3 = 1.22\lambda s_i / D \tag{45}$$

which leads to:

$$D_1 > \sqrt{3.66\lambda f (1/k_2 + 1/k_1)} . \tag{46}$$

From the geometry of Figure 3.3-6:

$$D_1 + \Delta_1 = 3D_2 + 3\Delta_2. \tag{47}$$

We will also assume symmetry such that $3D_2 = D$ and $2\Delta_2 = \Delta$. In order to minimize crosstalk between the lenslets in the replication stage $y_i < D_2 = D_1/3$ which leads to $k_2 < 1/3$. We will use as our baseline, a lenslet array with $D_1 = 300\ \mu m$ and $\Delta_1 = 45\ \mu m$ which is within the specifications of [Borelli]. From this, we can easily derive that the focal length of the first lenslet array must be f = 8.9 mm with an F#=30. The lenslet array must be a distance of s_o = 7cm from the object and its formed image is a distance of s_i = 1.02 cm from the array. These results are shown in Figures 3.3-6 and 3.3-7. A similar set of derivations can be performed for the neighborhood replication, summing over the filtered output, and summing over the second inner product lenslet arrays. The results of these calculations are shown in Figure 3.3-6 with the overall system size (and object/image distances) shown in Figure 3.3-7.

The system power is defined by the final active SLR, all the other components are passive. The SLR required power is assumed to be 3mW per pixel. The total power then becomes 3mW x $(500)^2$ = 750 Watts for the entire system. The power per unit volume is then 18mW/cm^3 (based on the calculated 41,000 cm^3 processor volume).

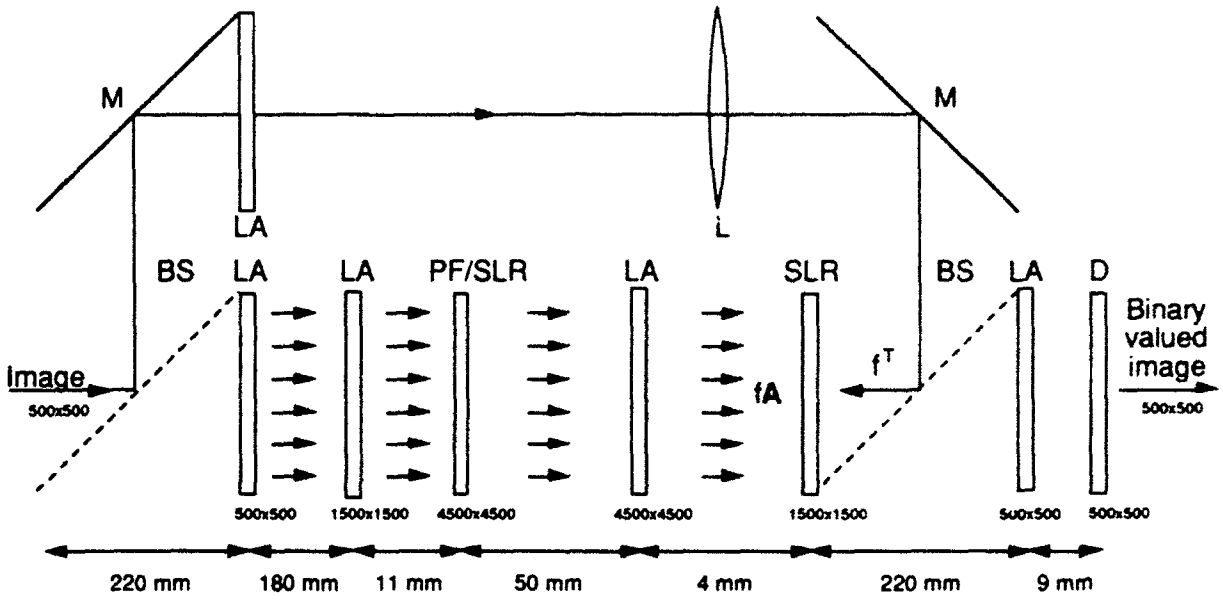

Length = 69.4 cm
Width = 2x17+1 = 35 cm
Height = 17 cm
Volume = 41,000 cm^3
Power = 3 mW x $(500)^2$ = 750 Watts
Power/volume = 18 mW/cm^3

Figure 3.3-7. Geometry of Optical Quadratic Processor used for Evaluation

The last calculation for system performance is the system signal-to-noise ratio. This determines whether or not there are sufficient photons in the system to produce a usable signal above the noise floor. In order to proceed, we must assume an operational scenario. This scenario was discussed in Section 2.1. We will just summarize the parameters here as:

Sensor range:	15 km
Sensor Lens Diam.:	17 cm
F5 system:	f=85 cm
Scene:	Sunlight veg. R_{veg}=.05 $F_{sun} = 4 \times 10^{-2}$ watts/cm^2/μm (λ = 0.6μm)

These specifications produce an average intensity at the image plane of the sensor as I = 0.282 Watts/m^2 (based on T_{lens} = 0.9, $\Delta\lambda$ = 0.5 μm). Figure 3.3-8 depicts the assumed transmission coefficients, responsivities and optical power division and increase (through summation) in the system. In addition, the optical power densities are shown at different points along the system. Lastly, the assumed specifications of the SLR (quantum efficiency, time constant, and spectral bandwidth) are given. Based on these specifications the signal to noise (photon) ratio is 51.4 (17dB). This signal-to-noise ratio, when completely used by target energy would provide a detection probability of P_D=.77 with a false alarm probability of $P_{FA} = 10^{-6}$. This is predicated on the use of Gaussian models for both the clutter and target and only the use of energy as the discriminant [VanTrees].

As noted in Section 2.3.2, the system throughput is related to the SLR response time. The best case response is 1 μsec. In this instance the system throughput rate is 42,500 Gops/sec (see Section 2.3.2 for analysis details). For a processor volume of 41,000 cm^3, and prime power of 750 watts, the throughput rate per unit volume is 1 Gop/sec cm^3 and the throughput rate per unit power is 57 Gop/sec W. These

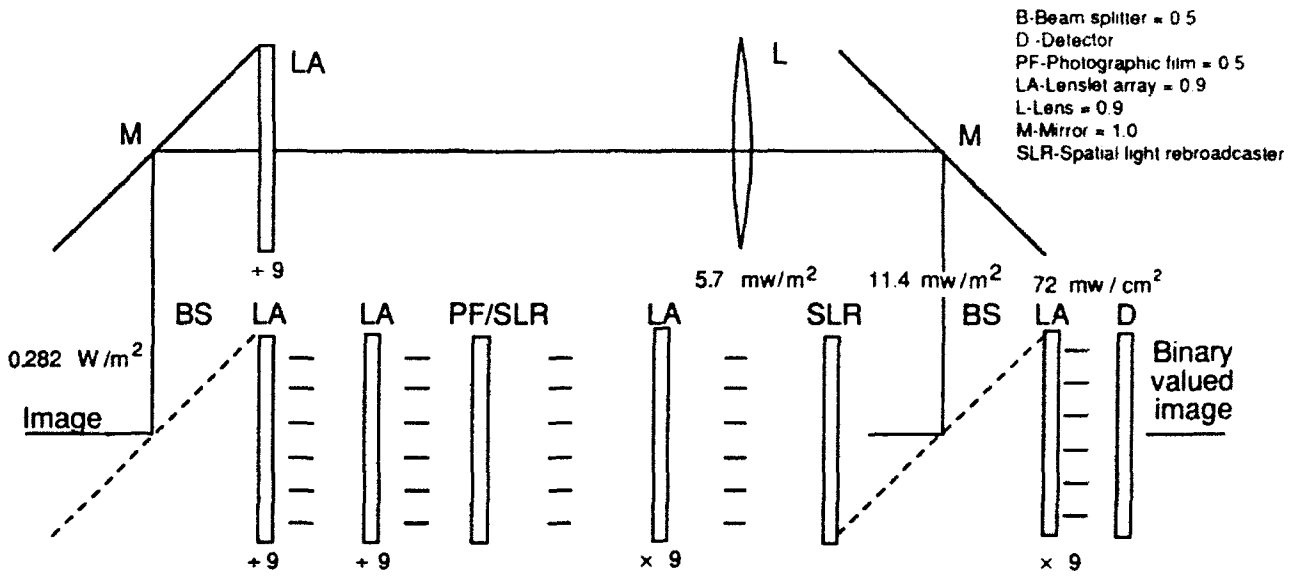

$\eta_d = \eta_{d'} = 0.6$ $\quad \eta_{d''} = 0.6$

$\tau_d = \tau_{d'} = 1\mu s$ $\quad \tau_{d''} = 1\mu s$

$\nu_d = \nu_{d'} = 5 \times 10^{14} s^{-1}$ $\quad \nu_{d''} = 3.75 \times 10^{14} s^{-1}$

$(\lambda = 0.6\mu m)$ $\quad (\lambda = 0.8\mu m)$

SNR = 51.4 (17 dB)

Figure 3.3-8. Optical Quadratic Processor and Assumed Optical Efficiencies Used in Signal-to-Noise Analysis

specifications are extremely high and provide a favorable comparison to state of the art electronic systems [Gary].

3.4 Morphological Processor

An important feature of morphological image processing is its inherent parallel nature where the same transformations operate on all pixel elements. Morphological processing can be performed at very high speed with an appropriate parallel processing architecture. There several basic architectures that can be used to implement a morphological image processor.

1) Parallel Full Array:

A full array of two-dimensional processors with each processor connected to other processors in its neighborhood. All processors execute the same instruction simultaneously which is broadcast from a central controller. This type of Single Instruction Multiple Data (SIMD) processor architecture is extremely difficult to be implemented with conventional microelectronics, requiring a hugh number of parallel processors and interconnects. A full parallel array has not been fabricated with conventional electronics.

2) Parallel Subarray:

A parallel subarray is simply a portion of a full array which reduces the hardware requirements. However, to process the full image, the image has to be partitioned and loaded into the subarray processor sequentially which adds to system complexity.

Several parallel subarrays processors have been built, most notably the Cellular Logic Image Processor (CLIP) series and the Massively Parallel Processor (MPP). These machines are still quite massive, requiring many processors and interconnects. In addition,the I/O time required to shift the subimages into and out of the subarrays

limits the processor performance. Extracting and combining information from multiple images are complex tasks which further limit the system throughput.

3) Raster Subarray: A raster subarray consists of a special memory unit to produce a complete set of neighborhood pixels for the computation unit. The input image is loaded serially in a raster format. Each time a pixel passes through the first register of the memory unit, the previously entered pixels are shifted along. The number of shift registers per line, M, is equal to the number of pixels per line in the image. A minimum of nine registers have to be available to the computation unit to form a 3 x 3 structure element which requires a total of 3M shift registers. The output is in same raster format as the input with in delay in time.

To maintain real time operation, the processor can be pipelined with a cascade of parallel subarrays such that the output of a raster subarray becomes the input to a next array in the cascade. The number of subarrays required is equal to the number of transformations needed to perform the algorithm. If the input data rate is slow or the processing speed is sufficiently fast, the number of cascaded subarrays required can be reduced by cycling the data back to the first array to continue the processing before the next stream of image data is loaded. ERIM's Cytocomputer is the most prominent processor of this type.

The ideal processor architecture in terms of performance is the parallel full array. All image pixels are transformed simultaneously, providing a tremendously high throughput. Its implementation, unfortunately, is not feasible with current microelectronics fabrication technology. The inherent massive parallelism of an optical processor, however, may make it possible to implement a parallel full array in a reasonably compact package, resulting in orders of magnitude improvement in system throughput.

The heart of an optical morphologic image processor is the computation unit which is composed simply of an input SLR, an imaging lens, a programmable pupil mask and an output SLR as shown in Figure 3.4-1 which performs the dilation operation. This basic module can be cascaded and arranged in a feed back architecture as illustrated in Figure 3.4-2. The data circle back after passing through and processed by the N stages. The processing throughput of such a processor is maximized when the time required to alter the transmittance of the SLMs is matched to the processing time through the N stages. If for example, the switching time of the SLR is 1 nsec and N = 50, the SLM and the SLR logic must be programmable within 50 nsec to keep up. Otherwise, the processing speed must be slowed down or the number of processing stage has to be increased.

The pupil functions can be complex and it may be difficult to obtain an SLM with independent amplitude and phase control and high switching speed. One possible design that can be used to circumvent to problem is to spatially multiplex the needed complex aperture functions on a transparency and make use of the fact that the output intensity distribution of an incoherent imaging system is independent of the spatial position of the aperture mask. Placed over the multiplex aperture mask is a binary SLM which blocks out all but the selected aperture function as illustrated in Figure 3.4-3. As the data are cycled through the n stage optical morphological processor, the desired aperture function is selected by controlling the on-off pattern of the binary SLM. Candidate SLM devices include the magneto optics SLMs which are capable of μsec switching speed..

Let us assume that the structure element is composed of 3 x 3 neighborhood pixels, a single transformation will require a minimum of 9 multiplies and 1 summation for a total of 10 arithmetic operations. If the space-bandwidth product (SBWP) of the SLRs is 256 x 256 pixels, then with the speed assumed in Table 1-1 for the active SLR devices, the processing speed of the optical morphological processor will be 256^2 x 10 ops/1 nsec = 6×10^{14} ops/sec.

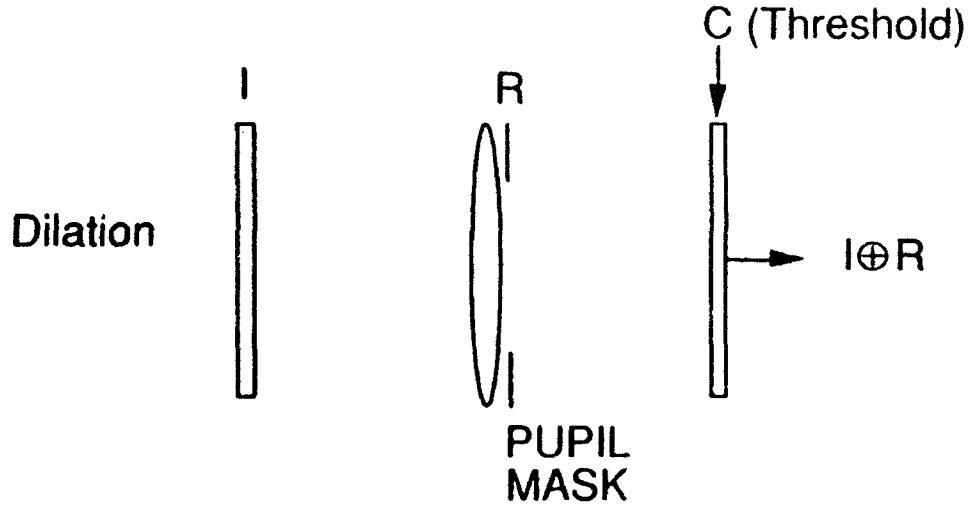

DILATION = T[I*R]

T = Threshold

* = Convolution

I = Input

R = Structure Element (Mask PSF)

Figure 3.4-1. Basic Element in Optical Morphological Processor

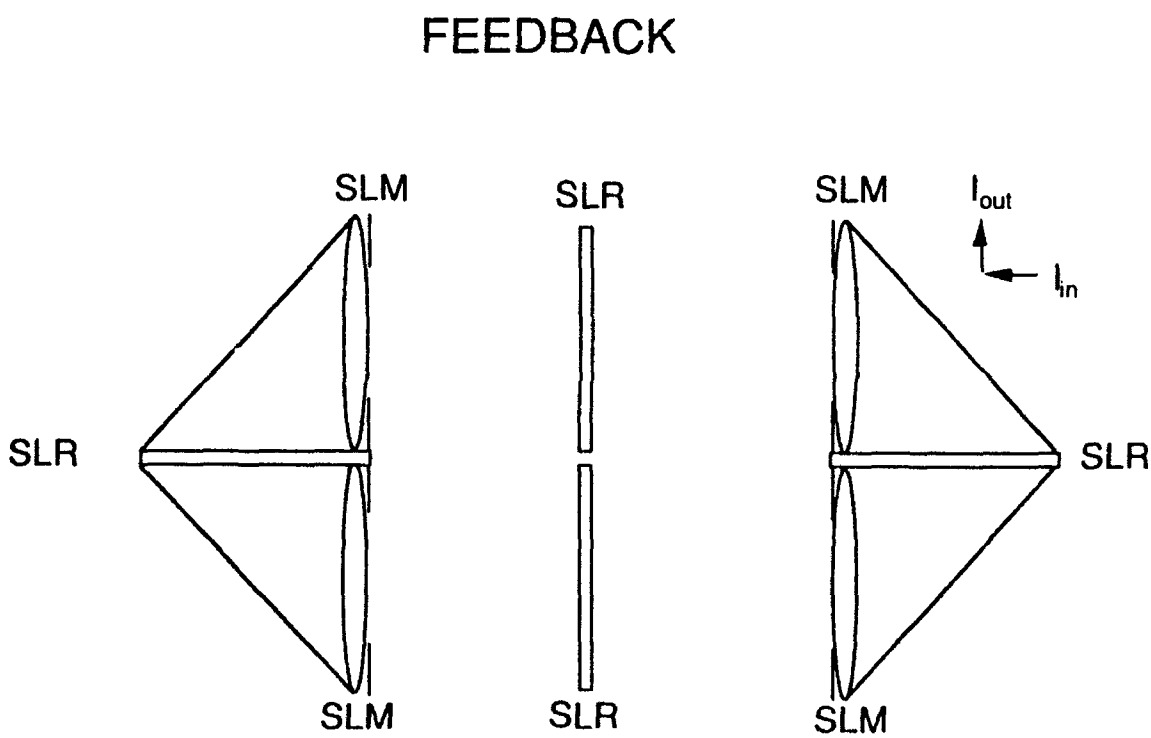

Figure 3.4-2. Optical Morphological Processor with Feedback

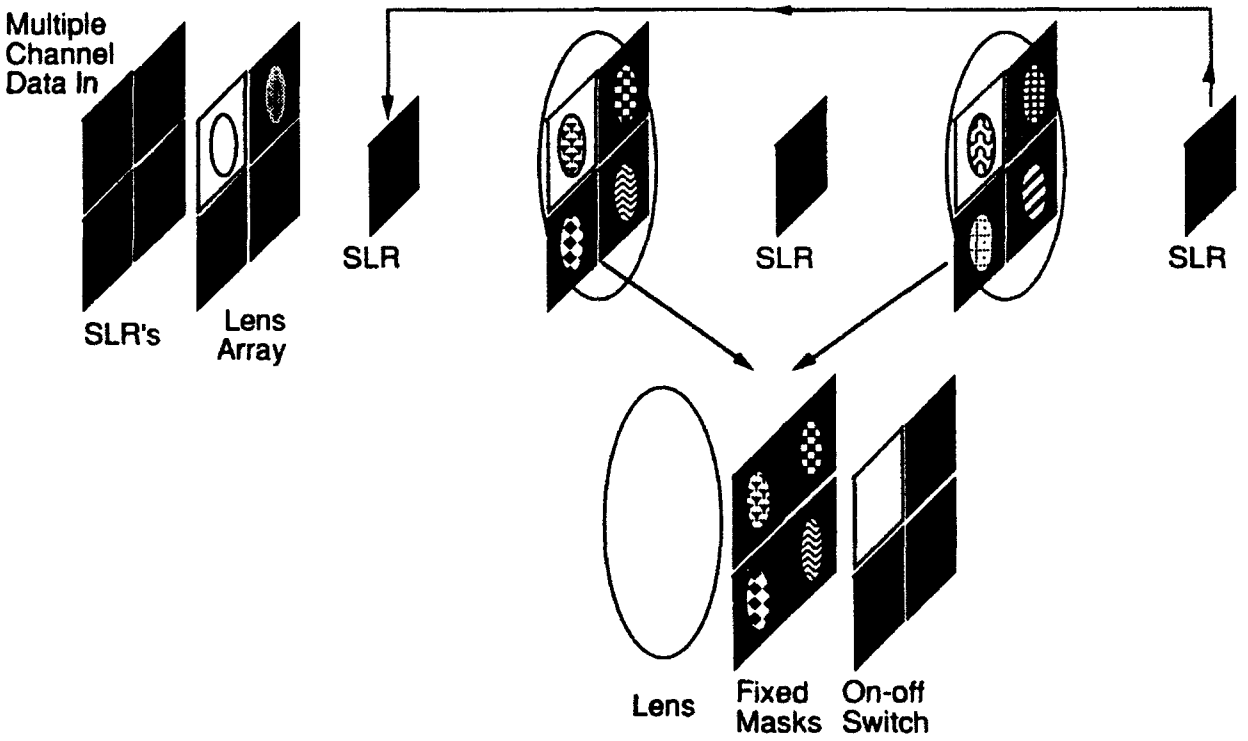

Figure 3.4-3. Optical Morphological Processor with Programmable Stages

A rough estimate of the processor size is about 5 cm x 5 cm x 10 cm for each optical stage. The optics of a 10 stage system will occupy about 2500 cm^3. Adding another 10,000 cm^3 for the control and driving electronics, the total processor volume is about 12,500 cm^3. The processor throughput per unit volume is then equal to 5.0×10^{10} operations/sec/cm^3.

If we use a more modest and realistic processor size with N=10 and a SLM switching speed of 10 μsec, the processing speed is lowered to 256^2 x 10 x 10 ops/ 10 μsec = 6.5×10^{11} ops/sec. The processing speed per unit volume achieved with these rather conservative parameters is then equal to 5.2×10^7 ops/sec/cm^3 which is still very high.

With electronic implementations, the small structure element (e.g., 3 x 3) is typically used to minimize hardware requirement. Larger structure element is obtained through successive dilation with smaller structure elements, taking advantage of the distributivity of dilation. With an optical processor, no such constraint is needed and a large structure element can be used directly. The dilation by a large structure element can be performed in a single step, further increasing the system throughput. For example, if the structure element is composed of 9 x 9 pixels instead of 3 x 3, the system throughput is increased further by almost an order magnitude.

The computation unit is only one component in an image processor. Other components required include input and output interfaces, image memories, controller, system interconnects and decision maker. A possible system architecture of a special purpose optical morphologic image processor may operate as follows. For simplicity only a single stage is shown. The input image, typically from video source, is read into two frame buffers with high read out rate. After a full frame fills one of the buffers, it is loaded rapidly into the SLR, either optically or electronically. While the data are being loaded into the SLR and processed by the optical processor, input image data are

directed to fill the second frames buffer. This is done to ensure there will be no loss of data. If the input image can be loaded into the SLR in parallel (e.g., a direct image of the scene), then a simple shutter can replace the dual buffer to freeze a frame of data to be processed.

The SLRs are controlled to produce either the direct image or its complement at the output, and the threshold level is set by the control computer. The SLMs are programmed by the controller to give the desired pupil function. The output of the Nth stage is fed back the first processor stage to continue the processing.

The optical processor filters and enhances the image and extracts target features. An electronic processor has to examine the features to recognize or classify the targets. The processed optical output is read out with a CCD detector array and digitized. The decision making will be performed by an electronic processor.

3.4.1 ATC Applications for Morphological Processor

Morphological processing has been successfully used in many difficult image processing applications, including ATC and ATR with low contrast infrared images and speckled radar images. It has also been employed extensively in medical image processing to, for example, recognize specific cells. Various image processing functions related to ATC can be implemented with a series of morphological operations and transformations. Some example of simple image processing functions are given below.

(1) Differencing or intersection can be used for change detection.

(2) Opening and closing can be used to remove salt and pepper noise, smoothing and size filtering.

(3) Difference between dilated and eroded images can be used to detect the edges of an target image.

(4) Dilation, hit and miss transform can be used for template matching.

(5) Thinning and thickening can be used to extract and enhance certain target features.

(6) Skeletonization can be used to extract target features and to establish the connectivity of features.

A complex imaging processing of algorithms can be implemented with a series of elementary operations or transformations in the form of an algorithm. For example, to perform feature extraction or dimension reduction, the algorithm may involve for example, removal of salt and pepper noise to smooth out the image, perform size filtering to find the features that look like wheels on a vehicle and to locate objects that match the overall size of the target, perform a skeletonization to extract the gross features such as the number of corners in the target image or to determine the connectivity of the wheels. To implement an algorithm may require the performance of hundreds of elementary operations and transformations on each pixels. To be able to perform the algorithm in real-time (video frame rate, or up 10^7 pixels/sec), special purpose processing hardware is required.

3.4.2 Summary Comment on the Optical Morphological Processor

The single instruction multiple data (SIMD) processing architecture is the most efficient architecture for morphological image processing but it is also the most difficult to implement with conventional electronics technology. The SIMD architecture, however, is ideal for optical implementation. An optical processor can process data at a very high rate with its massive parallelism but it is also relatively slow in changing the instructions to individual elements in the processor (e.g., reprogramming an SLM). It

allows a large amount of data to be processed simultaneously with the same instruction which are broadcasted optically to all processing elements.

We have shown that most morphological operations and transformations can be implemented as series of two fundamental local operations (complement and union) and one neighborhood transformation (dilation). The optical implementation of these three fundamental operations and transformation were described. An optical processing architecture for a target features extractor was presented around which an automatic target classifier can be built.

3.5 OTF Synthesis Preprocessor and Interferometric Processor

OTF synthesis preprocessing and interferometric processing are well established incoherent optical processing techniques. The basic operation of the two optical processors will not be changed by the use of SLRs. The most distinctive feature of an SLR based system is ability to perform bias subtraction on the detection device which contrasts with conventional implementation using a detector arrays where bias substraction is performed external to the detector. Since bias build up is the primary problem for both incoherent optical processors, the section will concentrate on addressing the performance of an SLR in bias subtraction.

Bias build up limits the performance of an incoherent optical processor because it occupies the bulk of the dynamic range of the detector. The optical output of the incoherent optical processor can be modelled as $B \pm mB$ where B is the bias, m is the modulation depth of the signal and $m \ll 1$. Utilizing the full dynamic range of the detector, $B(1+m) = N$ where N is the number of electrons in the well of a CCD detector array, we have:

$$SNR = \frac{2mB}{\sqrt{B(1+m)}} = \frac{2m\sqrt{N}}{1+m} \simeq 2m\sqrt{N} \qquad \text{for } m \ll 1 . \qquad (48)$$

The SNR can, therefore, be improved by using a detector with a larger storage capacity, N, or by increasing the contrast (m) of the signal or both. In the following section, the use of an SLR to enhance the output SNR of an interferometric processor is described.

3.5.1 Spatial Light Rebroadcaster for Bias Subtraction

A passive SLR typically consists of a uniform layer of electro-optic material such as an electron trapping phosphor [Lindmayar]. Incident writing energy at short wavelength (e.g., λ_i = green) is absorbed by the material, exciting electrons to the conduction band. The electrons then fall into traps where they are stored. When the material is exposed by a read out beam at a longer wavelength (e.g., λ_r=near infrared), the trapped electrons are excited out of the trapping level and fall back to the valance band.as shown in Figure 3.5-1, emitting light at wavelength λ_o where $\lambda_i < \lambda_o < \lambda_r$.

The rate at which electrons are filling the traps is determined by the product of the write beam intensity and the number of unoccupied trap sites. If the input radiation is far from saturating the SLR and the readout depletes only a small percentage of the trapped electrons, the intensity of the output emission is approximately proportional to the number of occupied traps times the intensity of the readout beam. The products of two arrays of values can be obtained by, for example, inputting a light pattern representing the values of one of the array and reading it out with a light pattern corresponding to the second array. The output intensity pattern of the emitted radiation is proportional to the products of the two arrays. The device has been used to implement vector-matrix multipliers and neural networks [Jutamulia, McAulay]. What we are interested in, however, is the dynamic behavior of a passive SLR.

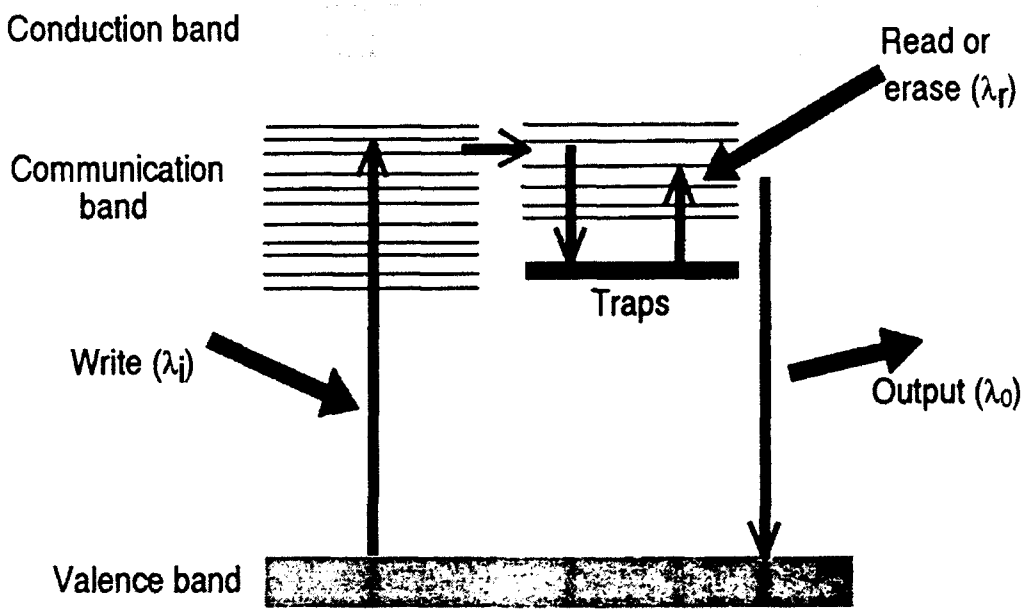

Figure 3.5-1. Operation of Electron Trapping Material

An impetus in utilizing an SLR for bias substraction in incoherent optical processing is the large dynamic range provided by an SLR. The number of traps available in an SLR is much larger than the well capacity of CCD detector arrays. A thin film SLR with a thickness of a few micrometers can have as many as 10^6 traps/μm^2 [Lindmayar]. With a cell or pixel size of $10\mu m$ x $10\mu m$, there are 10^8 traps per pixel. The well size of a typical CCD detector array by comparison has only about 10^6 electrons. Another reason for using an SLR is its simultaneous write and erase capability which allows the bias to be reduced as the output of an incoherent optical processor is being written onto the device.

3.5.2 Dynamic Behavior of Passive SLR

The rate at which the trap sites are occupied when an SLR is illuminated with the green (λ_i) write beam is given by:

$$\frac{dT_w(x,t)}{dt} = \delta_i \eta_i W(x)[T_s - T_w(x,t)] \tag{49}$$

where δ_i is the absorption cross section for the write wavelength, η_i is the quantum efficiency of the SLR in filling a trap, W(x) in the photon flux density of the write beam and T_s is the available trap density (i.e., total number of available traps per unit area) and $T_w(x,t)$ is the density of occupied traps at time t. The solution to the differential equation is given by:

$$T_w(x,t) = T_s\{1 - \exp[-\delta_i \eta_i W(x)\ t\ ]\} \tag{50}$$

assuming the initial condition of $T_w(x,0) = 0$.

In the case of read out by an infrared (λ_r) beam, some of the trapped electrons are excited out of the traps and fall back to the valance band. The rate that the trapped electrons are released is given by:

$$\frac{dT_r(x,t)}{dt} = \delta_o \eta_o T_r(x,t) R(x) \tag{51}$$

where δ_o is the absorption cross section for the readout wavelength, η_o is the transfer efficiency in releasing the electrons and R(x) is the readout photon flux density. The solution to the differential equation is:

$$T_r(x,t) = T_r(x,0) \exp[-\delta_o \eta_o R(x)\ t\ ] \ . \tag{52}$$

where $T_r(x,t)$ is the number of traps that remains occupied per unit area and $T_r(x,0) \neq 0$ is the initial condition.

If we first write on the SLR with a beam at wavelength λ_i over an exposure time of t′ with a flux density of W(x) and then read out the SLR with an IR (λ_r) pattern with flux density R(x) for a time period of t″, we have $T_r(x,0) = T_w(x,t')$ and the number of traps per unit area that remains occupied is equal to:

$$T_{wr}(x,\ t',\ t'') = T_s\{1 - \exp[-\delta_i \eta_i W(x) t']\} \exp[-\delta_o \eta_o R(x)(t'')] \ . \tag{53}$$

The final readout is accomplished with an uniform IR beam with photon flux density I_R. The emitted photon flux density is given by:

$$I_{out}(t) = T(x,0)\ \eta_e \delta_o \eta_o I_R \exp[-\delta_o \eta_o I_R\ t\ ] \tag{54}$$

where $T(x,0) = T_{wr}(x\ ,t',\ t'')$ and η_e is the transfer efficiency of the device in converting energy released by the electrons into photons. Detecting the output of the SLR, we have:

$$\begin{aligned} E_{out}(x,\tau) &= \int_0^{\tau} T(x,0)\ \eta_e \delta_o \eta_o I_R \exp[-\delta_o \eta_o I_R\ t\ ]\ dt \\ &= T(x,0)\eta_e\{1 - \exp[-\delta_o \eta_o I_R \tau]\} \end{aligned} \tag{55}$$

where τ is the integration time of the detector array. The output of the detector array

is linearly proportional to the distribution of the trapped electrons remaining in the SLR. In the following section, the use of an SLR to reduce the bias in the output of an incoherent optical processor is described.

3.5.3 Bias Subtraction in Incoherent Optical Processing

With the input and output both represented by light intensities which take on only positive real values, bias build up is a significant limiting factor for incoherent optical processing systems such as those employing OTF synthesis and interferometric techniques. Consider an interferometric output that is described by:

$$I_0(x) = B + mB \cos(fx + \theta) . \tag{56}$$

If we add a second channel with a π phase shift inserted between the interfering wavefronts, an inverted output is obtained. That is:

$$I_\pi(x) = B - mB \cos(fx + \theta) . \tag{57}$$

This form of output is obtained with OTF synthesis utilizing spatial frequency carrier or two pupil synthesis techniques. Two parallel output channels, one at wavelength λ_i and the other at wavelength λ_r can be obtained with the optical arrangement illustrated in Figure 3.5-2 and Figure 3.5-3 respectively.

The outputs described in Eq. (45) and (46) also represent the cosine transform of a single point in an incoherent input field. The transform output obtained with an interferometric processor can be described as a superposition of cosines of different spatial frequencies and phases. A two-channel interferometric processor that provides an inverted set of outputs at wavelengths λ_w and λ_r is shown in Figure 3.5-4.

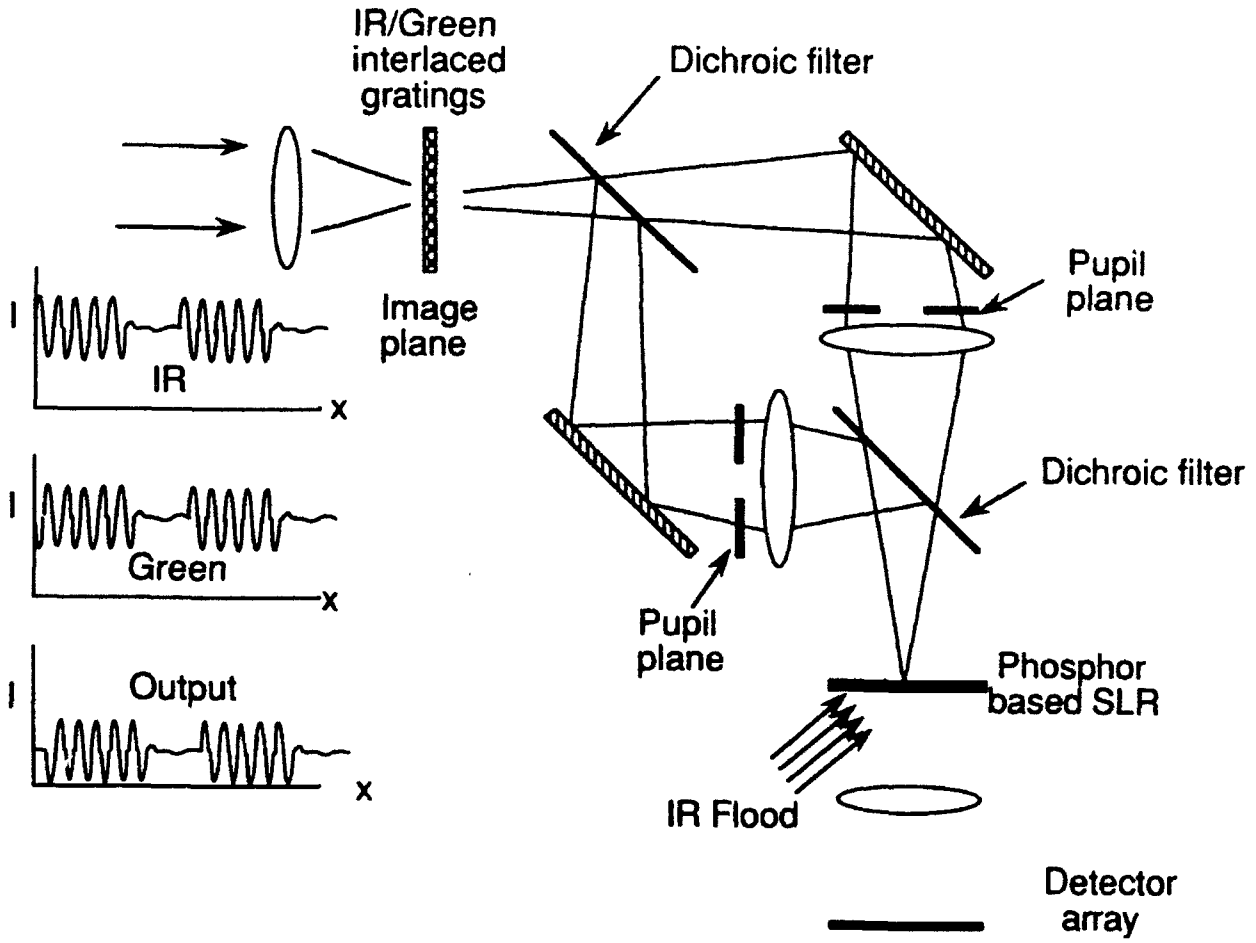

Figure 3.5-2. Two-Pupil Synthesis Interferometric Processor Using an SLR for Bias Subtraction

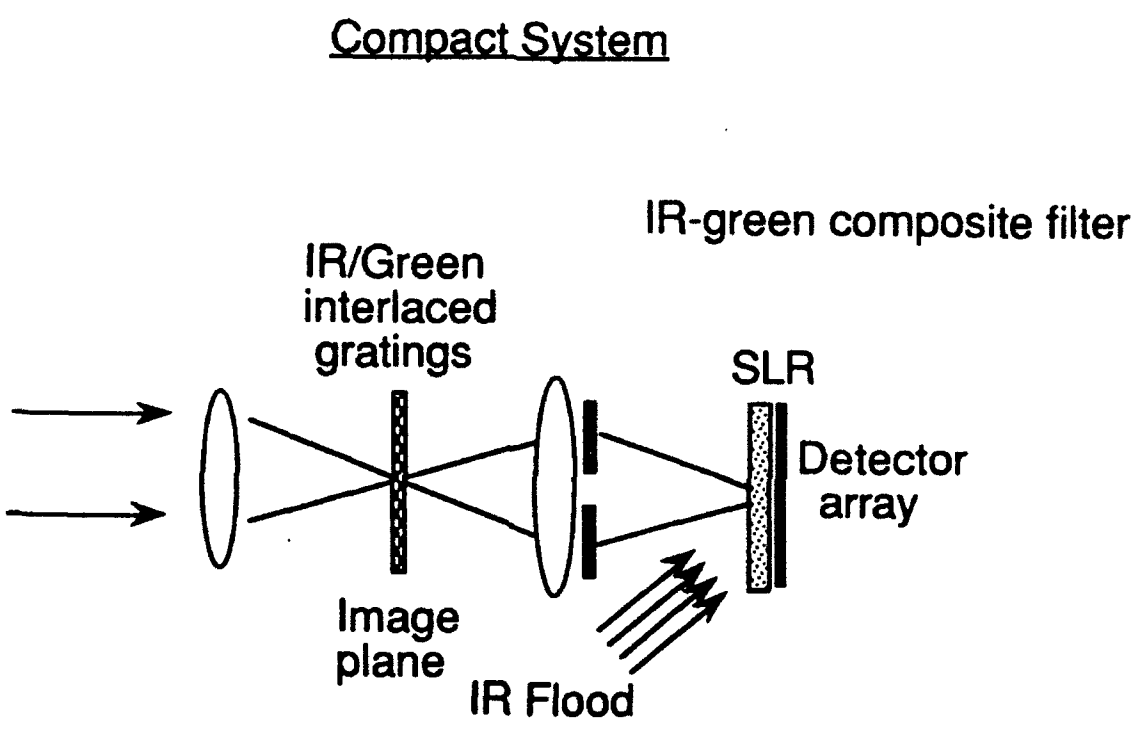

Figure 3.5-3. A Compact Aperture Synthesis Interferometric Processor Using an SLR for Bias Subtraction

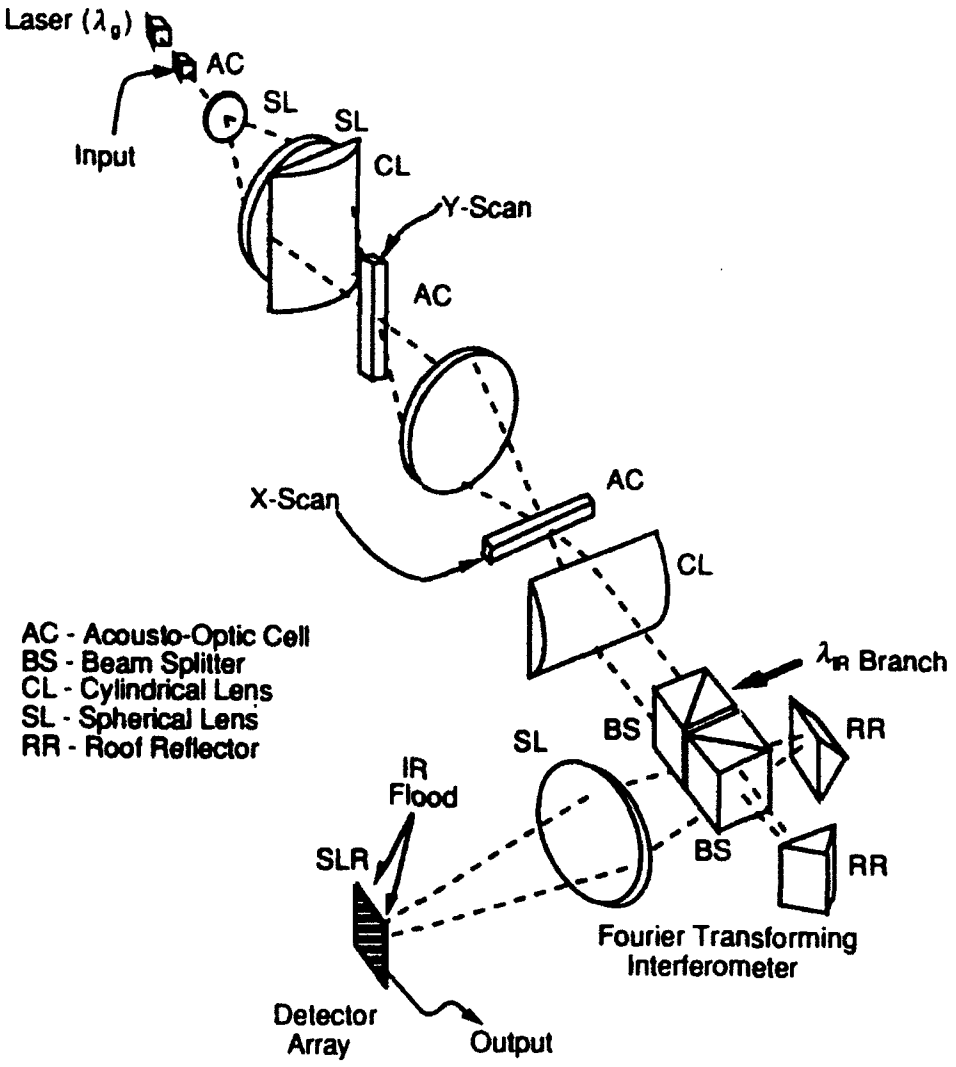

Figure 3.5-4. A Two-Channel Acousto-optic Based Interferometric Processor Using an SLR for Bias Subtraction

Let $W(x) = I_w I_0(x)$ and $R(x) = I_r I_\pi(x)$. From Eq. (11), the number of trapped electrons after t" sec of destructive readout is equal to:

$$\begin{aligned} T_{wr}(x,\ t',\ t'') &= T_w(x,\ t')\ e^{-\delta_o \eta_o t'' I_r [B - mB\cos(fx+\theta)]} \\ &= T_s\left(1 - e^{-\delta_i \eta_i t' I_w [B + mB\cos(fx+\theta)]}\right) e^{-\delta_o \eta_o t'' I_r [B - mB\cos(fx+\theta)]} \end{aligned} \tag{59}$$

where I_w and I_r are the relative brightness of the write and read beams. Reading out the SLR with a uniform beam, the intensity distribution of the emitted radiation is directly proportional to $T(x,t',t'')$ which is plotted in Figure 3.5-5 for different values of $\epsilon = \exp[-\delta_o \eta_o I_r t''/\delta_i \eta_i I_w t']$ and $B=1$, $m=0.1$. We see that the bias is gradually reduced as the bias removal exposure $\delta_o \eta_o I_r\ t''$ increases. The trend continues until ϵ falls below 0.3 where the signal level also begins to be reduced by the bias subtraction process. In Figure 3.5-6, the gain in signal-to-noise ratio is plotted against the erase exposure as expressed by ϵ. S_m denotes the highest SNR that can be achieved without bias subtraction. Since the characteristic of an SLR is nonlinear, the highest SNR is not achieved near saturation as with a CCD detector array. Instead, the optimum exposure is achieved when the mean or bias level occupies 45% of the available traps. With $T_s = 10^8$, $S_m = 982$ for an input signal with 10% contrast. From Figure 3.5-6, we see that the largest improvement in SNR is obtained when $\epsilon = 0.29$ where the gain is about 44%.

Instead of performing the write and bias subtraction sequentially, the processing can be speeded up by performing the input writing and the bias subtraction simultaneously. With both beam patterns illuminating the SLR at the same time, the rate of change in the number of trapped electrons is given by:

$$\frac{T(x,t)}{dt} = \delta_i \eta_i W(x)[T_s - T(x,t)] - \delta_o \eta_o T(x,t) R(x) \tag{60}$$

and the solution to the differential equation is:

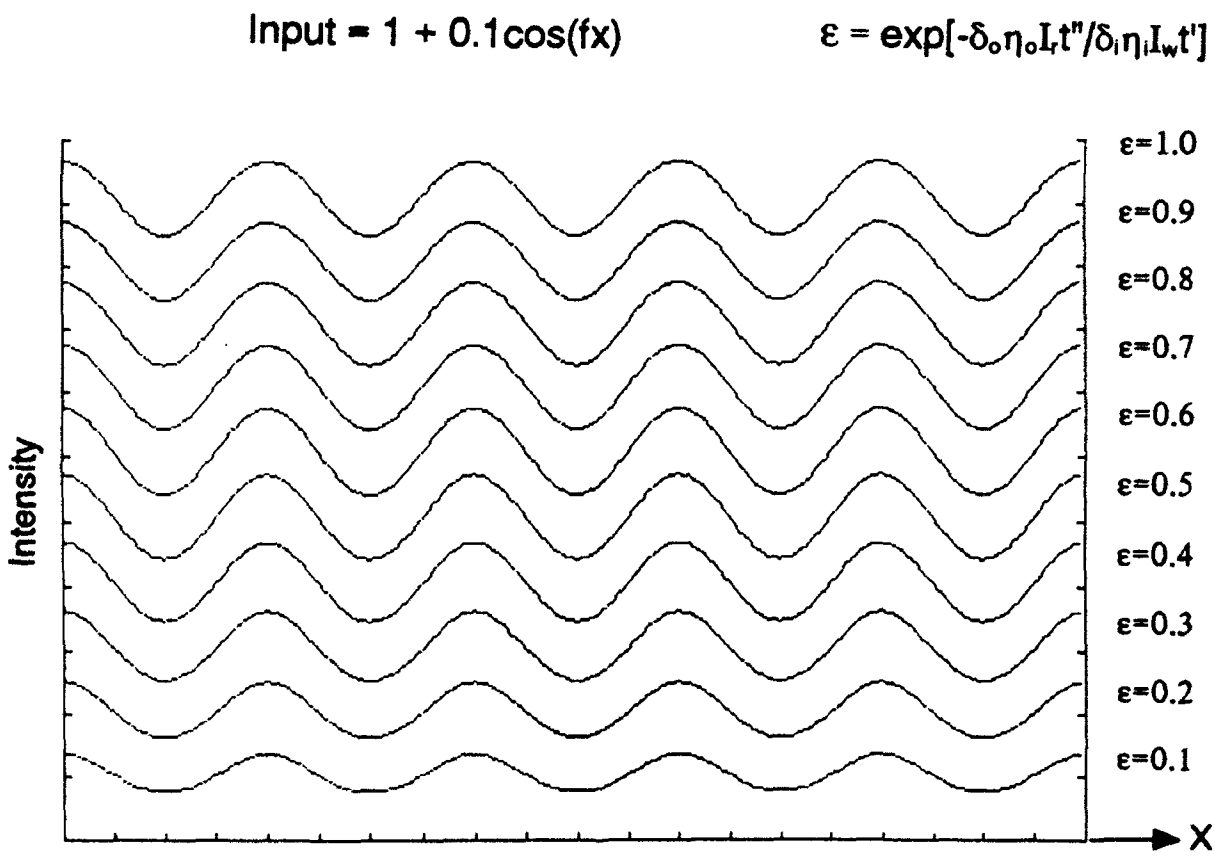

Figure 3.5-5. Bias Subtraction as a Function of Erasure Energy

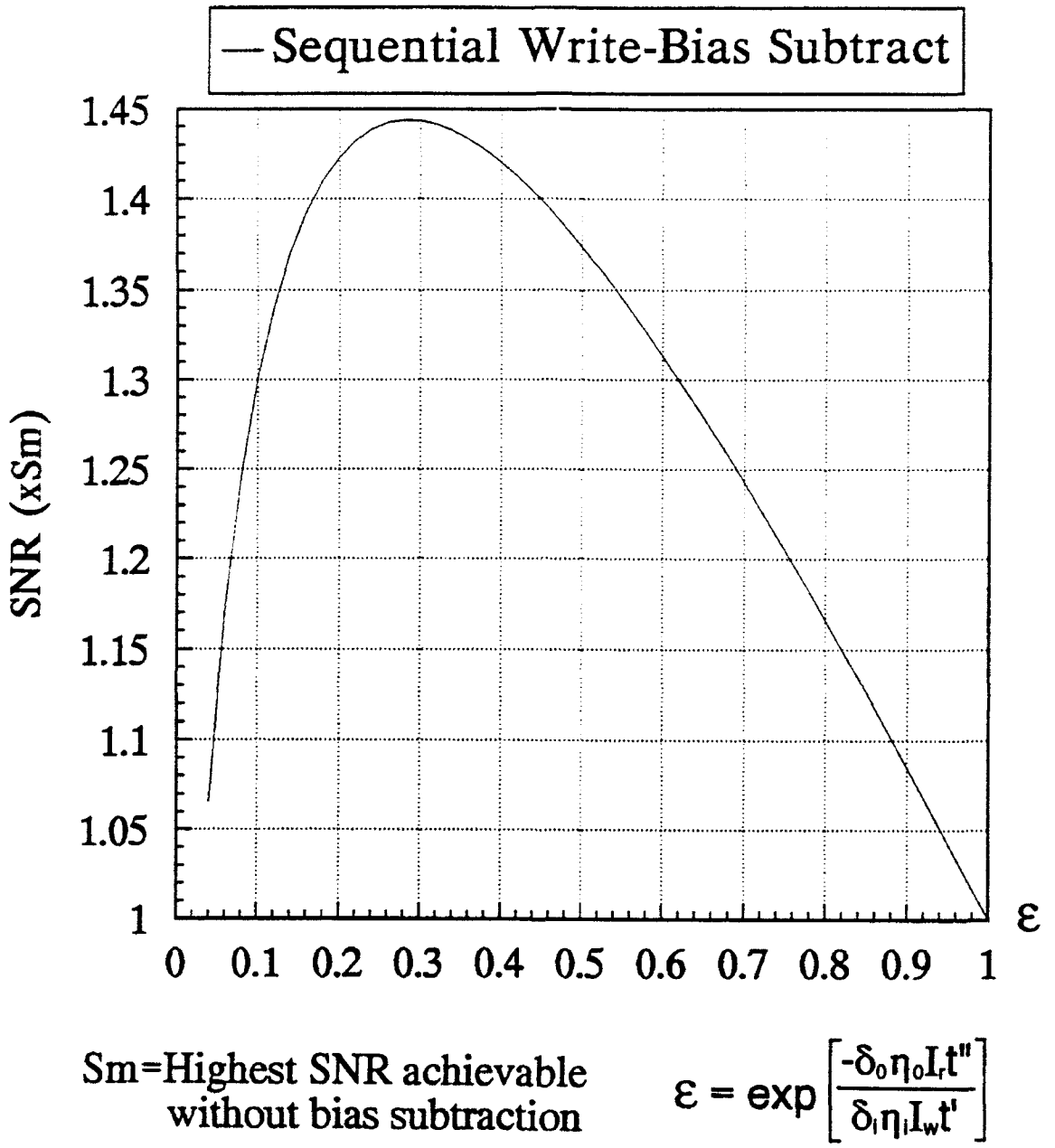

Figure 3.5-6. Gain in Signal-to-Noise Ratio as a Function of the Erase Beam Exposure

$$T(x,t) = \frac{\delta_i \eta_i W(x) T_s}{\delta_i \eta_i W(x) + \delta_o \eta_o R(x)} \left[1 - e^{-[\delta_i \eta_i W(x) + \delta_o \eta_o R(x)]\, t} \right] \qquad (60)$$

assuming an initial condition of $T(x,0)=0$. Using once again the write and read patterns given in Eq. (14) and (15) as the inputs, the outputs of the SLR are plotted in Figure 3.5-7 for different exposure times and different relative beam intensities. The SLR reaches a steady state after a certain amount of exposure. The amount of SNR enhancement achieved when the SLR reaches steady state is plotted in Figure 3.5-8 as a function of the erase-write beam ratio, $\zeta = -\delta_o \eta_o I_r t'' / \delta_i \eta_i I_w t'$. The largest gain in SNR is achieved when $\zeta = 2$ where the gain is about 57%. The SNR is zero when there is no erase beam because the SLR is driven to saturation.

Due to vignetting and other effects, the bias in the output of an incoherent optical processor output is typically not uniform. Often, the amount of spatial variation in the bias term is larger than the signal. The bias subtraction process achieved at steady state with the SLR is not dependent on the level of the original bias. The bias subtraction method produces a uniform residual bias which can be removed by simply subtracting a constant from the output of the detector array. This is illustrated in Figure 3.5-9. With a rectangular input window, the compressed output is a Sinc ($\sin \pi x / \pi x$) function. In Figure 3.5-6(a), we show the case where the output Sinc function is on a uniform bias. The bias level is as expected, reduced by the processing with the SLR. In Figure 3.5-9(b), the Sinc function is imbedded in a low frequency nonuniform bias. The residual bias in the SLR output is flat much like the case in Figure 3.5-9(a). The uniform bias can be easily removed by subtracting a constant value from the detector output. In Figure 3.5-9(c), the Sinc function is imbedded in a high frequency non uniform bias which makes it difficult to discern the presence of the signal. The processing by the SLR once again reduces the level of the bias and makes it constant over the entire output.

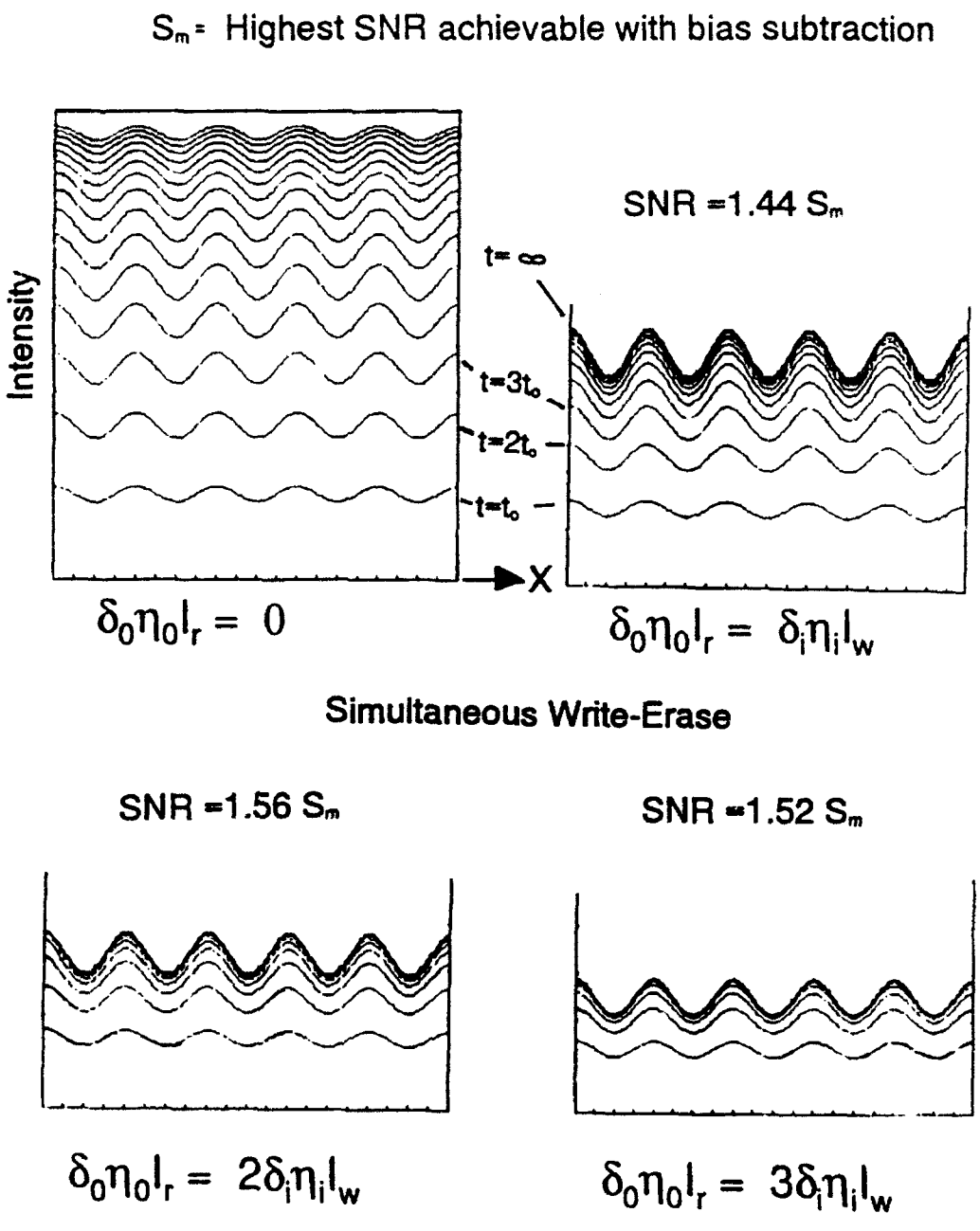

Figure 3.5-7. Bias Subtraction with Simultaneous Write and Erase

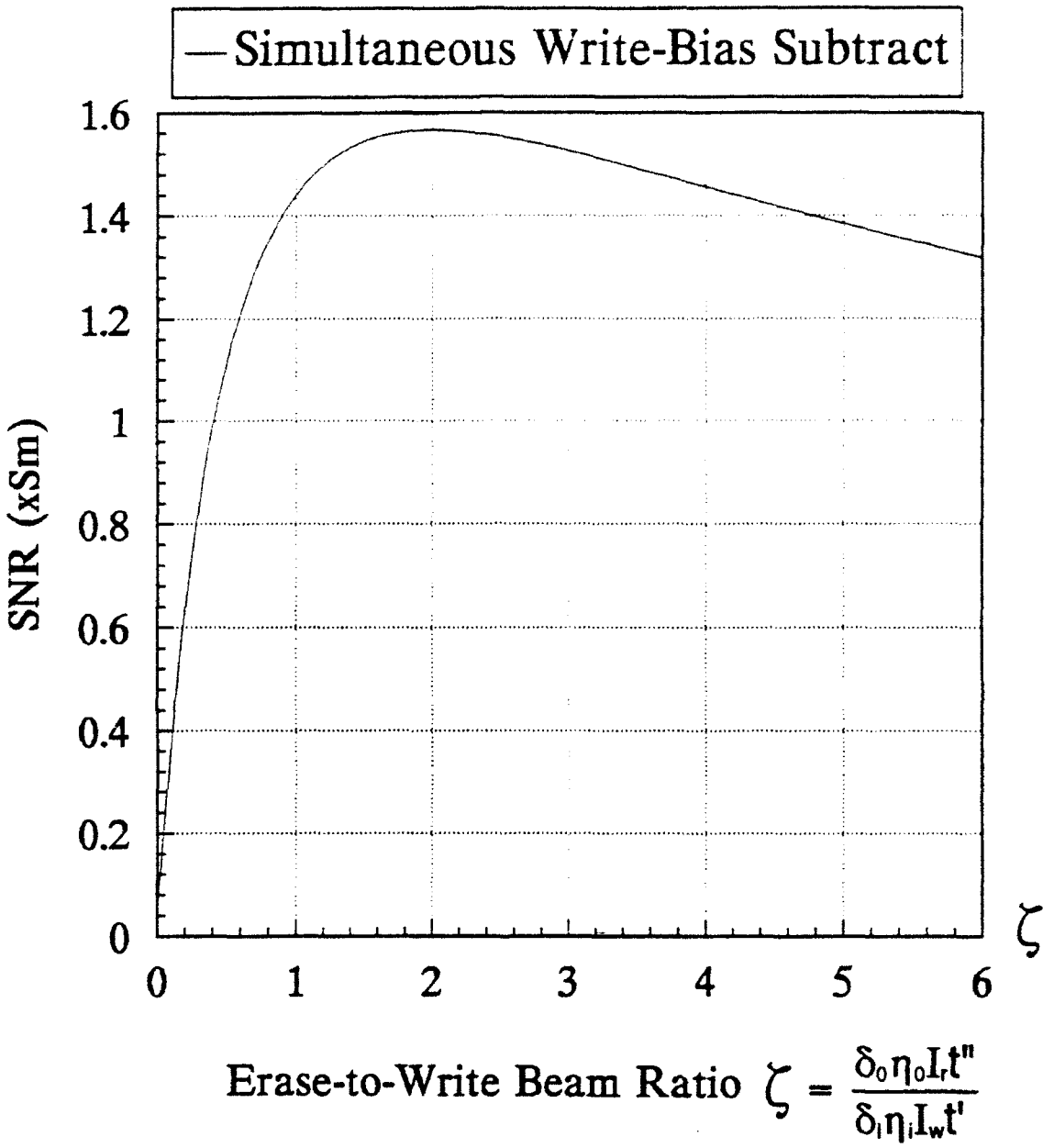

Figure 3.5-8. Gain in Signal-to-Noise Ratio with Simultaneous Write and Erase

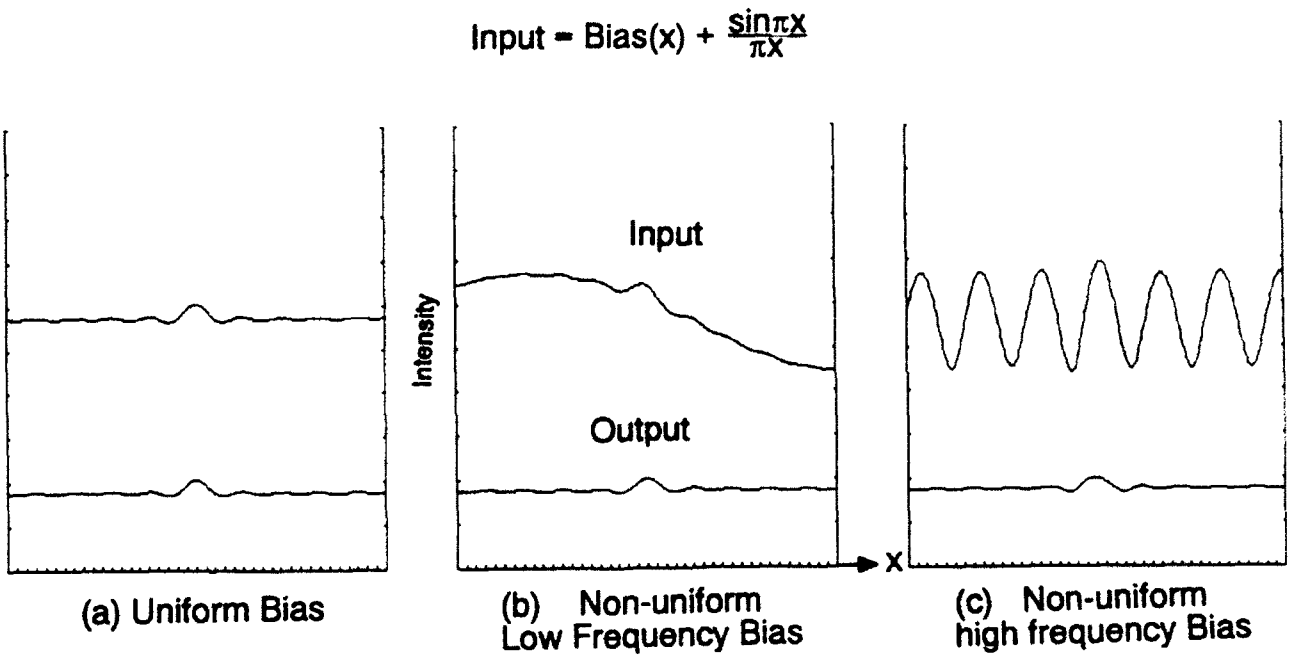

Figure 3.5-9. Removal of Space-Varying Bias: (a) Uniform Bias, (b) Nonuniform Low Frequency Bias, (c) Nonuniform High Frequency Bias

With the proposed processor architecture, the SLR reaches a steady state instead of saturating with increased exposure. The bias subtraction technique, therefore, adds robustness to the incoherent processing system as well. The exposure does not have to be controlled precisely. As long as the exposure is sufficiently long, an enhanced signal is achieved.

3.5.4 Projected Performance of Acousto-Optics Based Interferometric Processor

Consider an acousto-optic based interferometric processor as illustrated in Figure 3.5-4. Let the aperture time be τ, N be the number of pixels (on a carrier in the A-O cell and M^2 be the space-bandwidth product of the processor output. The processing speed of the processing system is then equal to M^2N/τ. As an example, with a Crystal Tech 40~5 A-O modulator, the carrier frequency f_c=75MHz, the bandwidth BW = 50MHz, τ = 80μsec and M = N = 4000. The processing speed is then equal to 1.25 x 10^{13} op/sec. The optics in the interferometric processor should occupy about 0.3 cubic feet. Including all the driving electronics, the overall processor size is estimated to be approximately 1 cubic foot. The predicted system performance of the optical interferometric processor per unit volume is about 1.25 x 10^{13} ops/sec/ft^3 = 4.2 x 10^8 ops/sec/cm^2.

3.5.5 Assessment

The optical interferometric performs the function of an array processor at very high speed. The large bias at the output, however, limits the performance of incoherent optical processors. A processing architecture utilizing a spatial light rebroadcaster as an intermediate detector can potentially enhance the output signal-to noise ratio by providing a larger dynamic range, removing a substantial part of the bias and all of its non-uniformity. By using the dynamic properties of an SLR, the bias reduction technique also provides the added benefit of making the system more robust. The exposure does

not have to be carefully controlled to achieve the optimum performance. The SLR reaches a steady state which prevents the device from saturating and losing the signal. The steady state can be reach rapidly if adequate laser powers are available for writing on and reading out the SLR.

Incoherent optical processors have the potential of utilizing the incoherent image of an object scene directly as the input, bypassing the bottle neck created by spatial light modulator. However, to utilize an SLR, the image of the input scene generally cannot be used directly because the natural scene may not possess enough of the desired ratio of energies at the write and read wavelengths of the SLR.

4.0 TASK 3: PRELIMINARY EXPERIMENTS

Preliminary experiments were performed to evaluate the hardware required to implement some of the concepts that were developed, specifically the waveguides of the integrated optics artificial neural network and the electron trapping material manufactured by Quantex that has been used as passive SLR.

4.1 Integrated Optics Architecture

In Section 3.2.3, the integrated optics architecture for artificial neural network processing applications was developed, analyzed, and a point design given. A proof-of-concept device was then designed, partially assembled, and preliminary experiments performed. It was found that many of the components needed for the proof-of-concept device were available off-the-shelf. A research quality waveguide array with the couplers did need to be fabricated, however. Preliminary experiments showed successful coupling of light into the waveguide array, but were only partially successful in coupling light of the waveguides.

4.1.1 Proof-of-Concept Device Design

The artificial neural network application chosen for demonstration was that of determining terrain type from airborne multispectral imagery of the ground. Other ERIM work had successfully demonstrated a Kohonen self-organizing network for this application [Kohonen]. The specific network chosen was a five input, five node, five output Kohonen network operating on five wavelength bands of visible to short wave infrared data. As discussed in Section 3.2.1, 5-bit accuracy in the input data and the weights is required for this application. From the earlier work, the desired weight values were already known.

The basic design of the integrated optics processor is shown in Figure 4.1-1. The off-the-shelf components will be described first. For the proof-of-concept device, the laser diode array was replaced by an LED array. The array chosen was the ROHM JA303012CL-01, an LED print head. It has 3,584 pixels at 84.5-micron spacing. The emitting area of each pixel is 50 microns by 65 microns. The intensity output is 0.83 microwatts at a wavelength of 0.66 microns and is focussed by a GRIN lens. The LEDs can be modulated at up to 5 MHz.

The LED array and interface electronics were connected to an IBM PC and software was developed to control the array. Because the LEDs only give a binary output (on or off), the software converts the 5-bit input data to pulse-width modulated form. The resulting maximum data rate is 100 KHz.

An EG&G TB series linear photodiode array was chosen. This array has 128 photodiodes, 50 microns in width by 2.5 mm in length. A fiber optic faceplate consisting of 6-micron diameter, N.A. = 1 fibers, couples light onto the diodes. The saturation exposure for the diodes is 0.05 microjoules/cm^2 resulting in a saturation charge of 29 picoCoulombs and a dynamic range of 175,000:1. The maximum readout rate is 2.5 MHz. This array was also interfaced to the computer and controlling software written.

4.1.2 Waveguide Array Fabrication and Preliminary Experiments

To match the characteristics of the off-the-shelf components, the waveguide array was designed to have waveguides 50 microns wide by 65 microns deep by 2.5 mm long. The center to center spacing of the waveguides is 84.5 microns. The waveguide core is made of Norland optical cement (index of refraction, n = 1.56) with a silicon oxide bottom and side cladding layer (n = 1.46) and a methylsiloxane polymer top cladding layer (n = 1.38). The initial coupling mechanism chosen was to place diffuse regions

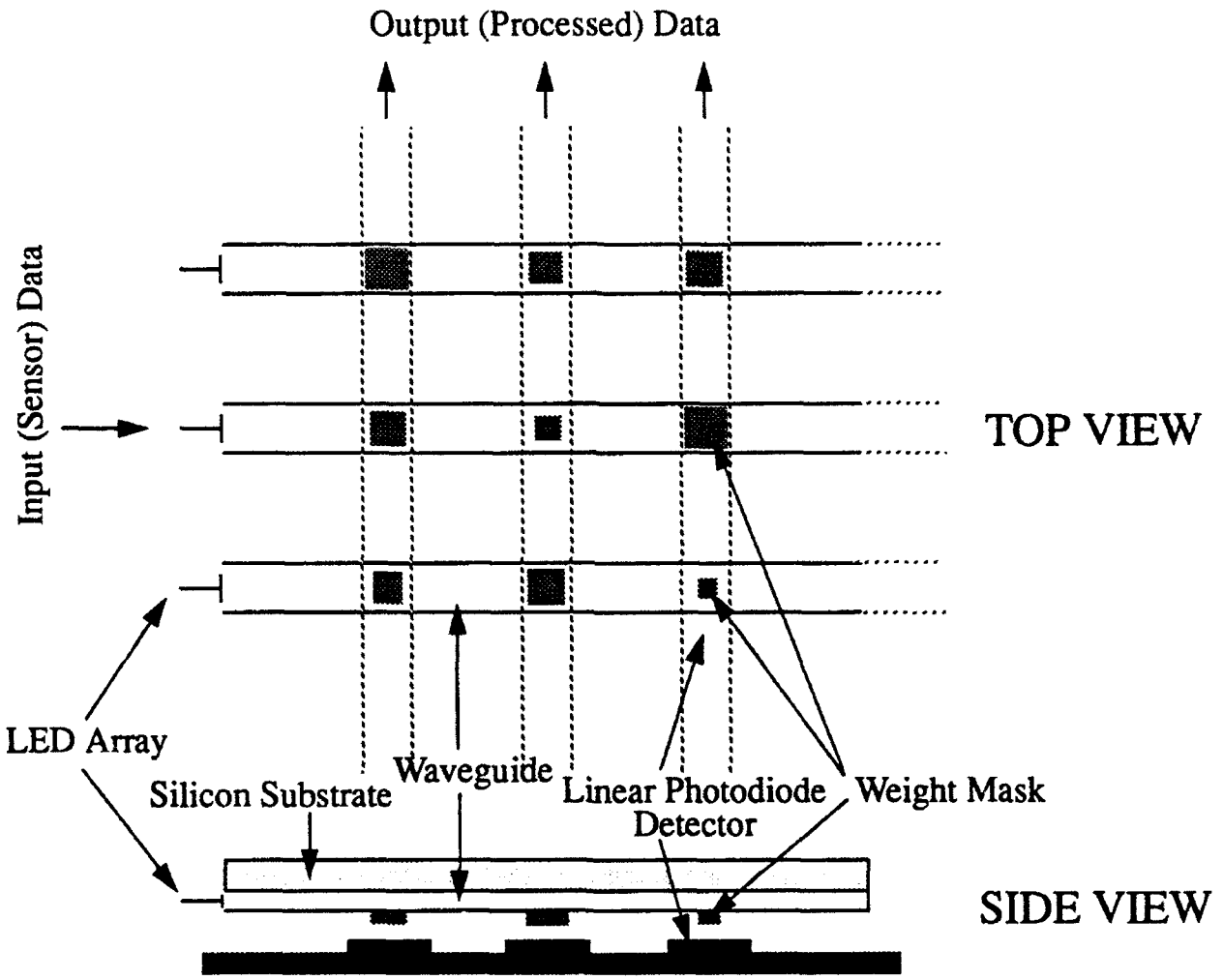

Figure 4.1-1. Integrated Optics Artificial Neural Network Processor

in the top surface of the waveguide to scatter light toward the photodiode array. The mask weights would be implemented by area encoding the diffuse regions and would be done as part of the waveguide fabrication process. Thus there would be no separate mask to align with the waveguide array during the experiment. The maximum size of an individual weight was chosen to be 10 microns by 40 microns which easily allows the necessary 5-bit array-encoding accuracy.

The waveguide fabrication process uses microfabrication technology. Masks were designed and made for the two photolithography steps. Mask 1 consists of long parallel stripes to form the waveguide pattern. Mask 2 consists of the known weight values area-encoded in five by five arrays as well as some test five by five arrays with non-zero weights only on the diagonal of the array. The fabrication process consists of the following steps:

1. Use high resistivity (P type Boron, 1 to 3 ohm-cm) intrinsic <110> silicon substrates polished on both sides.

2. Grow a 1.5-micron-thick layer of thermal oxide on the substrate in a furnace at 1000° C with oxygen and water vapor for 20 hours.

3. Use photoresist and Mask 1 to place the waveguide pattern on the thermal oxide layer.

4. Wet etch the waveguide pattern through the thermal oxide using NHsub4:HF for 28 minutes and remove the photoresist with stripper.

5. Wet etch the waveguides 65 microns into the silicon using a hot anisotropic KOH:Hsub20 etch for 108 minutes.

6. Grow a 1.5-micron-thick layer of thermal oxide on the waveguide wall and bottom surfaces. This is the cladding layer for the waveguide.

7. Fill the waveguides with Norland 61 optical cement, expose to UV, and cure the cement at 90° C for 12 hours.

8. Spin on a 0.5 micron methylsiloxane polymer (Accuglass 512) top cladding layer and heat cure at 150° C for 24 hours.

9. Use a 1.5-micron-thick photoresist layer and Mask 2 to place the weight mask (area-encoded) pattern on the top cladding layer.

10. Reactive ion etch through the cladding layer to the top surface of the Norland cement waveguides. This process leaves a diffuse surface on the Norland cement in the weight mask regions.

The fabrication process described above is the product of a collaborative effort between ERIM and WL/ELOT. The actual fabrication was done at WL.

Waveguide arrays were made at WL on several silicon wafers and delivered to ERIM for the preliminary experiments. The cross sections of the waveguides were examined under a microscope and found to be of the required size. A sample photograph is shown in Figure 4.1-2. Light was coupled into the waveguides from the LED array. Examination of light leaving the far end of the waveguides and microscopic examination of the top surface of the waveguides showed that, for the most part, light was indeed coupled into and contained within the waveguides and propagated to the far end with sufficiently low losses, crosstalk, and stray scattered light for a preliminary experiment to be successful. A few waveguides did have cracks in the Norland cement perpendicular to the direction of light propagation which scattered nearly all the light out of the waveguide at that point. The incidence of these defects was low enough so that, over the many redundant arrays fabricated on a 2-inch wafer, at least one would be found which was defect-free.

The weight masks were also subjected to careful examination under a microscope. A sample photograph is shown in Figure 4.1-3. It was found that the diffuse regions did not scatter very much light in a direction which would be within the acceptance angle of the fibers in the faceplate of the photodiode array. (The microscope had a greater acceptance angle than the fibers.) However, light propagating in directions very nearly along the length of the waveguide did leave the waveguide in the diffuse regions, strike the nearly perpendicular wall of the top cladding layer, and scatter into the microscope.

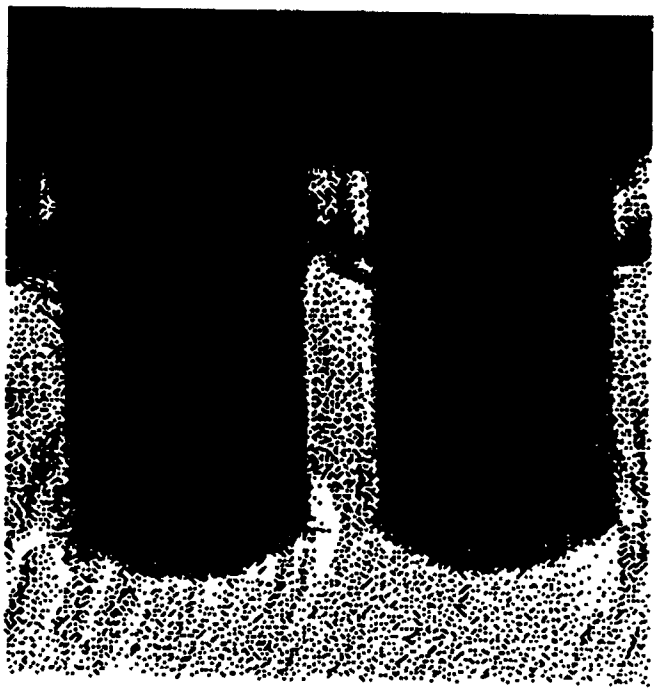

Figure 4.1-2. Cross Section of Waveguide Array Fabricated by the Air Force

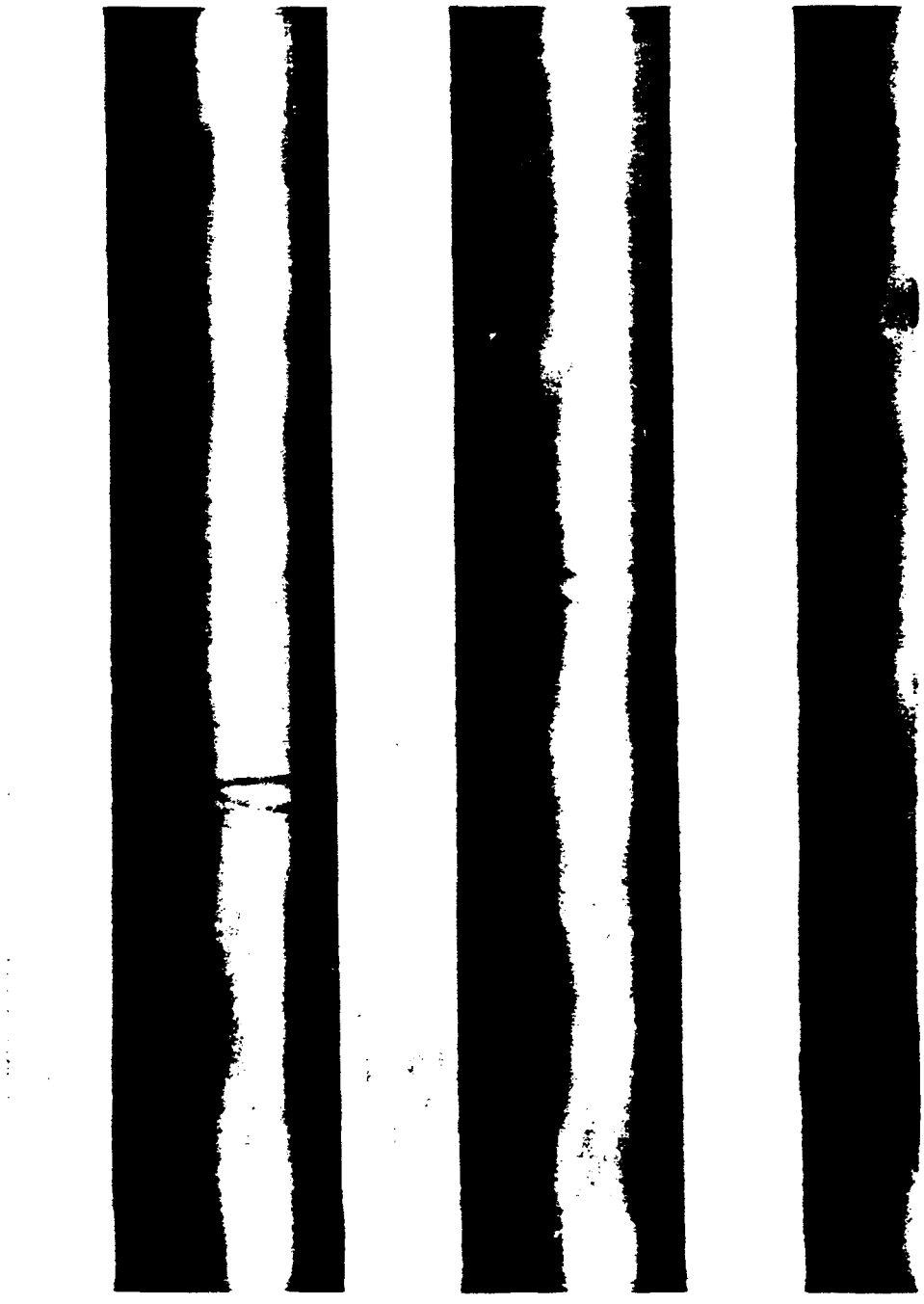

Figure 4.1-3. Waveguides with Weight Masks

This effect can be seen in Figure 4.1-3 as narrow lines of light at these perpendicular walls. This light appeared to be modulated only by the width of the weight masks and, therefore, would not be of the correct value.

Step 10 of the fabrication process was, therefore, modified. The substrate was placed on a 45 degree angle during the reactive ion etching to create walls angled at 45 degrees in the top cladding layer. An index matching fluid (n = 1.56 to match the Norland cement) would then be used to couple light out of the waveguide in the weight mask regions (no longer relying on diffuse scattering). This light would strike the angled wall at an angle of approximately 45 degrees to the wall normal and be reflected toward the fiber faceplate at near normal incidence to the faceplate. WL is currently fabricating this new waveguide array design. When ready, it will be used to continue these preliminary experiments.

4.2 Commercial Phosphor Based Passive SLR

An SLR based on electron trapping phosphor was acquired from Quantex Corp. and its read-write capability and temporal response was tested. The experimental setup is shown in Figure 4.2-1. The blue (488nm) beam from an Ar^+ laser was used to write onto the SLR and the near infrared (1.06μm) beam from a Nd:YAG laser was use to read out the device. To assure that the output detector detects only emission from the SLR, the laser light from the Ar^+ laser was spectrally filtered to remove any orange discharge glow from the laser tube and IR and blue blocking filters were used at the output to reject the read and write beams. The read and write beams from the Nd:YAG and Ar^+ lasers were modulated by shutters which sent a write pulse, a time gap and then a read pulse. The SLR emission was detected by a photomultiplier (PM) and monitored by a digital scope.

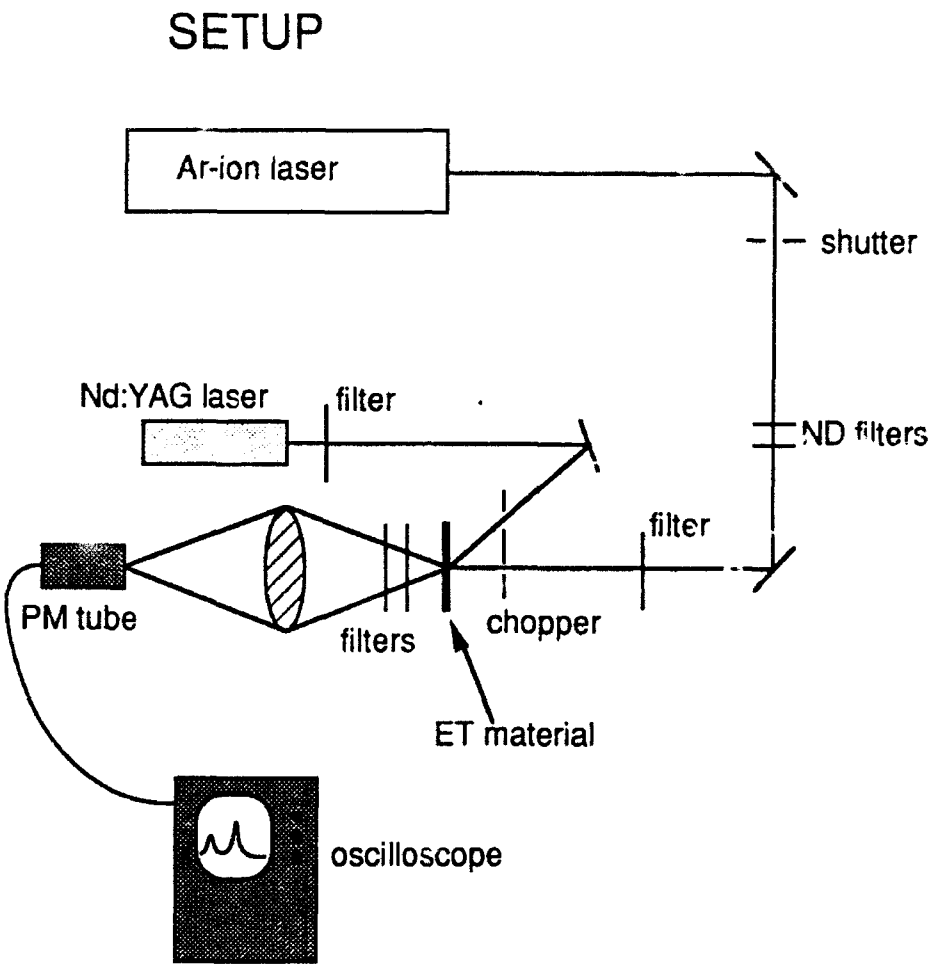

Figure 4.2-1. Experimental Setup to Test Phosphor-Based Passive SLR

There are two types of emission by the SLR, spontaneous fluorescence caused by the blue write beam and photoluminescence due to the IR readout beam. Fluorescence occurs because some of the excited electrons spontaneously fall back to the valence band instead of into traps. Photoluminescence occurs when the trapped electrons are excited by the IR beam out of the traps and give up the stored energy. The communication band is quite broad and some of the fluorescence emission are at the orange wavelength of photoluminescence. The write beam must, therefore, be turned off when the SLR is read out.

In Figure 4.2-2, the output of the PM is shown as a function of time. The write beam was turned on for about 20 seconds followed by an 8-second time gap and then the read beam. When the write beam was turned on, the fluorescence level steadily built up with exposure time because electrons were excited up to the communication band at a higher rate than they are falling back spontaneously to the valence band or into the traps. The increase in electrons population in the communication band produced a stronger fluorescence emission with time. When the IR read beam was turned on, the SLR emitted via photoluminescence. The emission fell off exponentially with time as the population of trapped electrons was depleted.

If a short IR pulse is used to read out the SLR and only a small percentage of the trapped electrons are released, the stored information can be readout repeatedly. The output beam brightness, however, will decrease exponentially with each subsequent readout. Repeated read out is illustrated in Figure 4.2-3. The SLR was written on by a strong blue pulse from an Ar^+ laser and then readout by two sequential pulses from a Nd:YAG laser. The first pulse in Figure 4.2-3 was due to fluorescence when the SLR was written by an Ar^+ laser and the subsequent two output pulses are photoluminescence induced by the read pulses. Some of the trapped electrons were released by the first read out pulse leaving a small population of trapped electrons. As expected, the intensity of the output due to the second readout pulse was slightly lower than the first.

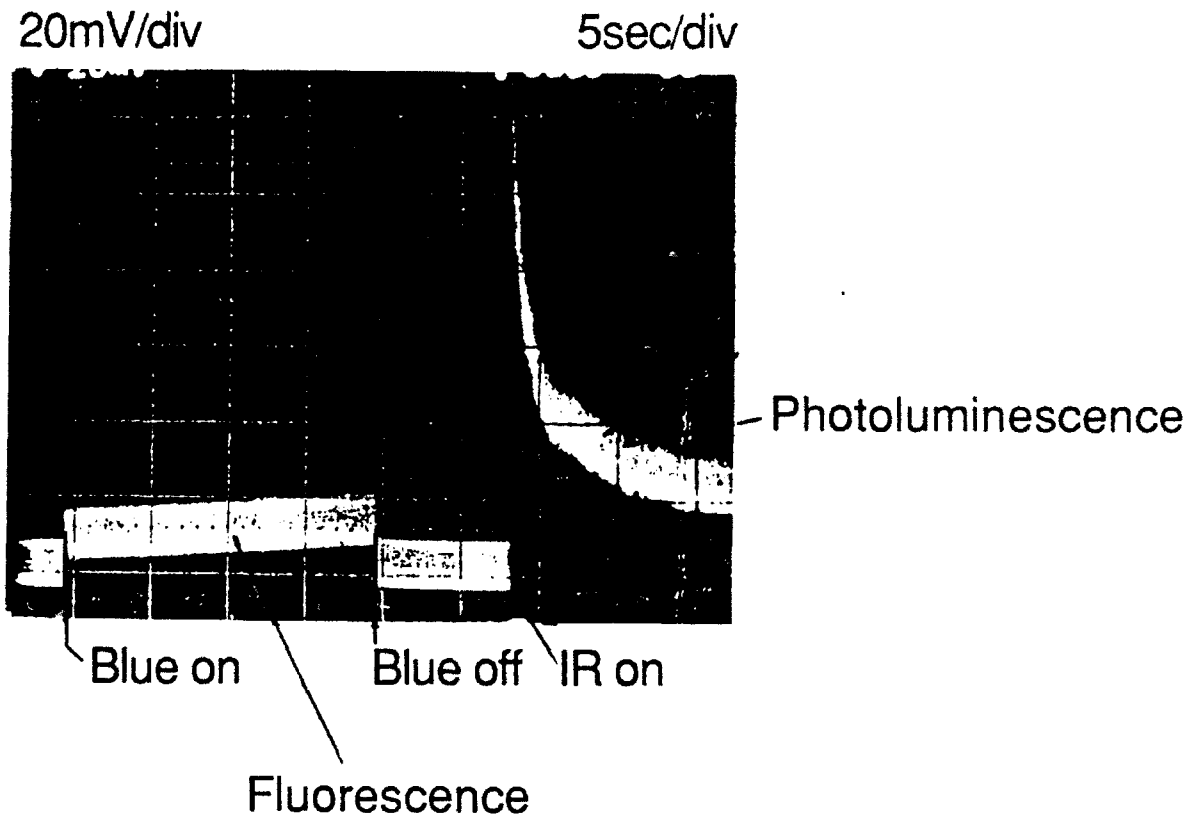

Figure 4.2-2. Photomultiplier Output in Write-Read Cycle

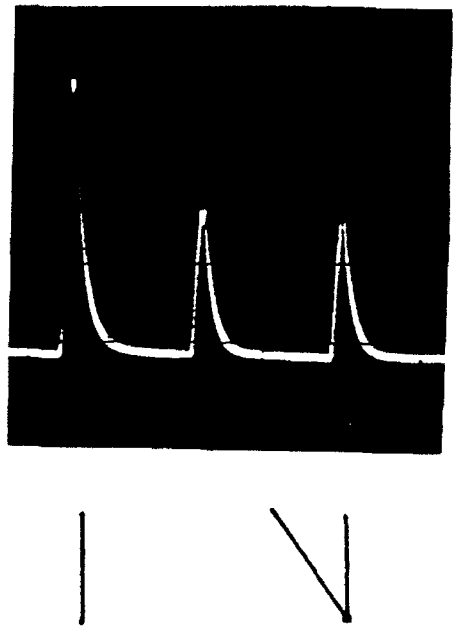

Figure 4.2-3. Demonstration of Repeated Readout

In the experiments, several drawbacks of the electron-trapping phosphor material as exemplified by Quantex's product became evident. (1) The light emitted by the SLR is very dim. One reason is that the SLR emits uniformly front and back over 4π steradian. A f/2 lens imaging one-to-one onto the detector gathers only 1/32 of the emitted light. (2) Rapid erasure of the stored information requires a large amount of energy (approximately 200 MJ/cm^2). In addition, the erasure did not appear to be complete, at least with the samples we obtained from Quantex. This resulted in a gradual build up of background bias with repeated write-read-erase cycles. (3) The readout is destructive. To use the device as a reference mask or matrix, for example, the device must be written periodically to refresh the memory. There is also a trade off between output brightness and the number of times the stored information can be read out. (5) The shift in wavelength between the input and the output makes it impossible to cascade two passive SLRs unless they can be doped very differently such that the wavelength of emission of the first SLR matches the wavelength of the write beam of the second.

5.0 CONCLUSION AND FUTURE DEVELOPMENT

The Spatial Light Rebroadcaster, particularly of the active type, can potentially be a powerful device that can serve as the heart of a compact high speed processor. The devices, however, are still in a very early developmental stage and they require significant amount of further development before they can be used competitively in optical processing architectures such as those described in this report.

5.1 SLR Performance Requirements

Passive SLRs such as those implemented with electron-trapping materials, exist today. Some of these materials were developed for wavelength down-conversion to visualize near infrared radiation and they are commercially available. The performance of these passive SLR materials and devices, however, require substantial improvement in several areas to make them competitive.

1) The slow temporal response of the passive SLR, particularly in erasure, limits the cycling rate. The throughput achievable is too slow to be competitive at this time.

2) Compounding the problem of low cycling rate is the low optical efficiency. The output is so dim that the output must be integrated over a significant amount of time to gather enough photons to provide the needed signal dynamic range.

3) The erasure is often incomplete unless very strong light or heat is used. The need for a powerful source for rapid and complete erasure impacts negatively on power consumption.

One solution to the problem may be to develop an SLR that emits light directionally (current devices radiate isotopically, over 4π radian). Improving the optical efficiency would allow the use of a thin layer of rebroadcasting material and improve the cycling speed of the device.

In addition, there are inherent characteristics of passive SLRs that limit their usefulness.

1) The readout is destructive. The material requires constant refreshing to keep the data stored in the device. A trade off between output brightness and the number of number of times the stored in formation can be readout is required.

2) The input and readout wavelengths are different which precludes the cascading of devices to perform sequential operations even if adequate optical efficiency can be achieved.

3) The nonlinearities exhibited by passive SLRs are weak and they cannot be easily changed. The type of operation that can be performed is, therefore, restricted.

Active SLR devices have the inherent flexibility and power to be a significant player in the future development of compact high speed processing systems. They may be utilized as interconnects and as the processing elements in an hybrid.electronic/optical processor. The programmable gain and nonlinearity provided by the device are particularly crucial to many optical computing architectures. The development of these devices, however, are still in an early stage. Specific area that requires further development includes the following.

1) Space-Bandwidth Product. The advantage offered by an optical processor is the massive parallelism of the computation. This advantage can be realized only if the space-bandwidth product of the input and output devices are sufficiently large. Devices being fabricated at this time are very small. The manufacturing technology to fabricate a large array with acceptable cost and yield remains to be developed.

2) Packing Density. The most attractive promise of optical processing is high speed processing in a small physical package with low power consumption. To fulfill this promise, the large space-bandwidth product must be accomplished in a small package that draws little power. Therefore, the device size must be small and the packing density must be very high. Considering that each element in an active SLR is consists of a detector, a signal conditioner and an emitter, a 3-dimensional structure is likely to be required to achieve the density desired.

3) Addressing Schemes. To maintain a high throughput, particularly with a pipelined, recirculating processing architecture, an efficient means must be available to address and program the elements in the SLR in parallel.

5.2 SLR-Based Optical Processors

We have analyzed several optical processing architectures that utilize either active or passive SLRs as processing elements, storage, input and/or output devices. The capabilities of those that employ passive SLRs are more restrictive. The advantage of using a passive SLR in lieu of conventional input, output and storage devices such as detector arrays and electronic memory is not compelling at this time. The lack of gain and the inability to be cascaded, in particularly, limit its usefulness. The potential strength of the passive SLR lies primarily in the large dynamic range it can provide. It may be able to enhance the performance of systems such as the interferometric processors where this feature is of crucial importance.

The active SLR is essentially an integrated array of elements each of which is composed of an input detector, a signal conditioner that is programmable electronically or by the output of a second detector, and an emitter. The ability to provide gain, non-linearity and high cycling rate, gives the active SLR unique power. It can perform simultaneously the functions of parallel optical interconnects and processing elements. The optical quadratic processor described in this report is an excellent example of the integration of these processor functions.

So far, the SLR is being developed as a general purpose device that can be utilized in different optical processing architectures. The system performance can be further optimized if the SLR is designed as an integral part of the processor. With such an approach, the SLR is not a stand alone component but is made specifically to match and operate with the other components. The integrated optics artificial neural network processor is a good example of this design approach.

It is recommended that future development of SLR based optical processors be directed towards the active SLR technology and optical processing architectures that combine the interconnects and processing elements with SLRs. In addition, instead of treating the SLR as a generic component to be inserted into an optical processor, the SLR should be considered as an integral part of the optical processor design. The pixel size, number and spacing, the temporal response, the packaging and integration of the SLR should be custom designed to match all other components to maximize the processor speed and efficiency.

Bibliography

Agranat, A., C.F. Neugebauer, and A. Yariv, "Parallel optoelectronic realization of neural networks models using CID technology," Appl. Opt., Vol. 27, pp. 4354, 1988.

Aleksoff, C.C. and N.S. Subotic," Compact Real-time Interferometric Fourier Transform Processor," Proc. Soc. Photo-opt. Instr. Eng., Vol. 1347, pp.427-439, 1990.

ATRWG (Automatic Target Recognizer Working Group), "Automatic Target Recognizer Component Definitions," ATRWG Report No. 87-002, April 1987.

Borelli, N., et al., "Photographic techniques for producing microlenses in photosensitive glass," Appl. Opt., Vol. 24, p. 2520, 1985.

Born, M. and E. Wolf, *Principles of Optics*, 5th Ed., MacMillan Co., New York, Chap. 10, 1964.

Boyd, G.D., "Optically excited synapse for neural networks," Appl. Opt., Vol. 26, p. 2712, 1987.

Cederquist, J.N. and S. Lee, "Coherent Optical Feedback for the Analog Solution to Partial Differential Equation," JOSA, Vol. 70, pp. 944-953, 1980.

Cederquist, J.N. et al.,"Multispectral Classification Algorithm Development," ERIM IR&D Report, No. 617124-1-F, December 1991.

Gary, C.K., "Comparison of Optics and Electronics for the Calculation of Matrix-Vector Products," Proc SPIE, April 1992, Orlando, Florida.

Goodman, J.W., *Introduction to Fourier Optics*, McGraw-Hill, New York, 1968.

Hopfield, J.J., "Neural Network and Physical System with Emergent Collective Computational Abilities," Proc. Natl. Acad. Sci. USA, Vol. 79, pp. 2554-2558, 1982.

Huang, K.S., B.K. Jenkins and A.A. Sawchuk, "Image algebra representation of parallel optical binary arithmetic," Appl. Opt., Vol.28., pp. 1263-1278, 1989.

Jutamulia, S., et al., "Use of electron trapping materials in optical signal processing 1: parallel boolean Logic," Applied Optics, Vol. 29, p. 4806-4811, 1990.

Lee, S.H., "Coherent Optical Processing," *Optical Information Processing*, Ed. S.H. Lee, Springer-Verlag, New York, Chap. 3, 1981.

Lindmayer, "A New Erasable Optical Memory," Solid State Tech., pp. 135-138, 1988.

Lippman, R.P. "An Introduction to Computing with Neural Nets," IEEE ASSP, p. 4, April 1987.

MacDonald, R.I. and S.S. Lee, "Photodetector sensitivity control for weight setting in optoelectronic neural networks," Appl. Opt., Vol. 30, p. 176, 1991.

Maragos, P. and R. Schafer, "Morphological system for multi-dimensional signal processing," Proc. of IEEE, Vol. 78, pp.690-710, 1990.

McAukay, A.D. and J. Wang and C.T. Ma, "Optical heteroassociative memory using spatial light rebroadcasters," Appl. Opt., Vol. 29, pp. 2067-2073, 1990.

Ohta, J., Y. Nitta, and K. Kyuma, "Dynamic opticalneurochip using variable-sensitivity photodiodes," Opt. Lett., Vol. 16, p. 744, 1991.

Rhodes, W.T., "Incoherent Optical Processing," *Optical Information Processing*, Ed. S.H. Lee, Springer-Verlag, New York, Chap. 3, 1981.

Rietman, E.A., R.C. Frye, C.C. Wong, and C.D. Kornfeld, "Amorphous silicon photoconductive arrays for artificial neural networks," Appl. Opt., Vol. 28, p. 3474, 1989.

Rugh, W.J., *Nonlinear System Theory - The Volterrn/Wiener Approach*, John Hopkins Press, Baltimore, 1981.

Seldin, J.H. and J.N. Cederquist, "Classification of multispectral data: a comparison between neural network and classical techniques," Government Neural Network Applications Workshop, Dayton, OH, 24-26 August 1992.

Serra, J., *Image Analysis and Mathematical Morphology*, Academic Press, London, 1982.

Shih, F.Y. and O.R. Mitchell, "Threshold decomposition of gray-scale morphology into binary morphology," IEEE PAMI, Vol. 11, pp. 31-42, 1989.

Sternberg S., "Grayscale Morphology," Comput. Vision Graphics Image Process, Vol. 35, pp. 333-335, 1986.

Sullivan, R.J., et al.,"Detection, Discrimination and Classification of Targets in Clutter: Results of Strategic Target Algorithm Research (STAR) (U)" ERIM Final Report to AFWL, Report No. 232400-10-F, October 1991 (SECRET/NOFORN/WNINTEL).

Tai, A.M. and C.C. Aleksoff, "Grating-based interferometric processor for real-time optical Fourier transformation," Appl. Opt., Vol. 23, pp. 2282-2291, 1984.

Taylor, G.W. et al., "A New Double Heterostructure Optoelectronic Switching Device using Molecular Beam Epitaxy," J. Appl. Phys., Vol. 59(2), 1986.

Van Trees, H.L., *Detection, Estimation and Modulation Theory*, Wiley, New York, 1968.